Foaming of Friction Stir Processed Al Precursor by Microwave Heating

Doctoral Thesis

by

Mandeep Kumar

Registration No.: 901908004

DEPARTMENT OF MECHANICAL ENGINEERING

THAPAR INSTITUTE OF ENGINEERING AND TECHNOLOGY

June 2023

Foaming of Friction Stir Processed Al Precursor by Microwave Heating

Submitted in partial fulfillment of the requirement for the award of the degree

of

Doctor of Philosophy

Submitted by

Mandeep Kumar

Registration No.: 901908004

Under the supervision of

Dr. Ratnesh Kumar Raj Singh
Assistant Professor
Department of Mechanical Engineering,
Thapar Institute of Engineering &
Technology, Patiala

Prof. Vivek Jain
Professor
Department of Mechanical Engineering,
Thapar Institute of Engineering &
Technology, Patiala

DEPARTMENT OF MECHANICAL ENGINEERING

THAPAR INSTITUTE OF ENGINEERING & TECHNOLOGY

June 2023

CERTIFICATE

Certified that the work presented in the thesis entitled "**Foaming of Friction Stir Processed Al Precursor by Microwave Heating**" being submitted by Mr. Mandeep Kumar (Regd. No. 901908004) in fulfilment of the requirements for the award of the degree of 'Doctor of Philosophy' in the Department of Mechanical Engineering, Thapar Institute of Engineering and Technology, Patiala, is an authentic record of the candidate's own work carried out during the period from June 2019 to February 2023 at this institute under our supervision. The matter presented in this dissertation has not been submitted for the award of any other degree in any university.

Dr. Ratnesh Kumar Raj Singh
Assistant Professor
MED, TIET, Patiala

Prof. Vivek Jain
Professor
MED, TIET, Patiala

DECLARATION

I hereby certify that the work which is being presented in this thesis, entitled "**Foaming of Friction Stir Processed Al Precursor by Microwave Heating**", in the fulfilment of the requirements for the award of degree of 'Doctor of Philosophy' in Mechanical Engineering submitted to the Department of Mechanical Engineering of Thapar Institute of Engineering and Technology (Deemed to be University), Patiala is an authentic record of my own work carried out under the supervision of Dr. Ratnesh Kumar Raj Singh , Assistant Professor, Mechanical Engineering Department, Thapar Institute of Engineering and Technology, Patiala and Prof. Vivek Jain, Professor, Mechanical Engineering Department, Thapar Institute of Engineering and Technology, Patiala.

The matter presented in this dissertation has not been submitted in part or full to any other university or institute for the award of any degree in India or abroad.

Mandeep Kumar

Mandeep Kumar

ACKNOWLEDGEMENT

First of all, I would like to express my gratitude to my supervisors Dr. Ratnesh Kumar Raj Singh, Assistant Professor, Mechanical Engineering Department, Thapar Institute of Engineering and Technology, Patiala and Prof. Vivek Jain, Professor, Mechanical Engineering Department, Thapar Institute of Engineering and Technology, Patiala for their invaluable guidance, moral support and encouragement during the entire period of this research which cannot adequately be expressed in words in this acknowledgement.

I would like to extend my acknowledgment to my doctoral committee member Dr. Tarun Kumar Bera (Head, Department of Mechanical Engineering), Dr. Dheeraj Gupta, Dr. Puneet Sharma and Dr. Satish Kumar Sharma for their valuable observations, suggestions, and feedback. I am very much grateful to my friends Parveen Kumar, Hemant Kaundal, and Avtar Singh for their help and support.

I would like to thank my parents, Sh. Pawan Kumar and Smt. Usha Rani whose consistent love and support motivated me throughout the period of research. I would also like to thank my brother, Mr. Harkesh Kumar for her understanding, patience and valuable support which helped me in achieving the goal.

Special thanks to my wife Ms. Pooja Sharma for her understanding and support during the entire period of research program. Special thanks to my daughters Ms. Aradhya and Anaya Sharma who was the source of my motivation.

Above all, I thank almighty whose blessings have enabled me to accomplish this research work.

Mandeep Kumar

Mandeep Kumar

LIST OF PUBLICATIONS

PUBLICATIONS RELATED TO PRESENT WORK:

Sr. No.	Title of Paper	Authors	Journal Name	Year or Status
1.	Effect of Tool Pin Profiles on the Properties of Foamable Precursor Developed by Friction Stir Processing	M Kumar, R Kumar, V Jain	Proceedings of the Institution of Mechanical Engineers, Part E: Journal of Process Mechanical Engineering (SAGE Publications) Impact factor: 1.822	Published (2022)
2.	Effect of Processing Parameters and Heat treatment techniques on Foaming Properties of Aluminium Foam Developed by FSP Route	M Kumar, R Kumar, V Jain	Proceedings of the Institution of Mechanical Engineers, Part L: Journal of Materials: Design and Applications (SAGE Publications) Impact factor: 2.663	Published (2022), Volume 237, Issue 2, Page no. 387-402
3.	Mechanical and Metallurgical Characterization of Foam Developed by Friction Stir Precursor Deposition Technique	M Kumar, R Kumar, V Jain	Journal of Adhesion Science and Technology (Taylor & Francis) Impact factor: 2.431	Published (2022)
4.	Aluminium Foam Development by Filling Architecture Techniques and Process Optimization	M Kumar, R Kumar, V Jain	Proceedings of the Institution of Mechanical Engineers, Part B: Journal of Engineering Manufacture, SAGE Publications) Impact factor: 2.759	Published (2023)

ABSTRACT

A substance with pores (voids) is known as a porous medium or material. The skeleton element of the substance is frequently referred to as the "matrix" or "frame." Many naturally occurring materials, including rocks and soil (such as aquifers and petroleum reservoirs), zeolites, biological tissues (such as bones, wood, and cork), and man-made materials, including metal, cement, ceramics, and polymers, can be categorized as porous media. These cellular materials are typically utilized in cases where weight needs to be reduced. Metals have a high energy absorption capacity during deformation caused by dislocation motion. As a result, metallic foams might offer an engineering material with the beneficial mechanical characteristics of polymeric foams, making them useful in applications where higher yield stresses and energy absorption are required. For many years, material scientists and technologists have worked to develop porous metals and metal foams. Metal foam is mainly composed of liquid and solid phases that coexist in a specific structure. A gas source is utilized to introduce pores into the structure. This gas source could be a blowing agent powder added to a liquid metal at a specific temperature, direct gas bubbles introduced to a liquid metal, or a blowing agent powder imbedded in the metal that expands when heated.

In the current technique, Titanium Hydride (TiH_2: blowing agent), Aluminum powder (Al powder) and Calcium Carbonate ($CaCO_3$: stabilizing agent) is embedded in the Aluminum AA7075 and AA6063 matrix using Friction Stir Processing (FSP) as the starting procedure. At this point, the metal is referred to as a precursor. This precursor creates a porous structure after being heated in a furnace/microwave at a specific time and temperature for the decomposition of the TiH_2. As a result of this decomposition, hydrogen gas is released, which remains in the matrix and forms pores. Metal foam is created when these holes have a spherical shape or a design that causes the density to be significantly reduced.

The results of various experiments such as powder filling techniques, tool pin profiles, and a new precursor development technique called as Friction Stir Deposition (FSD) are reported in this research work in order to ensure uniform TiH_2 distribution throughout the aluminum matrix for producing closed cell aluminum metal foam and its characterization. This indirect foaming method prevents the early melting of the material. This procedure opens the way for the creation of effective localized foam parts.

Based on the characteristic of the developed foam, it has been observed that the distribution of foamable mixture improved in the buried hole technique by creating an entrapped space to restrict the mixture to flow away and produce a porous Aluminum with a porosity of approximately 81% at 4-passes with 40% TiH_2 composition. As the number of FSP passes increases, pore size decreases. The percentage decrease in pore size from one pass to four passes during microwave heating is observed as 17.78 % as compared to 14.76 % in furnace heating. The time required for the development of foam in microwave heating is lower than that of furnace heating and the time needed for the development of foam in microwave heating is only 16.67% of the furnace heating. It is also observed from the results that the porosity in sandwich and groove techniques is 69% and 48%, respectively. The buried hole technique has higher porosity and improvement in porosity is of 17.92% and 71.25% as compared to sandwich and groove techniques, respectively.

It is also observed that during different tool pin profiles, the distribution of the foaming mixture improves with continuous material deformation by straight threaded cylindrical (STC) tool pin compared to the pulsating effect produced by square (SQ) and triangular (TR) pin. The foam developed at straight threaded cylindrical (STC) pin shows uniform deformation behavior during compression test than the foam developed by other tool profiles.

The foam developed by friction stir deposition (FSD) technique shows uniform distribution of foaming powder in 4 and 5 numbers of holes in the consumable rod as compare to other.

The hardness of the deposited precursor is lower than the base metal**.** The deposited material shows equiaxed fine grains that occurred due to dynamic recrystallization during deposition also have longer plateau stress due to optimum pore size which absorbs energy for longer duration.

TABLE OF CONTENTS

LIST OF TABLE

LIST OF FIGURES

Chapter 1: Introduction

A substance with pores (voids) is known as a porous medium or material. The skeleton element of the substance is frequently referred to as the "matrix" or "frame." Usually, a fluid is present in the pores (liquid or gas). Depending on the procedure and final density, a wide range of different materials are used to create various forms of foam. Many naturally occurring materials, including rocks and soil (such as aquifers and petroleum reservoirs), zeolites, biological tissues (such as bones, wood, and cork), and man-made materials, including metal, cement, ceramics, and polymers, can be categorized as porous media [1]. These cellular materials are typically utilized in cases where weight needs to be reduced. Since their relatively open structures can withstand high tensile and compressive strains, cellular structures also offer improved resistance to damage or sudden fracture. Due to its capacity to withstand considerable compressive stresses and absorb huge amounts of energy at a very low compressive stress [2], polymeric foams are frequently employed as protective casing in packaging and as an impact resistant material in applications like bike helmets and also utilized as a light structural material, for example as the core material in sandwich panels. The steps involved in the principle of foaming processes include polymer saturation or impregnation with a foaming agent, providing highly saturated polymer-gas combination by either sudden increase in temperature or drop in pressure, cell growth, and stability. In order to produce microcellular structure, temperature restriction is essential. Batch foaming, extrusion foaming, and foam-injection moulding are some of the numerous processing methods used to make polymer foam.

Metals have a high energy absorption capacity during deformation caused by dislocation motion. As a result, metallic foams might offer an engineering material with the beneficial mechanical

characteristics of polymeric foams, making them useful in applications where higher yield stresses and energy absorption are required.

1.1 Metal Foam

A volume proportion of 50-90% of the solid metal has uniformly distributed gas holes that define the metal foam [3]. It is described as the distribution of gaseous phase in a solid. As a result of its strong energy absorption capability, it can withstand greater strains [4]. Various research works [5] have examined the development and characterization of metal foams. According to their morphology, the metal foams may be divided into two main groups: closed cell and open cell as shown in Fig. 1.1 [3].

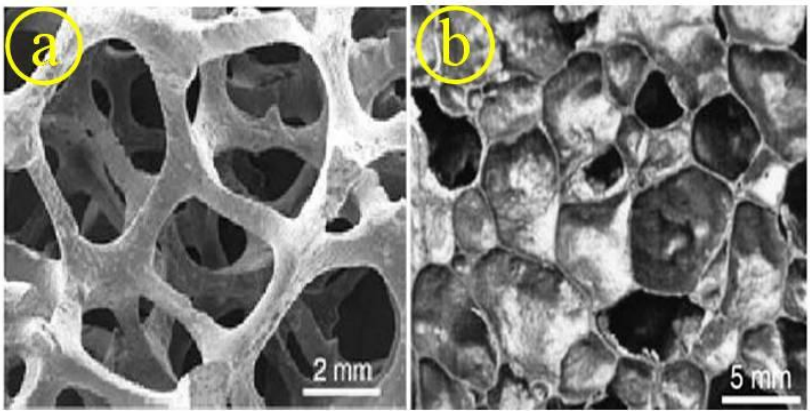

Fig. 1.1: Foam structure (a) Open and (b) closed-cell [6]

Due to their superior void connectivity, high internal surface area, and high thermal conductivity, open cell metal foams are employed inside of materials and in applications involving heat exchangers. These foams don't have effective mechanical qualities because of their honeycomb structure. As a result, practical applications where the material's stiffness is not a key concern, open cell metal foams are most often employed. Closed cell metal foams have the morphological

and physical characteristics that make them suitable for mechanical uses including load-bearing and structural ones [7]. When under compressive loading, they can serve as effective energy absorbers.

Steel, titanium, magnesium, zinc, and Aluminium are just a few of the metals that may be used to create closed-cell metal foams. Closed cell Aluminum metal foams are especially significant when it comes to mechanical applications like compressive strength, energy absorption capacity, and impact strength. Pure Aluminium makes up the Aluminium metal foams that are now on the market, whereas other Aluminium alloys have not yet been investigated for use in commercial manufacture [8]. Additionally, the commercially produced Aluminum foam sandwiches (AFS) and grooves are employed in a variety of mechanical applications [9]. In most cases, the foam may be recycled to create new foam.

1.2 Metal Foam Properties and Applications

Whether it is open-cell or closed-cell foam, metal foams have different properties. The techniques used for the foam production affects relative density, foam shape, and pore size due to this the mechanical and physical properties of the foam are also affected. The most significant factor influencing the mechanical property of foams among them is relative density. Electrical and thermal characteristics are regarded to be the physical characteristics of Aluminium foam.

1.2.1 Mechanical properties: The mechanical response of metal foams is closely related to its relative density. The relative density of the foam is defined as the ratio of the density of foam to that of the density of solid. The increase in the density of the foam causes the strength of the foam to increase [10].This increase in the strength is attributed to the fact that the thinner cell walls tend to buckle easily as compared to the thicker cell walls. Particularly for energy

absorption applications, the compression property of metal foam is important. Closed cell foams made of Aluminium exhibit the typical compressive stress-strain behaviour under uniaxial compressive loads.

1.2.2 Thermal properties: Metal foams naturally have a low thermal conductivity in compared to their parent metals since they are mostly made up of voids that are filled with air. In comparison to metals, the presence of gas bubbles in metal foams alters their thermal conductivity [11]. Metal foams are therefore attractive choices for a variety of thermal shielding applications, including nuclear fuel casks, to ensure superior thermal isolation, fire retardancy, energy absorption capabilities at lightweight, etc. [12]. It is obvious that air has a much lower thermal conductivity than metals.

1.2.3 Electrical property: Metal foams' conductivity is lower than that of solid metals because they contain nonconducting gas-filled pores. Depending on whether they have a closed or open shell structure, metal foams have different properties [11].

1.3 Practical Application of Foam

Metal foam is a commonly used material in many engineering applications, including those involving structural, functional, biological, and chemical requirements [13]. The primary goals of researchers nowadays are to scale up fabrication processes and create novel methods for continuous manufacturing that is both high-quality and affordable. Due to their comparably high cost, metallic foams currently have a restricted number of industrial applications. The lack of acceptable low-cost manufacturing processes for the mass manufacture of metal foams is one of the key limiting constraints. Metal foams are actively sought for weight-critical structural

applications and lightweight design. The functional uses for metal foams are fairly varied and look promising, as seen below:

1. The weight of the vehicle has to be raised as a result of the need for improved vehicle safety. On the other side, this reduced fuel economy, which calls for lighter vehicles. These problems called for the creation of multifunctional materials, and metal foams are one of the workable solutions.
2. Metal foams are the preferred material for noise management and control. Foams made of Aluminium may be utilized well in these situations to regulate and reduce noise.
3. The aircraft industry also demands lightweight components and structures, much like the automotive industry does. Metal foams are beneficial because they provide greater resistance to buckling and crippling forces.
4. Additionally, Aluminium foams are now being used in satellites, energy absorber parts, and spacecraft. Metallic foams have shown to be very suited for usage in satellites and space stations due to their lightweight and isotropic characteristics.
5. Shipbuilding requires low-weight, high-strength components, much like any other structural application. Aluminum foam cores play a crucial role in shipping constructions as a strong core that supports upper layers. These layers are in capable of carrying the weight.
6. Metal foams are utilized in the construction sector in a variety of ways. In place of expensive honeycomb structures, metal foams can be employed in building frontages as lightweight, rigid, and fire-resistant constructions. Moreover, Aluminium foams are increasingly commonly employed to safeguard building materials from fire.

7. Metal foams are used in a variety of ways for machine construction. To improve damping capacity and decrease inertia, stiff foamed sections of machinery components or foam-filled pillars may be utilized in place of standard metal axles or platforms.

Fig. 1.2 indicates the most important commercial applications where the metal foam is used [14].

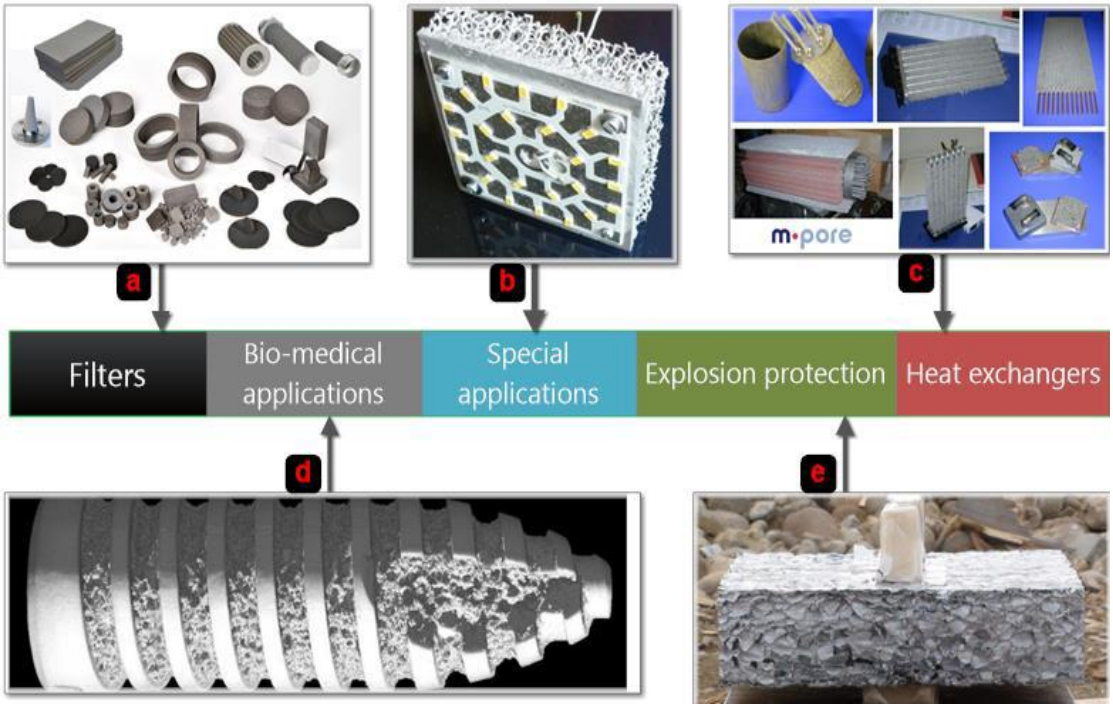

Fig.1.2: (a) shows high temperature filters made from porous metals, (b) shows using open cell foam in special applications as passive thermal cooling of LED lamps, (c) heat exchangers based on Al- and Cu-foams, (d) displays porous titanium as dental implant for Bio-medical applications, (e) aluminum foam for blast mitigation test [14].

1.4 Manufacturing Techniques of Metal Foam

Conventionally, a variety of techniques have been utilized to create metal foam [15-18]. As illustrated in Fig. 1.3, the foaming techniques may be divided into two categories: direct foaming

and indirect foaming. In direct foaming techniques, a blowing agent is directly added into the liquid metal. The metal turns into foam when in contact with gas. There are three types of direct foaming: injecting gas into the melt (the "Alcan line"), adding a chemical blowing agent to the melt, which breaks down and releases gas (the "Alporas line"), or dissolving gas in the melt first and releasing it during foaming (the "Gasar line"). The technique of "indirect foaming" (also known as "precursor foaming") entails melting a solid substance that has a gas source embedded in it; this gas source releases gas when the solid material melts, which then supports the foaming process. The following provides a detailed description of each method:

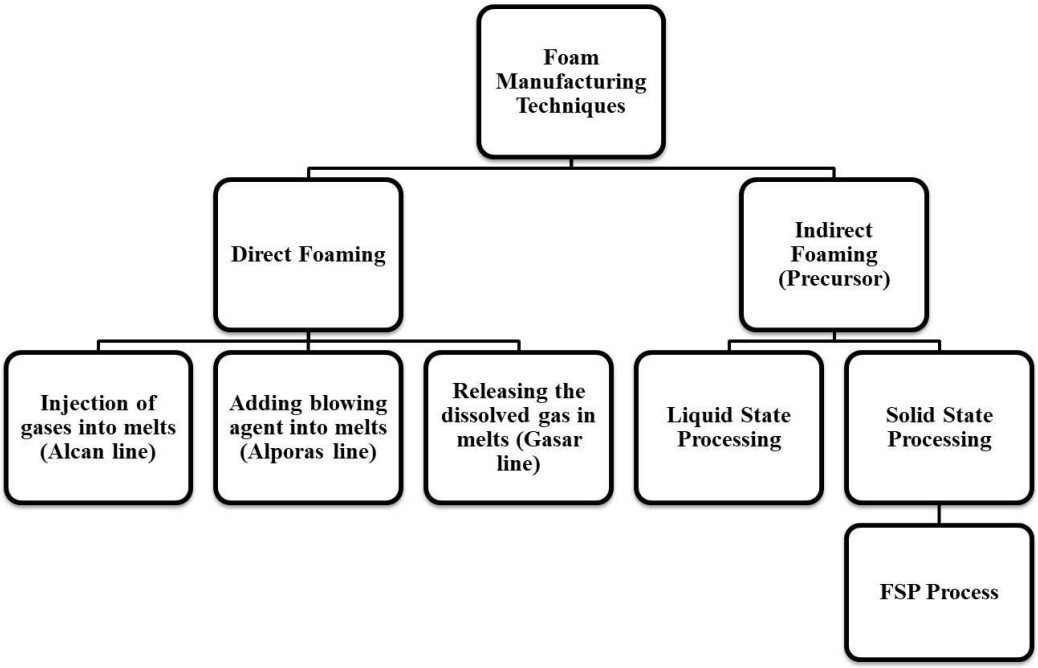

Fig. 1.3: Foam manufacturing techniques

1.4.1 Direct foaming

1.4.1.1 Air bubbling: By directly pushing gas into the molten metal, as shown in Fig. 1.4, these bubbles are collected on the top surface of the molten metal due to the buoyancy force [15].

When the bubbles solidify, foam is produced. Despite the ease and cost-effective technique, the pore development and dispersion during processing, continue to be a significant drawback.

1.4.1.2 Foam by adding blowing agent into melts: In this process, Aluminium is melted and stabilized between 670 and 690 ^{o}C. Titanium hydride (TiH_2) is the most popular foaming substance added to melts [19]. TiH_2 decomposes and releases hydrogen (H_2) gas when heated over 465 ^{o}C, which causes bubbles that can eventually form a closed-cell foamed structure as seen in Fig. 1.5. The TiH_2 and cooling conditions have the greatest influence on the cell size, which varies from 0.5 to 5 mm.

1.4.1.3 Releasing the dissolved gas in melts (gasar line): By using directed solidification, the metal foam is created using this technique. During solidification, a gas-eutectic reaction happens in which a solid metal and hydrogen are both created at the same time, resulting in the gas-filled pores and subsequently the porous material. As a result, porous material that contains up to 30% of its volume is pores. Controlling and optimizing of the pore shape is challenging because of the many of process factors involved. This method is still only used in labs since the materials produced in this way are expensive.

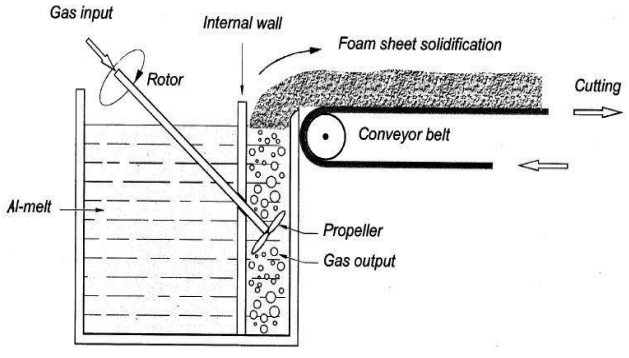

Fig. 1.4: Air bubbling foaming method [15]

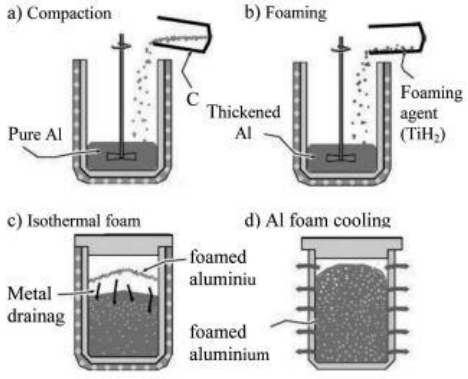

Fig. 1.5: Adding blowing agents into melt [19]

1.4.2 Indirect foaming (precursor foaming)

In the indirect foaming method, a blowing agent is embedded into the metal matrix. This combination of the bulk metal and the blowing agent is called as the precursor.

1.4.2.1 Liquid state processing route: In liquid state processing the materials is heated to a molten state and allowed to solidify as per requirement. In this method, blowing agent is added to the melt but is prevented from decomposing. To create a foamable precursor, the melt in which the blowing agent is mixed is quickly cooled at room temperature. This precursor material is divided into small pieces, sealed, and heated to a temperature just over the solidus temperature of the alloy. As a result of the severe internal pressure created by the decomposition of the foaming agent, voids are formed. The method also results in relative densities as low as 0.08. The foam's closed cells have a diameter of between 1 and 3 mm.

Process benefits

1. As long as desired, continuously transform a liquid metal or alloy into foam by this process.
2. Less expensive process.
3. Lowest density and highest homogeneity continuously produced.
4. No special fixture is required for the manufacturing of the precursor.

Process limitations

5. Restriction on producing shaped parts.
6. Distribution of the foaming into the melts is not uniform.
7. Large energy consuming process for precursor heating.

8. Cutting the foam is necessary in order to open the cells.
9. The handling of throughout the process is quite dangerous because high temperature process.

1.4.2.2 Solid State processing route: This process involves mixing the foaming agent into the metal matrix under solid state condition by using the friction tool for the manufacturing of the precursor. A foamable precursor are extracted from the processed zone of the tool and heated by some heat treatment techniques for the decomposition of the foaming agent. At a specific temperature, the metal matrix softens and the blowing agent decomposes and the foam is developed. Highly porous metal foam is developed when the blowing agent distributed more uniformly and releases gases that create pores inside the matrix more uniform.

Process efficiencies

1. Used for near net shapes and complicated parts
2. Mass production process because works under solid state condition.
3. Sandwich and grooves type's panels of multi materials are easily manufactured.
4. Less energy consuming process and easy to handle.
5. Distribution of the foaming is more uniform.
6. Used in variety of materials for the manufacturing metal foam.

Process drawbacks

1. Limited size foam is developed.
2. Material wastage only tool processed zone is used for foam development.
3. Foaming agent wastage in some techniques which enhanced the cost.

4. Special fixture is required for the manufacturing of the precursor.

1.5 Friction Stir Processing (FSP) Technique

The processing method known as friction stir processing (FSP) was invented by Mishra et al. [20]. Friction stir processing uses the fundamentals of friction stir welding (FSW) and works under the solid state condition route [21, 22]. In this process a non-consumable rotating tool with a pin and shoulder that are made especially is inserted into a plate as shown in Fig. 1.6. Depending on the nature of the work piece, a hardened material, such as HSS, EN31 and H13, is utilized to make the cylindrical tool. The tool is made up of three crucial components: the shank, tool shoulder, and tool pin. The tool produces a refined grain structure by heating the workpieces due to frictional heat [23]. FSP results in substantial material mixing, temperature exposure, and plastic deformation.

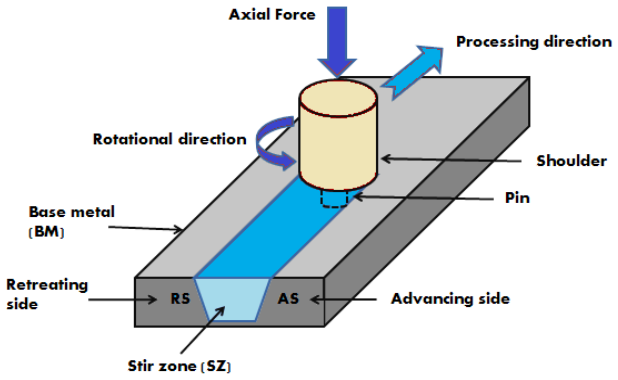

Fig. 1.6: Friction stirs processing technique

1.5.1 Capabilities of the friction stir processing technique

1. Produce fine-grained equiaxed microstructures
2. Eliminate the majority of liquid based defects

3. Can be used for a broad material range of ferrous and nonferrous metals
4. Easy to operate and does not involve any environmental pollution
5. The FSP methodology has the ability for producing a foamable precursor.
6. High mixing ability process.
7. FSP is an easy and high-speed process, so it can provide higher efficiency.

1.6 Metal Foam manufacturing by FSP technique

Due to its unique capabilities, FSP may create metal matrix composites by uniformly combining a reinforcing powder with the base metal serving as the matrix [24, 25]. The surface composite that was so produced is said to have greatly improved surface characteristics. This FSP technique is successfully used by Yokoshiko Hangaii et al. [26] for the development of a precursor. In order to fabricate metal foam, there are mainly two phases involved. First, the metal matrix is mixed with a blowing agent (such as TiH_2, ZrH_2, MgH_2, $CaCO_3$, etc.) for the manufacturing of the precursor. The manufactured precursor is heated above the decomposition temperature of the foaming agent in the second phase as shown in Fig. 1.7. Consequently, it might be considered one of the indirect methods of foaming (where the precursor is formed in the first step). By simply moving the rotating tool used in FSP back and forth, it is possible to create intensive stirring, which makes it simple to mix powder into an Al plate and combine segregated microstructures and gas holes in an even, uniform way. The use of FSP as a foaming technique provides a number of benefits over traditional foaming techniques.

1. One-step processing technique, depth of processed zone can be controlled by the pin length.
2. It reduces the environmental effect and decreases the cost of Al foam.
3. No chemical effects and no cracking.

4. FSP is an easy, quick technique that has a great potential for productivity.
5. The precursor can be produced without the need for time-consuming heating processes that use a lot of energy.

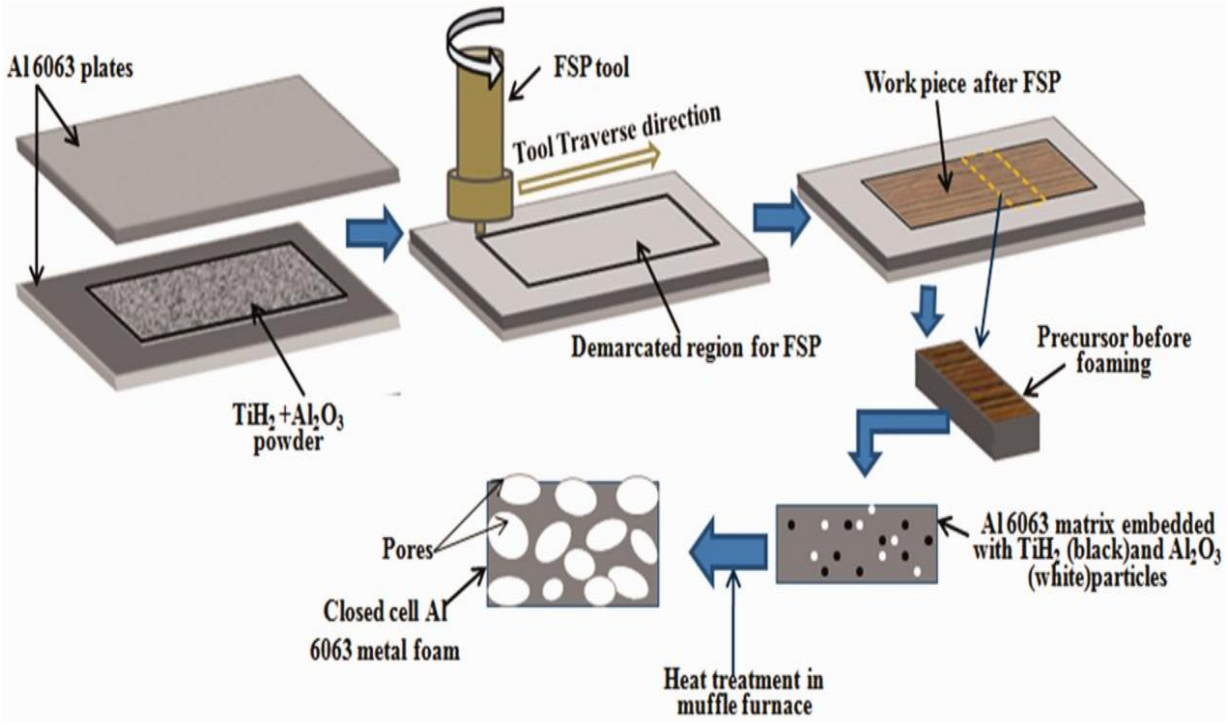

Fig. 1.7: Foam developed by FSP technique [26]

1.6.1 Drawbacks of FSP using as foaming technique

1. New processing technique, so more effort and knowledge is required for the development of metal foam.
2. Keyhole at the end of each pass
3. Need of a suitable fixture
4. Lack of predictive models in FSP
5. Difficult to developed bulk size metal foam.

1.7 Process Parameters

The property enhancements in metal foam are influenced by the distribution of foaming mixture particles inside the metal matrix. However, a number of factors including the methods are played significant role in metal foam that how the mixture is dispersed. These factors are FSP tool parameters, machine process parameters, types of blowing agent and precursor heat treatment technique. Each process variable has a varied contribution since some have a bigger effect on enhancing characteristics. The aim of the high-quality metal foam is depicted in a detailed cause and effect diagram in Figure 1.8. In the relevant sections, the variables in the figure are discussed in more detail.

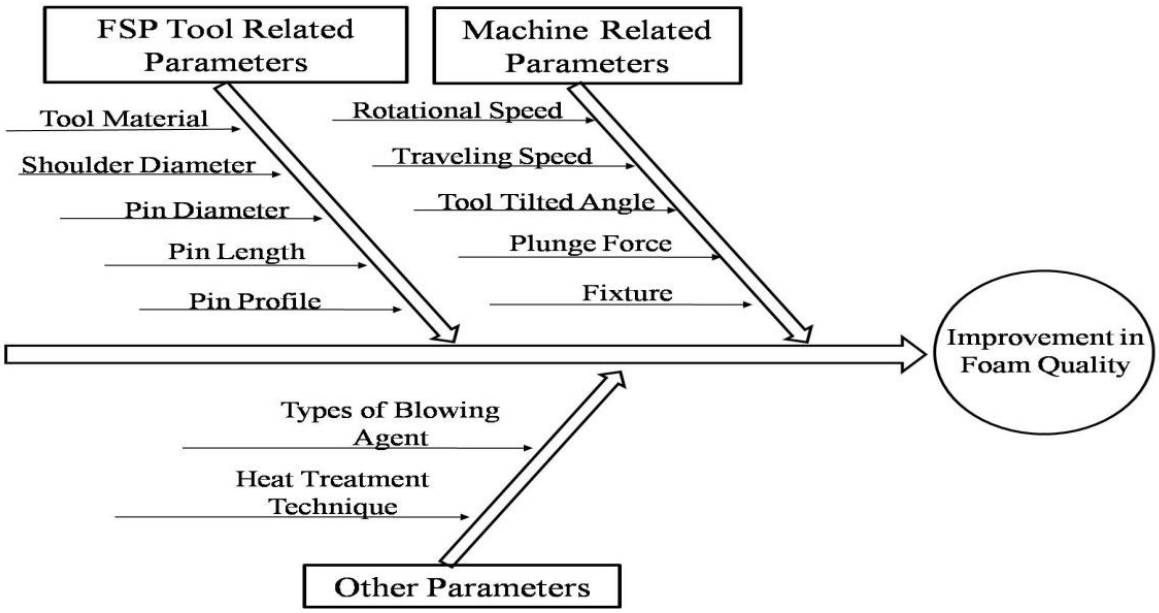

Fig. 1.8: Cause and effect diagram for improvement in foam quality

1.7.1 FSP tool process parameters

The tool geometry and their process parameters are crucial in determining heat generation, material deformation, particle dispersion, and properties of manufactured metal foam. Depending

on the type of workpiece to be used for the production of metal foam, the selection of tool material with the necessary hardness must be determined. The revolving tool generates heat primarily for two reasons: (1) Friction between the revolving tool and the workpiece. (2) Plastic deformation, which happens when the material of the workpiece stirs, mechanically mixes, and generates as a result of the tool's stirring motion. Designing of the shoulder to pin diameter (D/d) ratio can help to attain the best properties. The pin's geometry is more significant than other factors when it comes to tool pin design. The distribution of foaming particles and material movement are both significantly influenced by the tool pin profile [27], which in turn has an impact on the characteristics of manufactured metal foam.

1.7.2 Machine process parameters

The main machine variables that affect the quantity of heat produced and the pace of material movement throughout the process are the rotational and travel speeds. The combination of greater rotating speeds and slower travel speeds has been demonstrated in the literature to increase heat input, improve material flow, and enhance particle dispersion [28, 29]. Despite the fact that increasing rotational speed leads to better particle dispersion in metal matrix. Axial force, tool tilt angle, and plunge depth are additional machine-specific factors [30-32]. The angle of tool tilt and plunge depth have a close relationship. It is necessary to simultaneously optimize the tilt angle and plunge depth in order to achieve the optimal tool-to-work contact area. This may be explained as follows: As the tilt angle increases while the plunge depth remains constant, less of the tool's shoulder contacts the workpiece, which results in less heat production. Thus, more penetration depth is necessary to balance off the heat generation and decreased contact area. The typical tilt angle ranges from 0° to 3°. The contact pressure between the leading edge

and the shoulder is also impacted by tilt angle. Even at larger tool rotational to traversal speed ratios, low tilt angle causes the creation of voids.

1.7.3 Other process parameters

These variables are those that are used in the production of metal foam and have a significant impact on the quality of generated foam.

1.7.3.1 Blowing agents

The foaming agents have also a significant impact on the qualities of the metal foam that will be manufactured. In order to create high-quality metal foam using the powder metallurgy process, the appropriate blowing agent must be used. The composition and purity of the gas or foaming agent; the particle surface interactions; the composition of the matrix alloy; and the thermal processing conditions are the main factors that affect the quality of foams. The two different types of foaming agents (hydrides and carbonates) are used in metal foam manufacturing as given below:

Hydrides as blowing agent: When heated to its decomposition temperature, this foaming agent must be able to produce the desired amount and size of gas bubbles which creates pores in metal matrix. It is challenging to estimate the temperature at which the hydride begins to emit hydrogen. The temperature range at which hydrides decompose is substantially influenced by a number of variables, including hydride particle size, the degree of initial surface oxidation, the environment in which they are heated, and the pace of heating. TiH_2, ZrH_2, and MgH_2 are a few hydrides that have been employed as foaming agents. A very little amounts of metal hydride contain enough hydrogen gas to produce a significant amount of porosity [33].

Carbonates as blowing agents: As foaming agents, carbonates can effectively replace hydrides. $CaCO_3$ and $MgCO_3$ are better blowing agents for creating magnesium foam because Mg has the ability to absorb hydrogen. When employing carbonates to create foam, there is a noticeable shrinkage that is hidden when using hydrides.

1.8 Precursor Heat Treatment Technique

The stability of the foam is determined by the time and temperature used to heat the precursor in some particular heating technique, which results in proper sphericity and pore size. In this procedure, the precursor samples are heated by different heating techniques like direct torch flame heating, direct friction tool heating, furnace heating, and microwave heating and so on. According to the necessary metal foam shape and qualities, the time and temperature parameters need to be optimized [34, 35].

These factors have a significant impact on the types of intermetallic produced and the stability of the pores inside the matrix. If these parameters are not adjusted, drainage of the metal, thin or broken cell walls, large cell sizes, fluidity of the base metal, and development of undesired intermetallics can all result in brittleness in the foam, reducing its mechanical and morphological properties. Several studies have attempted to refine the parameters and explain how they affected the final metal foam [36].

1.9 Thesis Organization

Chapter 1 introduces metal foams briefly and shows the various characteristics of this unique material. This chapter gives a comprehensive overview of the background, categorization, and

prospective applications of these materials. The many methods of producing metal foam are also covered in the end of this chapter.

Chapter 2 provides a summary of the most recent findings from the research of Aluminium foams. To determine the present state of research in the topic, a thorough literature review has been conducted. The manufacturing of metal foam, its characterization, and its applications have been divided into three categories in the literature that is currently available.

Chapter 3 explains the detailed design and production process used to manufacture Aluminium foams. It contains information on the design and construction of the machinery used to manufacture Aluminium foam, as well as a study of the raw materials utilized in the foaming process.

Chapter 4 reports of the experiments done to evaluate the mechanical and metallurgical characteristics of the created material, together with their results. For the purpose of analyzing the parametric combinations to manufacture Aluminium foam of high quality, a thorough methodology built on the Taguchi technique has been adopted and applied. The study comprises characterizations of the precursor based on its macro- and microstructure, temperature generation throughout the process, and hardness data. Aluminum foam's compressive property, including pleateau stress, is discussed. This chapter also reports on the porosity and pore size of the developed foam under various heating conditions, as well as under various filling techniques and tool pin profiles.

Chapter 5 The chapter highlights the constraints of the friction stir processing (FSP) for foam development and gives an overview of new technique named as friction stir deposition (FSD). In

this technique, the optimum parameters obtained from the previous work (chapter 4) are used for further characterization and optimum use of work material.

Chapter 6 presents the conclusions drawn after the complete study of foam manufacturing. The chapter also list out some furture scope in the domain area for further exploration by the next researchers.

All researchers and scientists involved in this field are expected to find the study given in this thesis to be extremely helpful in understanding the production and characterization of Aluminium foam.

Chapter 2: Literature Review

As discussed in the introduction chapter that the metal foam is used in various fields due to its unique properties. The numbers of processes are used for the manufacturing of metal foam. The techniques that work in liquid state are more dangerous and also time consuming but the techniques that work in solid state are more famous now days because this process works in solid state condition. Compared to the other technologies, liquid metallurgy is significantly less expensive, but it produces structures that are more uneven. So, extensive literature survey has been carried out to find the current status of solid state process for the development of metal foam.

2.1 Historical Development

Due to their distinctive features, naturally occurring cellular materials including pumice stone, wood, cork, bone, etc. have inspired researchers to create manmade cellular materials [37]. For the purpose of creating high-quality foams, research on foam production techniques began in the 1920s and continues today [38]. Foams can be made in a variety of ways, including using liquid metal, solid metal powder, metal ions, and metals in the vapour or gaseous phase. The most extensively discussed techniques under this categorization are those for producing foams from solid metal powder and liquid metal. The development of metal foam is depicted in Table 2.1.

Table 2.1: Historical development

Sr. No.	Author and Year	Foam Development
1	Benjamin [39]	The first attempt used mercury vapours to create Aluminium metal foam.

2	Elliott [40]	For the U.S. Navy, Bjorksten Research Laboratories (BRL) developed a technique for foaming Aluminium.
3	Fiedler et al. [41]	Suggested an alternative way to make metal foam using an alloy and ground metal hydride (titanium and zirconium hydride).
4	Erb [42]	Developed a technique for moulding foam metal products by progressive localised crushing.
5	Berry et al. [43]	Melting the dross and adding it basically created cellular structured metal foam.
6	Niebylski [44]	Through a US Patent, the production of high-quality lead-zinc foams was disclosed.
7	Niebylski [45]	Increased the efficiency of a method for making fiber-reinforced metal foam.
8	Kendall [46]	Described the fabrication of copper foams with outstanding potential for vacuum applications.
9	Davies et al. [47]	Studied the several techniques used to manufacture metallic foams, such as casting, powder metallurgy, and metallic deposition.
10	Cocks [48]	Invented hyper-ballistic protective materials to manufacture metal foams
11	Miyoshi et al. [19]	Developed the Alporas technique, which used a batch casting method to successfully fabricate foamed Aluminium.
12	Jin et al. [49]	Presented a technique for creating metal foam in which gaseous bubbles were kept inside a mass of molten metal while the foam

		was being manufactured.
13	Chen et al. [50]	Used the holographic interferometry technique to report the elastic characteristics of the copper foam.
14	Clancy et al. [51]	Devised a method for creating low-density metallic foam hollow spheres.
15	Knott et al. [52]	Metal foams are manufactured using the die-casting method.
16	Dobesberger et al. [53]	Developed a method to produce free-flowing metal foam with certain physical properties.
17	Dunand et al. [54]	Used the sintering method to create metal foam.
18	Hangai et al. [55]	Creating foamed metal precursors using friction stir processing
19	Campagna et al. [30]	The condenser fins on the heat exchanger are made of metal foam.
20	Jung et al. [56]	A nano crystalline nickel coating using an electro-deposition method is applied before coating open-cell Aluminium foams.
21	Banhart et al. [57]	Developed a procedure for producing metal foam using powder metallurgy that contains a metal and a metal alloy.
22	Cochran et al. [26]	Outlined the casting and powder metallurgy processes used to create syntactic foam.
23	Babcsan et al. [58]	The size of the bubble may be customized using a novel manufacturing technique to create metal foam, which is formed

		by oscillations caused by longitudinal waves inside the bubble.
24	Reesink et al. [59]	Discovered a technique for creating the heat exchanger's opencell porous-shaped body.
25	Noraas et al.	Employed a solid mould process with dual investments to create reticulated metal foam.
26	Wood et al. [60]	Carbon foam and metal foams were used to improve acoustic absorption and heat transmission.
27	Aronsson et al. [61]	Hybrid metal foams were created using the electroplating procedure.

In the field of metal foams, researchers like J. Bnahart [15, 62, 63], M. F. Ashby [64], and L. J. Gibson [65] have made major contributions and published a number of reviews and books on the field. Their research explores the design, manufacturing, and mechanical characteristics of metal foams used in a variety of applications. Following is an overview of the literature in the context of the current study on metal foams:

In their "design guide to metal foams," Norman Fleck et al. [64] referred to this category of materials as "met foams." Both a variety of procedures and the elements that influence foam production are provided.

The key categories of melt route, powder route, and precursor route are among the conventional methods for creating metal foam, according to Banhart [66]. Commercial production of the Aluminium metal foams goes under the brand names ALPORAS, ALULITE, and CYMAT. They create closed-cell Aluminium metal foam using the melt-foaming technique.

The procedures used in powder metallurgy to create metal foams have been thoroughly outlined by Kennedy [67]. His work focuses on a number of features of powder metallurgy's ability to create foams that are close to net shape. According to their manufacturing processes, open and closed cell foams are both discussed.

In order to generate metal foam for applications such as heat exchangers and biomedical equipment as shown in Fig. 2.1, Zhao et al. [5] studied the mechanism of pore development and compared several procedures, including powder metallurgy and additive manufacturing. They came to the conclusion that while there has been significant progress in the production of porous materials, there are still problems with achieving uniform pores and managing the foaming process.

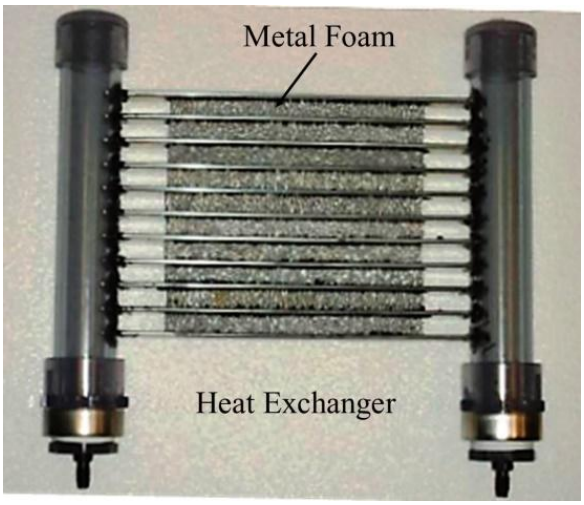

Fig. 2.1: Metal foam heat exchanger

The powder metallurgy technique of metal foam creation was created in 1995 by Banhart et al. [68]. By sintering the Aluminium and blowing agent powders and then heating it at a certain temperature to cause the decomposition of the blowing agent powder, they were able to create Aluminium metal foam with a porosity of around 90%.

The impact of alloy composition on the foaming behaviour of Aluminium alloys generated by powder processing was examined by Moreno et al. [69]. They stated that the particular metal composition had a major impact on the foaming behaviour. Consequently, the AlSi8Mg4 base alloy's composition was changed by slightly changing the Mg and Si contents. With an increase in Si concentration and a reduction in Mg content, they noticed greater expansions. The ideal magnesium concentration, however, was said to be 4%.

Using a melt injection approach, Pamidi et al. [70] developed aluminum metal foam with a porosity of 80%. They created the foam both with and without the stabilizing TiB_2 particles. According to the research, foams containing TiB_2 had smaller, more uniform pores and demonstrated higher stability and strength.

The stability of several Aluminium alloy foams stabilized by particles and produced using the gas injection method was described and compared by Heim et al. [71]. They discovered that microscopic particles, like TiB_2, could create pores that were more stable and smaller if they were distributed uniformly.

By heating the precursor to about 520°C before foaming, Fan Deng et al. [72] attempted to increase the stability of Al-7Si-4Cu foam produced using the powder processing route. Outcomes improved as a result of heat treatment-induced high temperature oxidation.

A new approach for fabricating Aluminium foam that uses in-situ TiC-TiB_2 reinforcement during the melt processing route was proposed by Xuguang An et al. By using this reinforcing method, it was shown that the compressive and energy absorption properties greatly improved when compared to the pure Aluminium foam. Because of the homogeneous loading during compression, the stress-strain curve of this foam seems to be more uniform.

The current state of closed cell Aluminium foams as of the year 2008 has been examined by Lefebvre et al [7]. They have gathered a lot of information regarding the large-scale production of Aluminium foams up till 2008.

When Aluminium metal foam is formed via the melt processing approach, Kadoi et al. [73] have examined the decomposition behavior of TiH_2 and its heat treatment behavior. This study discovered that the decomposition of TiH_2 powder happens in two stages, the first of which takes place between 460 and 490°C and the second of which occurs above this temperature. The heat treated TiH_2 was found to be more effective when used in the casting process.

A study by Shadi Mehjoob et al. [74] focused on "the synthesis of fluid and thermal transport models for metal foam heat exchangers." They explain how the performance of the heat exchanger is affected by the micro structural metal foam parameters of porosity, pore and fibre diameters, pore density, and relative density.

By using the sintering and dissolution processes, K L A Khan et al. [75] focused on the synthesis and characterization of Al foam. They discovered that adding an alloying element and silicon carbide increased the compressive strength at the same relative density.

The impact of Al_2O_3 particle addition on the structure, hardening capacity, and mechanical characteristics of closed cell PCM 6061 foams was studied by Mahmutyazicioglu et al. [76]. This study shows that closed cell Aluminium foams include Al_2O_3 particles in their cell walls. It is also elaborately discussed how Al_2O_3 particles form a mechanical barrier between two gaseous pores to prevent them from coalescing with one another.

The methods for producing metal foam in the above mentioned literature include gas injection, melt processing, powder metallurgy, etc. But in 2010, Hangai et al. patented a novel technique for creating Aluminium metal foam that used friction stir processing (FSP) as the initial procedure for precursor generation. In their patent 2014 [77], they also described this technique for producing functionally graded materials.

2.2 Friction Stir Processing (FSP) Technique

The processing method known as friction stir processing (FSP) was invented by Mishra et al. [20] and this technology uses the fundamentals of friction stir welding (FSW). By rotating the tool into the base metal with a pin and shoulder, FSP is frequently used to generate heat for friction and excessive plastics deformation [78]. While FSW is typically employed as a joining technique, FSP has made a significant contribution to the field of surface composites by improving the surface characteristics of materials [28, 79-81]. FSP may create metal matrix composites by uniformly combining a reinforcing powder with the base metal serving as the matrix [82, 83]. Many aspects have been shown to affect the uniform distribution of reinforcements and their impact on attributes in recent studies [79], [84]. Moreover, effective surface composites and in-situ bulk composites produced using FSP have been reported in a number of studies. The following list includes some of the major work that is essential to the current study:

Using FSP, Daneshifar et al. [85] produced the in situ Al-Si/Mg2Si composite. In Al-Si matrix Mg was embedded using a grooving method. Four FSP passes were made while the FSP was running at 2500 rpm and 8 mm/s. The homogeneous distribution of Mg2Si particles in the matrix as shown in Fig. 2.2 and a little improvement in hardness were demonstrated.

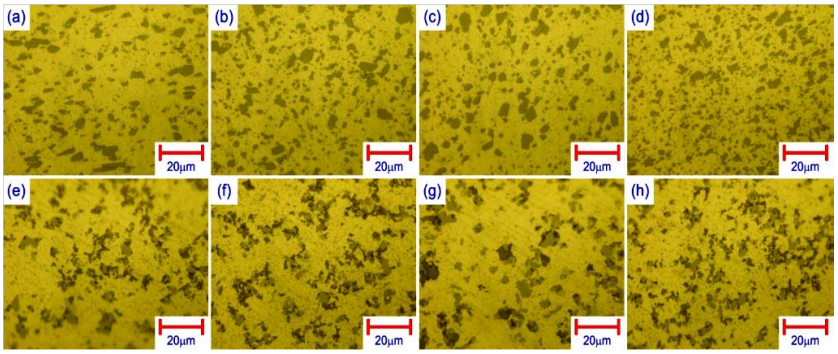

Fig. 2.2: Optical micrographs showing the microstructure of the SZ at (a) top, (b) center, (c) leading edge, (d) trailing edge of the neat sample, and (e) top, (f) center, (g) leading edge, (h) trailing edge of the composite sample [85].

Through FSP, Rohit Shandley et al. [86] described numerous methods for attaining uniform reinforcing agent distribution in the metal matrix. The stirring action, or tool passes was the FSP characteristics that had the biggest impact on the distribution. The dispersion of the particles in the AA5083 matrix became more regular as the number of passes increased, however at lower passes, SiC particle agglomerates were observed. Fig. 2.3 shows the distribution micrographs that were acquired in various situations.

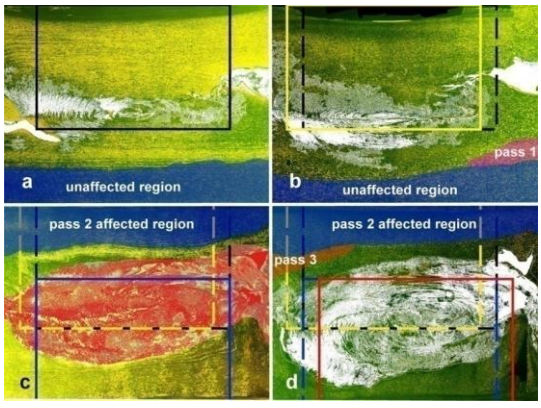

Fig. 2.3: The mixing of the foaming agent and the affected areas after (a) pass 1, (b) pass 2, (c) pass 3 and (d) pass 4.

The optimization of process parameters for producing metal particle reinforced 5083 Al composite by FSP was recently reported by Bauri et al [87]. To achieve a defect-free stir zone and a uniform distribution of particles, a wide range of parameters including tool rotation speeds from 1000rpm to 1800rpm and a range of traverse speeds from 6mm/min into 24mm/min were investigated. From these studies, the ideal rotation and traversal speed was discovered.

The mechanical characteristics of a fine-grained Aluminium alloy generated by the friction stir technique were studied by Kwon et al [88]. They discovered that when tool rotation speed was reduced, the hardness and tensile strength of the friction stir-processed 1050 Aluminium alloy considerably enhanced.

The Carbon Nano tube (CNT)/aluminum composites were made by Z. Y. Liu et al. [89] using powder metallurgy and subsequent friction stir processing (FSP). The CNTs were found to be uniformly distributed in the composites, according to micro structural investigations. The yield strength of 1 weight percent and 3 weight percent CNT/A composites improved by 23.9% and 45.0%, respectively, above that of unreinforced Aluminium.

The influence of the shoulder diameter to pin diameter (D/d) ratio was examined by P. Vijayavel et al. [90] who discovered that a ratio of 3 was optimal for the study as shown in Fig. 2.4. The strength and ductility of the LM25AA-5% SiCp metal matrix composites made via FSP were based primarily on this ratio. It was decided to use a tool with a 1000 rpm rotation speed and a 40 mm per minute traverse speed.

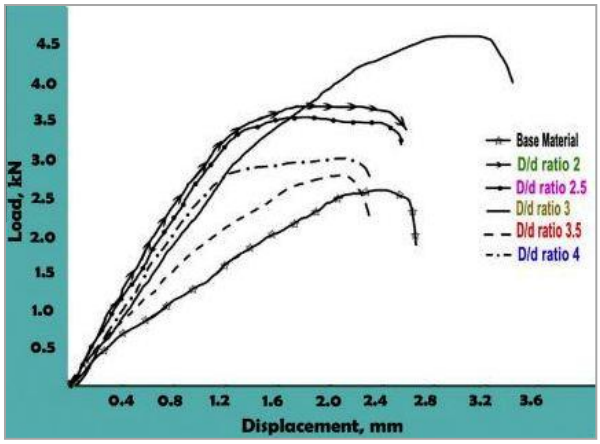

Fig. 2.4: Load displacement curve

For the first time, M.N. Avettand et al. [91] demonstrated the FSP's capacity to combine yttria particles with copper to create an oxide dispersion strengthened material.

The in-situ composite production of Aluminium alloys via FSP was reviewed by N. Gangil et al [92]. They discussed the current state of Aluminium metal matrix composites and the various manufacturing methods.

In their overview of FSP research in 2019, Kan Li et al. [93] went into considerable detail on the process's general functioning and how it might be used to create composite materials.

2.3 Development of Metal Foam by FSP

The production of metal foam has employed this FSP application. A foamable precursor can be created quickly using the FSP process [94]. Yokoshiko Hangaii et al. [26] successfully developed a novel foaming technique which works on the FSP for precursor development. Using FSP, the blowing agent powder is mixed with the metal matrix to create the pores, which decomposes and releases gas when heated in a furnace at a given temperature and for a specific

period of time. They said that their technique for creating metal foam offers a few benefits. The rolled Aluminium plates were utilized in place of expensive Aluminium powder or Aluminium melts. This technique consuming less energy, it also makes way for green technologies. It takes less time since; following precursor creation, heating only takes a few minutes.

Hangaii et al [95] porous 4045 Al alloy was created utilizing expensive Al plates. Through eight passes of FSP, 12 minutes of holding time, and a holding temperature of 923 K, 50% porosity was achieved as shown in Fig. 2.5. The findings demonstrate the significant potential of FSP technology for producing porous Aluminium at cheap cost and with a greater consideration for the environment.

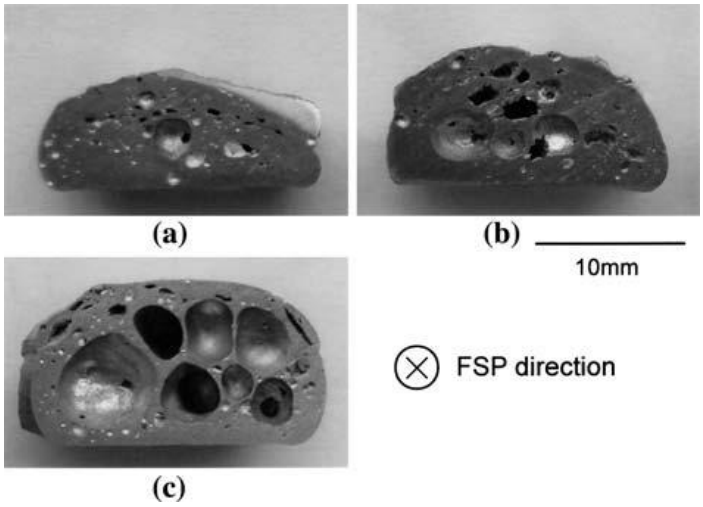

Fig. 2.5: Morphology of the pores of porous aluminum produced at a holding temperature of 923 K and 12 min holding time: (a) two-pass FSP, p = 16.3 pct; (b) four-pass FSP, p = 31.0 pct; and (c) eight pass FSP, p = 46.4 pct [95].

The influence of additional alumina and holding time on the production of porous Aluminium using FSP was studied by Utsunomia et al. [96]. It has been demonstrated that porous Aluminium with a porosity of up to 80% produced by carefully controlling the amount of

alumina supplied and the holding time. The Fig. 2.6, shows the developed foam sample at different holding time intervals.

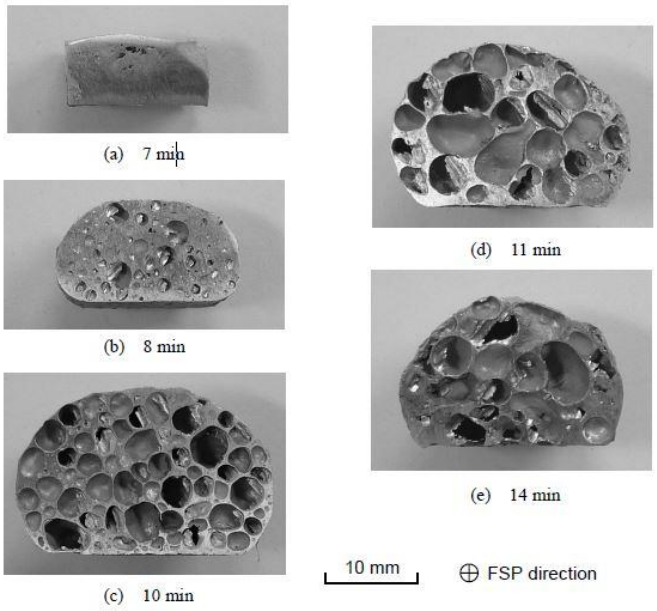

Fig. 2.6: Change in pore structure with holding time [96]

The effectiveness of the former was discovered by Hangai et al. [97] while development of Al alloy metal foam without the use of a blowing agent and compared its tensile qualities and fracture behaviour with commercially available ALPORAS.

Friction stir processing was employed by Pang et al. [98] to integrate the CNT+TiH_2 combination into the Aluminium matrix. The precursors were heated to form a porous structure with up to 46.3% of porosity and a peak stress of 8.5–11.1 Mpa is obtained.

The impact of tool rotation rate on the foaming characteristics of porous Aluminium created by FSP was discussed by Hangaii et al. [99]. The impact was examined in A1050, and it was found that the quantity of stirring action (tool rotation rate and number of FSP passes) is the only factor

that affects the porosity of Aluminium. The maximum porosity was achieved with a holding temperature of 998 K and a holding period of 10 min.

Compression testing was carried out on the FG Aluminium foams made by Hangaii et al. [100] using the three combinations of 1.0-0 mass%, 0.4-0 mass%, and 0.2-0 mass% TiH_2. They concluded that there were three plateau zones visible on the compression curves of this type of material, one for each density that existed along its length.

A1050-A6061 Functionally Graded Aluminum Foam was manufactured by the friction stir processing route by Hangai et al. [101]. The seamless FG Aluminium foam may be manufactured using the FSP technique; it was demonstrated by the point analysis results that the Mg content progressively changed in the bonding area.

The localised metal foam was manufactured by Papantoniou et al. [102] using the FSP approach to include a combination of TiH_2 and MWCNT to create a precursor. The powder was inserted into the metal matrix using the grooving procedure. The level of porosity was around 54% as shown in Fig. 2.7.

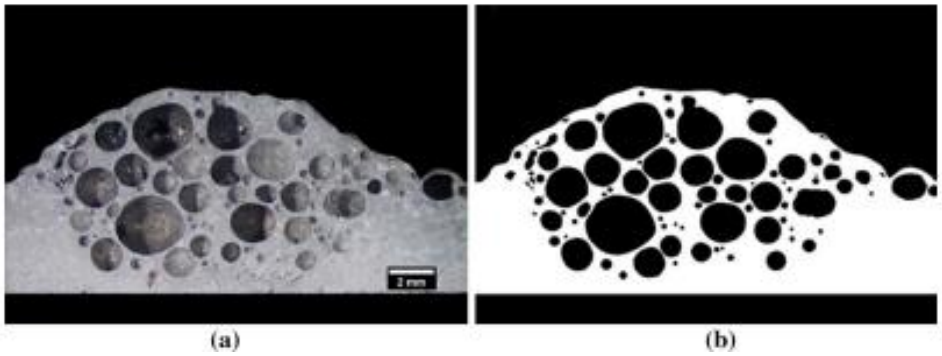

Fig. 2.7: (a) Macrograph of cross section of the final foam (cross section perpendicularly to FSP direction) and (b) binary image of the porous structure (obtained by ImageJ) [102].

Aluminum 1050 and ADC12 alloy foam-filled tubes were manufactured by Hangai et al. [103] using the FSP technique. In two different trials, by spinning the tool over the precursor-filled tube, the ADC12 precursor was attached to the inner surface of the A1050 and steel tube. The interior of this joined tube was made foamy by further heat treatment. The fabrication of the foam-filled tubes therefore proven to be a successful technique.

2.4 Development of Precursors by FSP

For the fabrication of precursors, which refers to the technique of pre-placing the foaming agent over the metal matrix before FSP, many strategies are used. To achieve the defect-free precursor, proper selection of the foaming agent strategy must be made in addition to the previously mentioned process parameters. Numerous studies looked at various filling strategies for blowing agents after the development of FSP as a method for manufacturing of metal foam.

The introduction of these new techniques was mostly done to stop the waste of particles sputtered throughout the operation. Various powder techniques for placing blowing and stabilizing agents on the substrate before conducting FSP have been reported in the literature. Foaming agents are inserted into metal matrix via different-shaped like holes, grooves, and sandwiches on the substrate [26]. The homogeneous dispersion of foaming particles in the precursor is now widely acknowledged to be a significant and difficult task during FSP.

Here, the numerous filling methods for foaming powder are described along with their features.

Functionally graded aluminum (FG) foam with varying pore structure was fabricated by Yoshihiko Hangai et al. [104] in sandwich style by utilizing friction stir processing. FG foam with a varying pore structure was developed and the compressive properties of the fabricated FG

foam were demonstrated. It was shown in that such FG foams have the potential for their deformation location to be controlled and that two plateau regions with a seamless bonding interface can be obtained. The compressive strength graph of the developed foam samples are shown in Fig. 2.8.

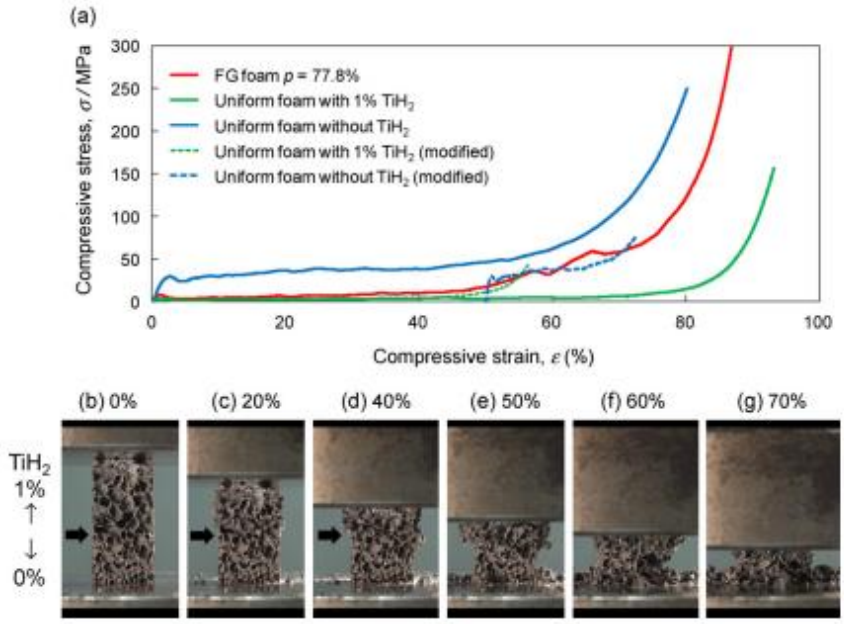

Fig. 2.8: Stress–strain curves and sequential deformation images of FG foam (p = 77.8%) [104].

Yoshihiko Hangai et al. [101] developed functionally graded (FG) Aluminium foam using friction stir processing (FSP) by sandwiching the blowing agent between the plates and employing Aluminium alloys A1050 and A6061. Their results revealed that the Mg content progressively changed in the bonding region and that the FSP approach may be used to produce continuous FG Aluminium foam.

In order to fabricate precursors, Sharaf U. Nisa et al. [105] used the friction stir processing method by sandwiching Aluminium alloy plates with a combination of blowing agent powder and stabilising agent powder. Using FSP, closed-cell Aluminium 6063 metal foam was created.

An estimated 60% porosity was attained with various pore sizes. The SEM image of these pores are shown in Fig. 2.9.

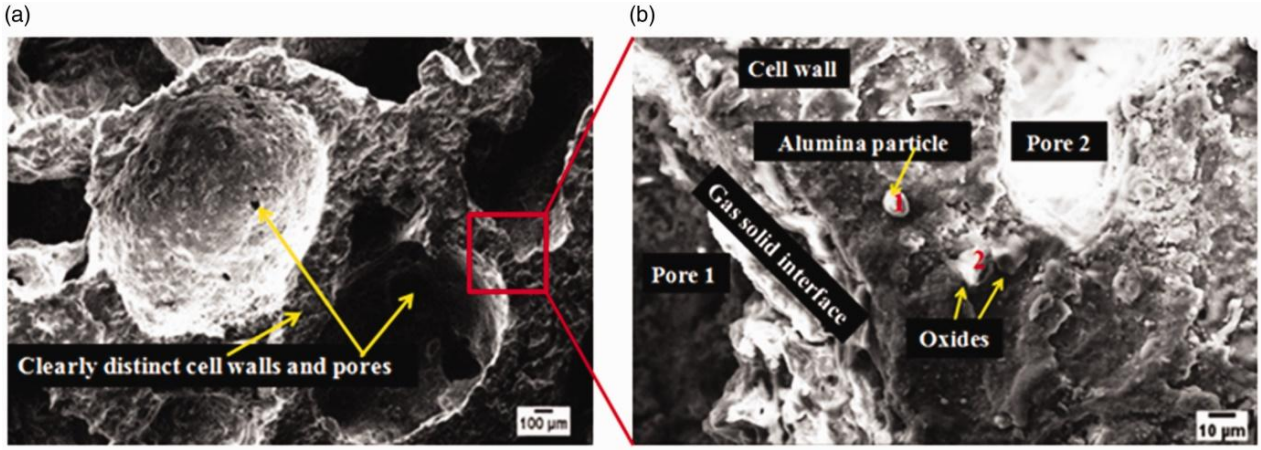

Fig. 2.9: (a) SEM image of the foam and (b) Enlarge view of pores

Closed-cell carbon nanotubes (CNTs)-reinforced Aluminium composite foams were effectively manufactured by Q. Pang et al. [98] using a friction stir welding and sandwich approach combination. The precursor to composite foam develops at 680 °C for 15 minutes with sufficient expansion and extremely spherical pores. Peak stresses of CNTs/Al composite foams were 3–4 times greater than those of pure Al foam, ranging from 8.5–10.3 MPa at a strain rate of 0.01 mm/s.

The precursor was fabricated by Takao Utsunomiya et al. [106] by utilizing a sandwich powder filling technique and the intense stirring action of FSP to mix a blowing agent powder and a stabilizing agent powder into an Aluminium alloy matrix. On the porosity and pore structure of A6061 porous Aluminium, the effects of the tool rotation rate and the number of passes were examined. They concluded from the results as shown in Fig. 2.10, that the tool should rotate at a

rate of between 1000 to 2200 rpm in order to produce porous Aluminium with high porosity and excellent quality.

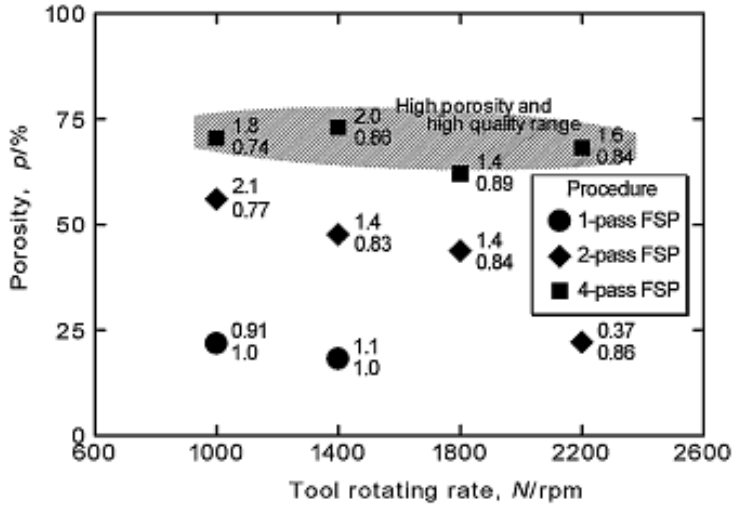

Fig. 2.10: Relationship between tool rotating rate and porosity [106]

Papantoniou et al. [107] used the groove technique and FSP procedure to manufacture the A5083 Al-Mg alloy foam. According to the results, a porosity of 60% and an equivalent pore diameter ranging from 0.2 to 3.3 mm can be attained after the foaming procedure.

By inserting foaming agents into grooves, M. Azizieh et al. [108] manufactured foams made of magnesium-based nanocomposite materials using friction stir processing (FSP). On the pore distribution and porosity, the effects of the number of FSP passes, TiH_2 to Al_2O_3 weight ratio, and foaming temperature were discussed. The outcomes indicate that for the optimal pore distribution and porosity, a minimum TiH_2 to Al_2O_3 weight ratio was required.

Mustufa Haider Abidi et al. [109] developed a precursor with $MgCO_3$ powder serving as the blowing agent via friction stir processing. By using a groove method, this blowing agent is blended into the plate. On the size and porosity of the foam produced, the simultaneous effects of

tool rotation speed, traverse speed, and shoulder diameter were examined. An average pore size of 10.5 m was used to achieve the greatest porosity of 16.67%. The highest pore size, 17.8 m, was found to be connected to 14.40% porosity.

Azizieh et al. [110] developed the Aluminium alloy A1100 foam. Before FSP, there was a groove in the Aluminium sheet that had the proper width and depth for the TiH_2 and Al_2O_3 powders to be fed into. Successful fabrication of Aluminium foam with up to 40% porosity was achieved. They discovered that samples generated with more FSP passes had lower foaming times gives the more uniform pore structures. The combine effect of all process parameters on porosity is shown in Fig. 2.11.

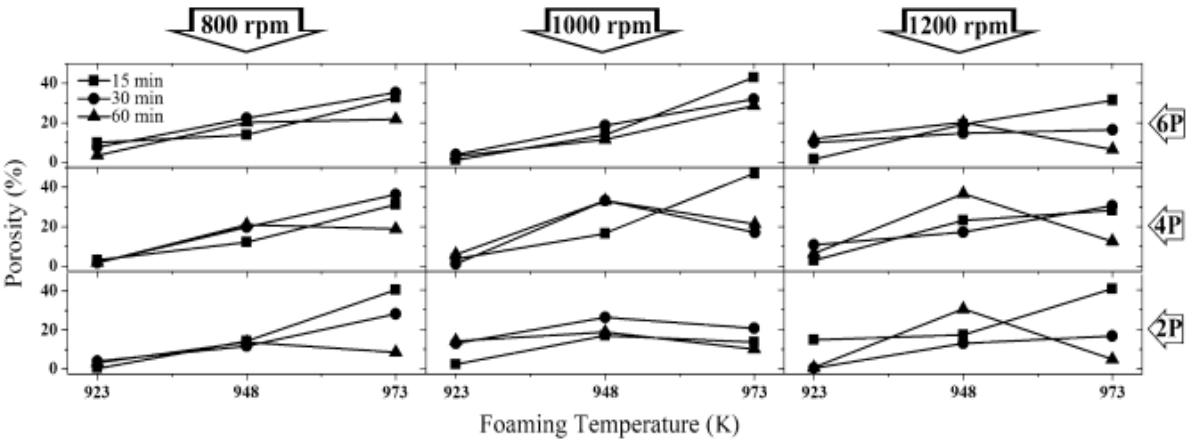

Fig. 2.11: Effect of different process parameters on the porosity [110]

Multi-pass FSP was used to create the Aluminium foam precursor, which contained magnesium carbonate as the foaming agent. By using a sandwich-based slot technique, Rohit Shandley et al. [86] filled slots between two Al 5754 plates with foaming agent. Foam with a porosity of 54% was successfully developed.

By mixing TiH_2 and pure Aluminium powder into the plate with the use of a drilled hole approach, Sachin Rathore et al. [111] manufactured the Aluminium-yttrium oxide (Al-Y_2O_3) MMC foam using the FSP process. The pores are uniformly distributed throughout the Aluminium matrix and are consistent in size. When more titanium hydride (TiH_2) is incorporated into the metal matrix as shown in Fig. 2.12, the foam's compressive strength starts declines.

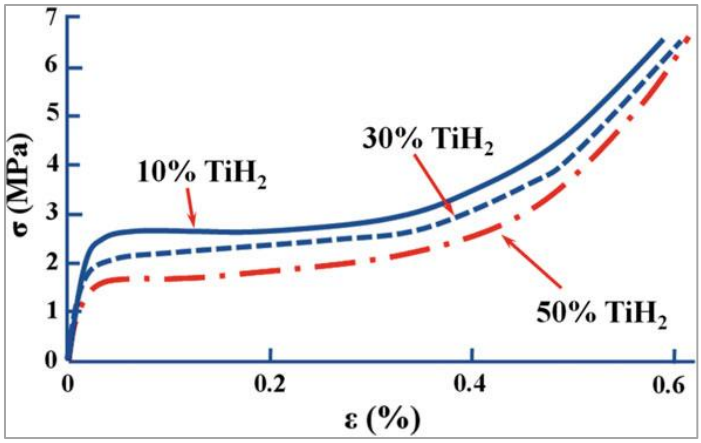

Fig. 2.12: Effect of foaming agent wt. % on compressive strength of foam [111]

Yamamura et al. [112] fabricated tungsten carbide (WC) particulate and silicon carbide (SiC) whisker reinforced Aluminium alloy plate for local reinforcement of 6061Al by utilizing a guide hole method on the top surface of the plate and FSP technique. Local titanium hydride (TiH_2)-containing Aluminium composites are another product that FSP can manufacture. These results, which show that local metallic foam production via FSP is feasible, are explored in terms of microstructure and mechanical attributes.

By drilling holes in the lower plate, Lim et al. [113] developed composites of AA7075 and multi-walled carbon nanotubes using AA6111 plate of 1.1 mm thickness as the cover plate. Friction stir processing was used to examine the effects of processing parameters on particle dispersion

and hardness in an Aluminium alloy reinforced with multiwalled carbon nanotubes. The dispersion of nanotubes in the Al-alloy matrix was found to be enhanced by increasing the tool rotation speed from 1500 to 2500 rpm and the tool shoulder penetration depth.

The composite material of A356 with SiC particles was successfully created by Choi et al. [114] utilizing FSP, and Aluminium tape was utilized in place of thin or thick sheet to cover the drilled hole prior to processing.

Silicon carbide particles reinforced AA5083 alloy surface composite was fabricated using different friction stir processing strategies by Vipin sharma et al. [83] Prior to FSP, covered the grilled hole opening with a 2 mm thick Aluminium (Al) plate and discovered that it was a great idea to prevent the loss of reinforcement particles.

2.5 Mechanical Characterization of the Metal Foam

Understanding a material's mechanical behaviour is essential before using it in a particular application. Numerous studies have examined the closed-cell Aluminium metal foam's mechanical behavior [36, 115-117]. Nickel [118] and Titanium foams [119] have also been studied in addition to Aluminium alloy foams. According to typical studies of foams produced by FSP utilizing dolomite as the blowing agent powder through the precursor approach, it is possible to produce foam with the appropriate mechanical properties [120]. The compressive behaviour of the metal foam created in this way was further studied [117].

2.5.1 Compressive strength property: Particularly for energy absorption applications, the compression property of metal foam is important. Closed cell foams made of Aluminium exhibit the typical compressive stress-strain behaviour under uniaxial compressive loads. Fig. 2.13

depicts the stress-strain curves for metal foams subjected to compression loading. There are typically three zones that make up the compressive stress-strain curve of metal foam: linear elastic deformation, plateau, and densification zone [121-123]. In a region with linear elasticity, cell edge bending or cell face stretching controls foam deformation. Highly localized cell edge buckling, crushing, and ripping causes the collapse region. A plateau stress that is either constant in value or gradually increases with strain defines the collapse region. When the foam's cell walls started to touch one another, which caused the foam to become densifies. The stress in this area suddenly rises and becomes close to the strength of the of the Aluminium metal.

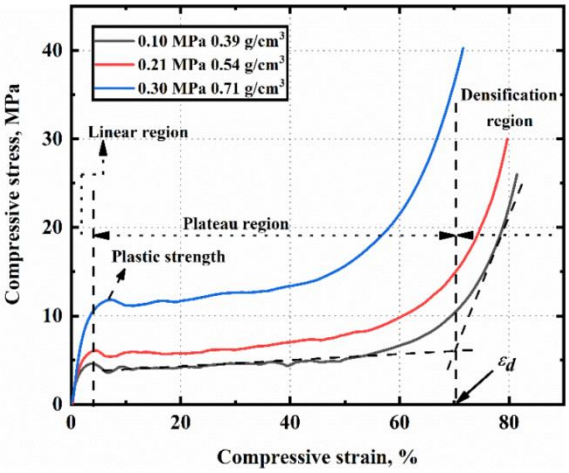

Fig.2.13: Compression stress strain curves of Al-closed cell foam

Since the metal foams are known for their excellent energy absorption capabilities, therefore the plateau region plays a significant role in determining the efficiency of the foam [36]. Usually the energy absorbed up to densification is used to determine the maximum energy absorption capacity of the Aluminium metal foam [4]. This subsequent collapse mechanism is pivotal in determining the energy absorption behavior of particular metal foam. [124].The summary of the

literature review dedicated to the compressive response of closed cell aluminum foam is given in Table 2.2.

Table 2.2: Summary of the literature review dedicated to the compressive response of closed cell aluminum foam

Sr. No.	Title of the Paper	Type of Metal Foam	Compressive Behavior of Foam
1.	Coupling effect of porosity and cell size on the deformation behavior of al alloy foam under quasi-static compression [125].	Closed-cell Al-Cu5-Mn alloy Foam	The foam is ductile because it has porosities under 74%, which makes the curve smoother. Given that their walls are thinner and more easily distorted, foams with large cell sizes are more likely to collapse.
2.	In situ observations of compressive behavior of Aluminium foams by local Tomography using high-resolution X-rays [126].	Al-Zn-Mg foam	The highest fracture nucleation was caused by micro pores with diameters greater than 30μm.
3.	The role of foaming agent and processing route in the mechanical performance of fabricated aluminum foams [127].	Pure Aluminum foam	The processing route was discovered to have a substantial impact on compressive behavior.

4.	Effects of cell wall property on compressive performance of Aluminium foams [128].	A356 Alloy foam	The plateau stress of Aluminium foams shows a linear relationship with the materials' yield strengths for the cell walls.
5.	A novel method for producing Al-foams and evaluation of their compression behavior [117].	Closed cell Al foam	Due to the continual mechanism of hardening, these foams lack a defined plateau zone.
6.	Powder metallurgy route Aluminium foams: a study of the effect of powder morphology compaction pressure, and foaming temperature on the porous structure [34].	Aluminium powder + titanium hydride developed foam	The plateau region is smooth, and the plateau's compressive strength was 5 Mpa.
7.	Effects of alumina (Al_2O_3) addition on the cell structure and mechanical properties of 6061 foams [129].	6061- Al_2O_3 foam	The mechanical characteristics are not considerably altered by the addition of Al_2O_3.
8.	The temperature effect on the compressive behavior of closed-cell aluminum-alloy foams [130].	356 Aluminum alloy foam	With an increase in temperature, the mechanical properties of the start decreasing.

The difference in the morphology and relative densities of the metal foams results in a variety of characteristics. The fluctuation in the characteristics of closed cell metal foams is caused by the

absence of cell walls and morphological wiggles [131]. According to the composition of the cell wall, elastic buckling, yielding, or fracturing causes the cells to start collapsing at nearly constant load during compression [132].

2.5.2 Tensile property: Understanding a material's tensile response is always important for a design engineer. Typical metal foam's tensile behaviour is shown in Fig. 2.14. The ultimate tensile strength (uts), which is known to as the maximum value, is reached after the stress grows extremely quickly with a very slight increase in strain. Up to this point, metal foam hardens; after this point, metal foam fails and stress starts to decrease with an increase in extremely tiny strain [133].

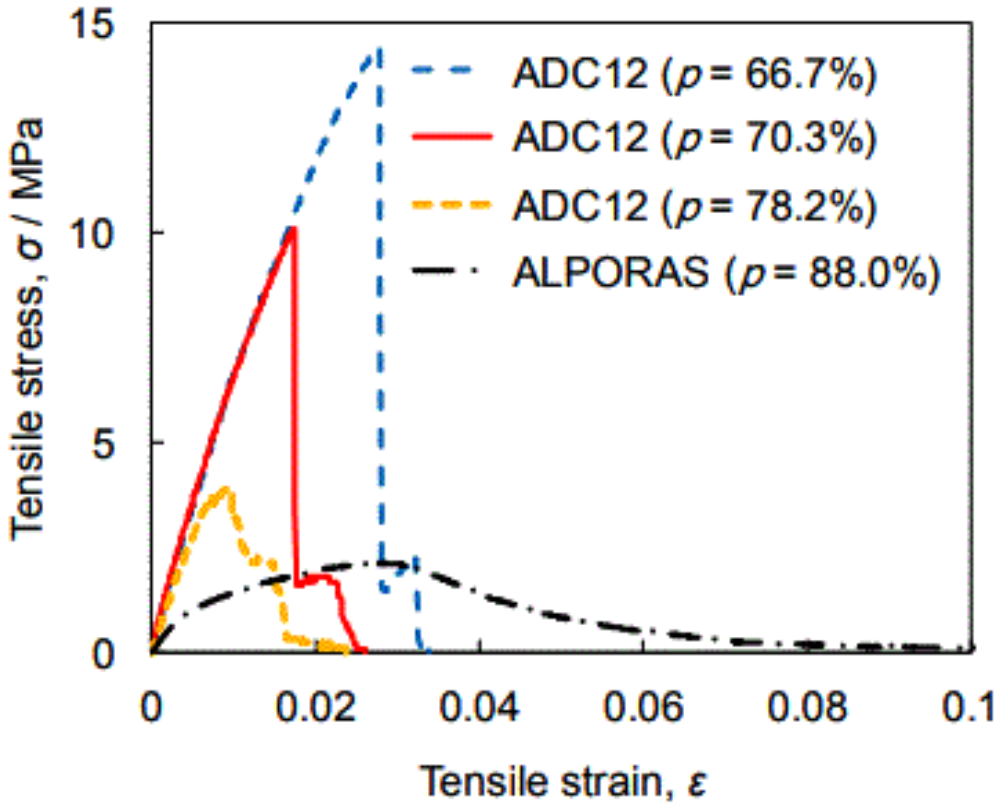

Fig. 2.14: Tensile behaviour of Al-closed cell foam [134]

2.6 Research Gap

1. On the basis of literature survey, it has been found that the FSP is used only in case of sandwich or groove conditions and these processes limit the benefits of FSP.
2. No attempt has been made for maximum utilization of foaming agent during friction stir processing.
3. The heating has been done in furnace which is a time consuming process. Hence an alternate heating method is needed to be explored.
4. The different methodologies/strategies of FSP are not explored for further enhancement of foam quality.

2.7 Research Objectives

The main focus of this research work is to produce low cost, less energy consuming and low density Aluminium foams by new designed powder filling strategy and alternative heating technique. On the basis of research gaps identified through the available literature survey, the proposed research plan was developed and the following research objectives have been established, which are given below:

1. To study the feasibility of development of foam using friction stir processing technique with microwave heating.
2. To investigate the influence of the processing parameters of friction stir processing.
3. To optimize the microwave heating conditions for development of foam.
4. To characterize the developed foam through different Mechanical and Metallurgical techniques.

2.8 Research Methodology

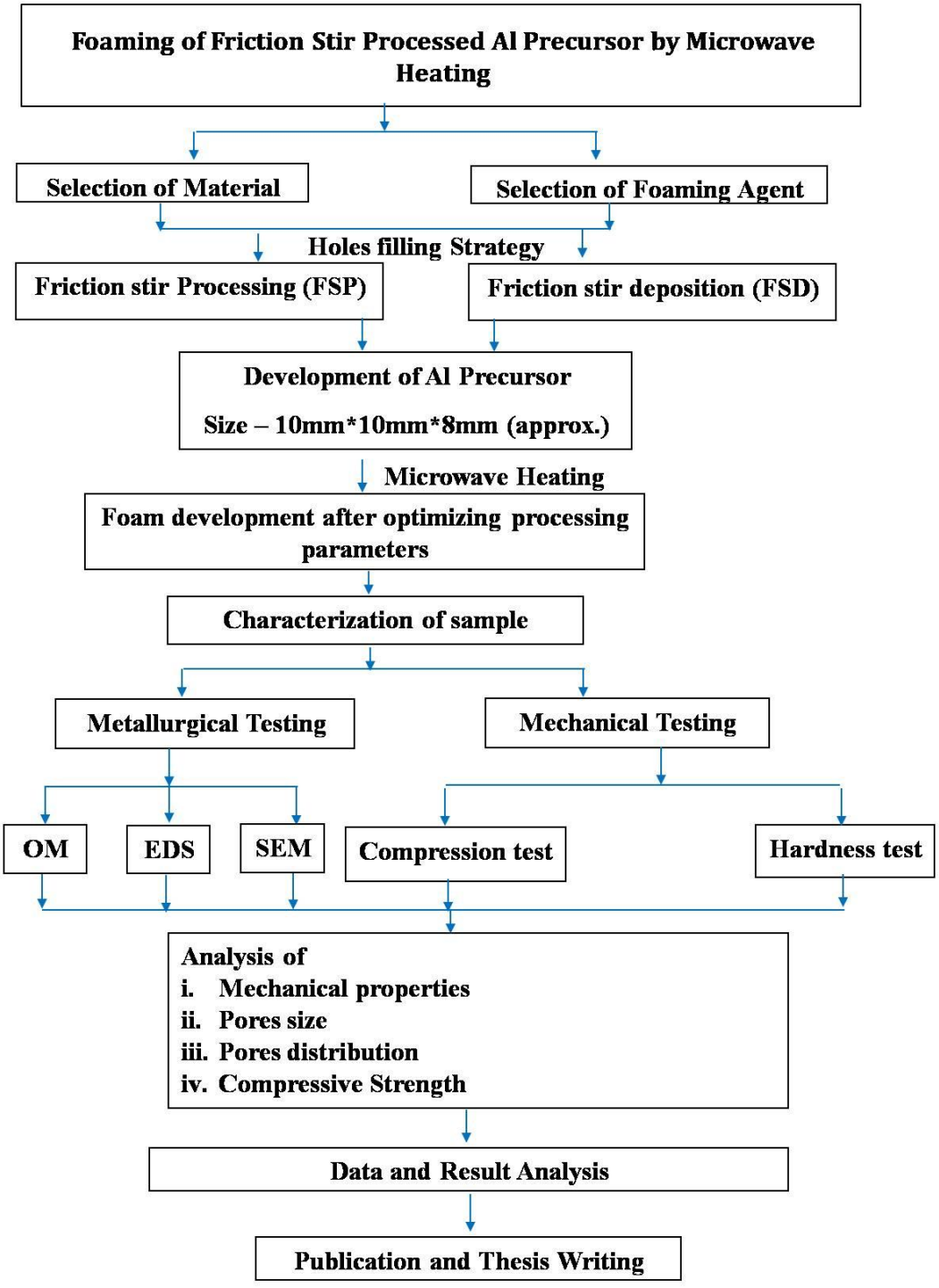

Fig. 2.15: Work plan of research

The methodology has been designed for achieving the objectives of the proposed research proposal, which is as shown in Fig. 2.15. The aim of the research proposal is to develop new technique for developing foam by using the FSP with microwave heating. The experiments will be conducted by using vertical milling machine for application of friction heat and speed for the proper distribution of foaming agent and stabilizing agent. The initial feasibility analysis on Al alloy for developing foam will be carrying out. The optimization of processing parameters like hole size, powder composition, friction stir processing parameters and heating time will be carried out. The macro and micro-structural evolution will be carried out on developed foam to understand the distribution and size of the pores for quality assessment of the developed foam. The relevant techniques will be used for the study of microstructures, which includes scanning electron microscopy (SEM), X-ray diffraction (XRD), energy dispersive spectroscopy (EDS) and optical microscopy. Mechanical characterization will help in understanding fatigue strength, compressive strength and hardness test of developed foam.

Chapter 3: Experimentation

The present research is focused on manufacturing metal foam (indirect foaming) with the help of solid state metallurgical approach. The initial step in the creation of the metal foam in this approach is friction stir processing (FSP) and used to manufacture the precursors. Later, this precursor is heated to develop the Aluminum metal foam. Fig. 3.1 illustrates the key steps of this process.

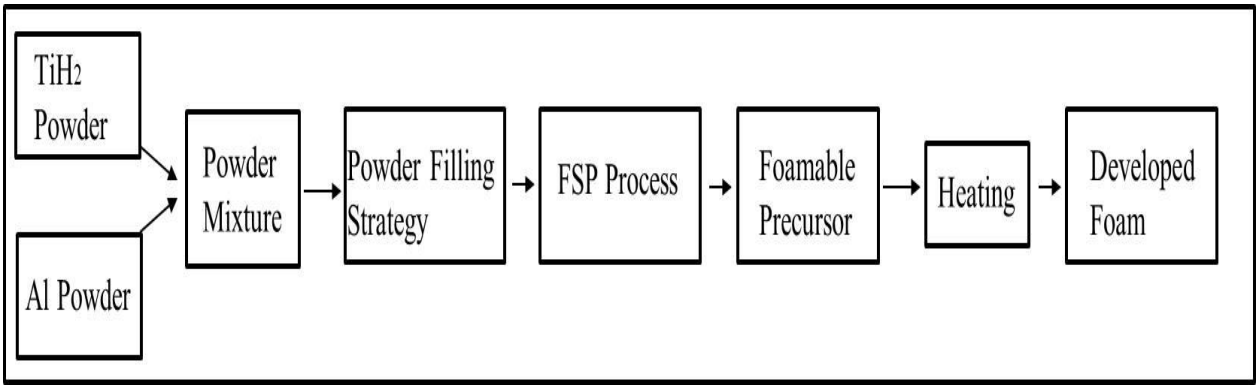

Fig. 3.1: Foam development Procedure

The following sections describe the use of machine, work piece material and tool required for the FSP.

3.1 Selection of Machine, Work Material and Tooling

3.1.1 Work material

In this study AA6063 and AA7075 plates of size 150 × 100 × 10 mm are selected as a base metal (shown in Fig. 3.2). The composition of the base materials is given in Table 3.1 and 3.2, respectively. These Al alloys shows good strength and high corrosion resistance which make it

suitable for the variety of applications including aircraft, automobiles and shipbuilding. Thus, these materials were chosen and explore for their foam development.

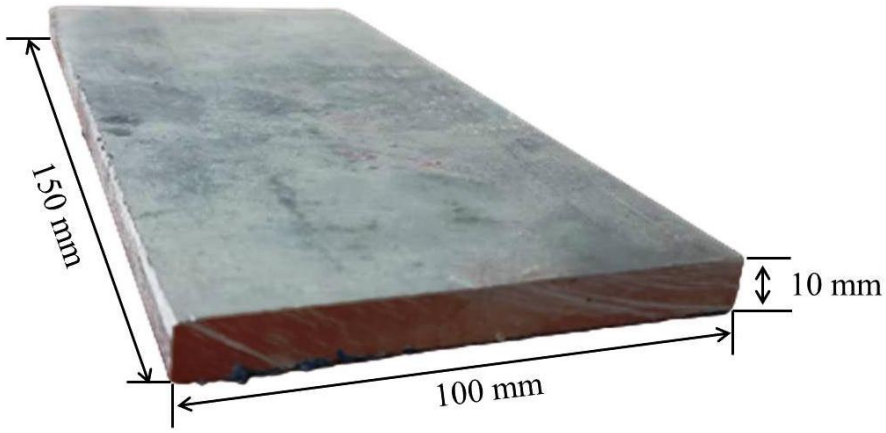

Fig. 3.2: Base plate shape and size

Table 3.1: Aluminum 6063 Composition [53]

Al	Si	Fe	Cu	Mn	Mg	Cr	Zn	Ti	Al
98.41%	0.2%	0.35%	0.10%	0.10%	0.55%	0.10%	0.09%	0.10%	Balance

Table 3.2: Aluminum 7075 composition [53, 135]

Elements	Si	Fe	Cu	Mn	Mg	Cr	Zn	Ti	Al
As per ASTM standard (%)	0.4	0.5	1.2-2	0.3	2.1-2.9	0.18-0.28	5.1-6.1	0.2	Balance
As obtained (%)	0.38	0.45	1.7	0.2	2.5	0.19	5.7	0.2	Balance

3.1.2 Tool material

The tool's hardness, strength, and abrasion resistance must be higher than those of the work piece. High speed steel (HSS), high carbon high chromium steel (HCHR), EN31 steel and H13

are common tool materials [136]. In this study H13 steel is used as the tool material. Table 3.3 provides the typical composition of this steel. As illustrated in Fig. 3.3, the pin profile is 7 mm long and 7 mm in diameter. The shoulder has a consistent diameter of 20 mm throughout the experiment.

Table 3.3: Composition of H13 steel

Element	**Content (%)**
Chromium, Cr	4.75-5.50
Molybdenum, Mo	1.10-1.75
Silicon, Si	0.80-1.20
Vanadium, V	0.80-1.20
Carbon, C	0.32-0.45
Nickel, Ni	0.3
Copper, Cu	0.25
Manganese, Mn	0.20-0.50
Phosphorus, P	0.03
Sulfur, S	0.03
Fe	Balanced

As the thickness of the workpiece is taken as 10 mm, therefore, the length of the tool pin is maintained at 7 mm for the sufficient penetration. The diameter of the tool pin is selected according to powder filling strategy into the base material.

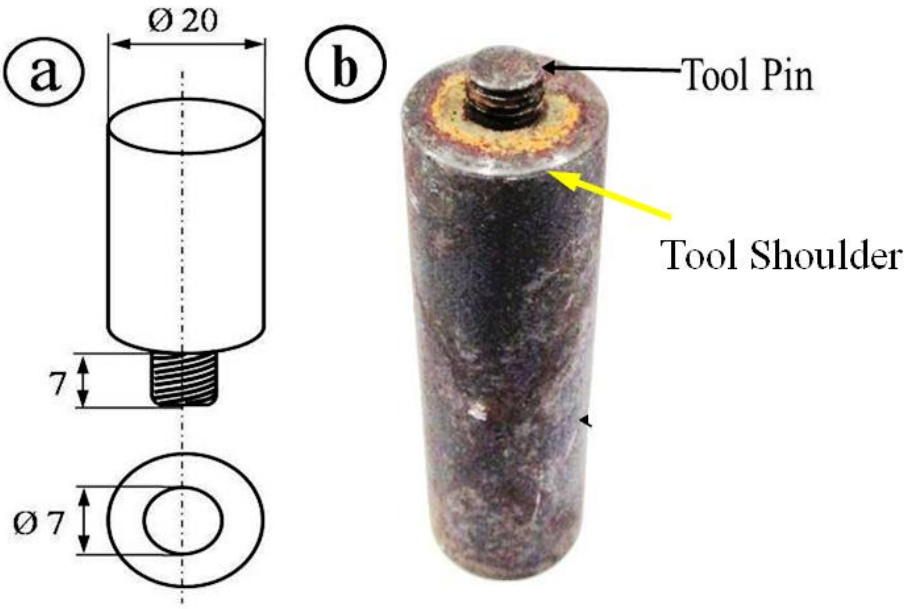

Fig. 3.3: FSP Tool; (a) Schematic diagram and (b) Original Image

The threaded profile pin expected to provide superior material processing owing to downward movement of materials along the probe threads enhances material flow. The straight cylindrical threaded profile pin is therefore chosen for the experimental work.

3.1.3 Foamable mixture

To get the desired level of porosity and also the cell sizes in the Aluminium foam the Titanium Hydrate (TiH_2) of 325 mesh size has been used as a blowing agent. The viscosity enhancers are added to enhance the viscosity of the metal matrix, so that the foaming process will be stable. For this purpose the Aluminium powder of average size of 50 micron with 98% purity and Calcium Carbonate ($CaCO_3$) with 98% purity are used as a stabilizing agent. These powders are shown in Fig. 3.4.

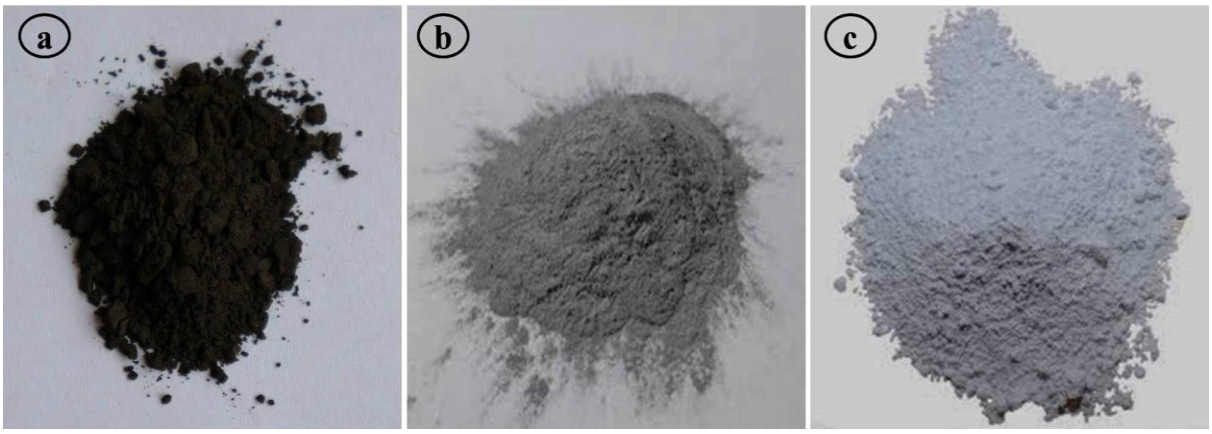

Fig. 3.4: Different powders used in process are; (a) Titanium Hydrate, (b) Aluminium powder and (c) Calcium Carbonate

3.1.4 Machining setup

For conducting the FSP experiments under various conditions, a traditional milling machine (HMT: Model-FN2V) as shown in Fig. 3.5 with a vertical spindle is used to fabricate the precursor. The detailed specifications of the machine are given in Table 3.4.

Table 3.4: Specifications of the machine HMT (Model-FN2V)

Machine Model		**FN2/FN2E (H,U,V)**
Overall dimensions (LxW)	Mm	1520x310
Clamping area (LxW)	Mm	1350x310
Power operated table traverses Longitudinal Cross Vertical	mm mm mm	800 265 400
Max. safe weight on table	Kg	350(H&V), 250(U)
Number of speeds		18
Speed range	Rpm	35.5-1800

Main Motor	kW/rpm	5.5/1500
Feed Motor	kW/rpm	1.5/1500
Space required (LxBxH)	Mm	255x250x207(H) 255x196x197(V) 255x313x201 U)
Packing Case (LxWxH)	Cm	230x195x210
Weight-Net / Gross	Kg	2400 / 3200 (H) 2500 / 3300 (V&U)

The machine table is moved in X, Y and Z directions with the help of lever arrangements. The transverse speed (X axis) is maintained automatically with help control switches. The workpiece is mounted over the worktable with the help fixture. The spindle head is responsible to maintain the different RPM of the FSP tool.

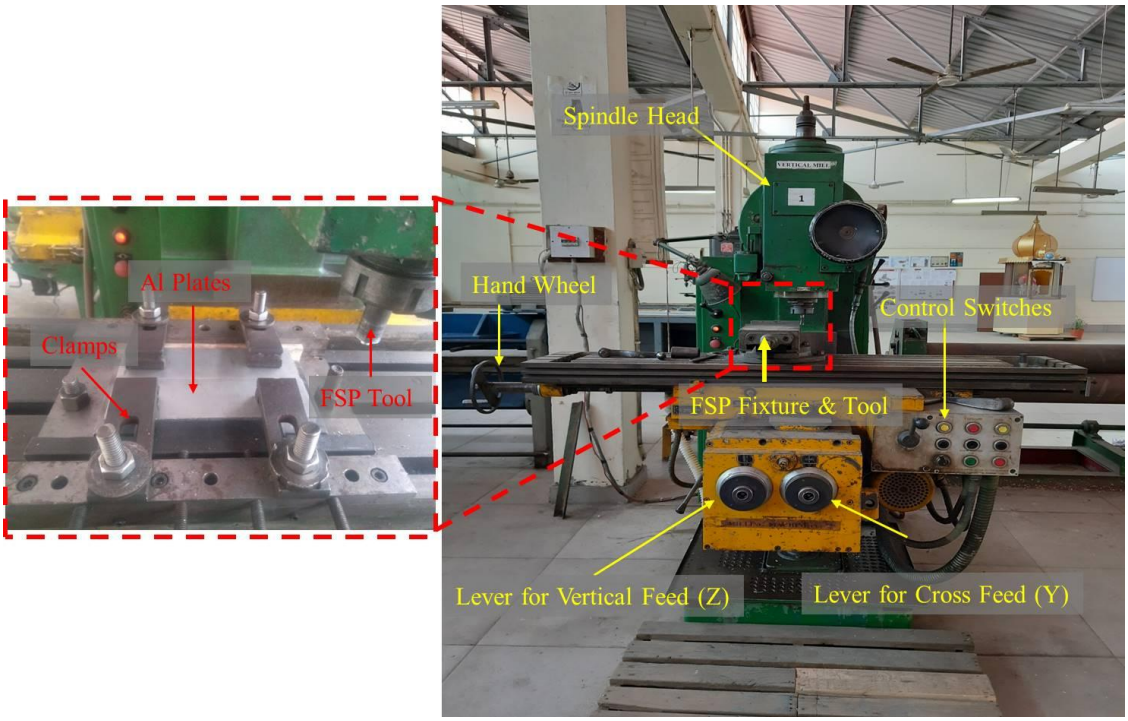

Fig. 3.5: HMT vertical milling machine setup for FSP; Zoomed view of fixture

To improve the quality of the produced Aluminium foam, experiments are conducted on the machine in two different phases:

1st Phase: Employment of different foamable mixture filling techniques for the development of aluminum foam by FSP approach.

2nd Phase: Employment of different tool pin profiles to mix the foamable mixture into the substrate.

3.2 Foamable Mixture Filling Techniques (1st Phase)

The foamable precursor is developed using a flat plate substrate. The foamable powder mixture (TiH_2+$CaCO_3$+Al7075) is filled into the Al substrate using the three different techniques, and then it is subsequently mixed using FSP. These techniques are discussed below:

3.2.1 Buried hole technique

In this technique, buried holes are drilled in AA7075 plates with 4 mm diameter from one end to another along the length of the plate, as shown in Fig 3.6 (a). To prevent processing interference a gap of 25 mm is maintained between two adjacent drilled holes. These holes are tightly filled with the foamable material, and they are then sealed using readily available epoxy compound. The foamable material is subsequently blended by FSP into the substrate. In this technique, it is expected that the buried hole will produce a closed area where it will be challenging to move the foamable mixture away from the processing region and all the foamable mixture is entrapped in the processed zone. Some amount of H_2 gas released during decomposition of TiH_2 will also expected to be entrapped owing to no availability of open space in the processed zone, as shown

in Fig. 3.6 (b). Thus the utilization of foaming mixture is expected to be highest to improve the quality of the foam.

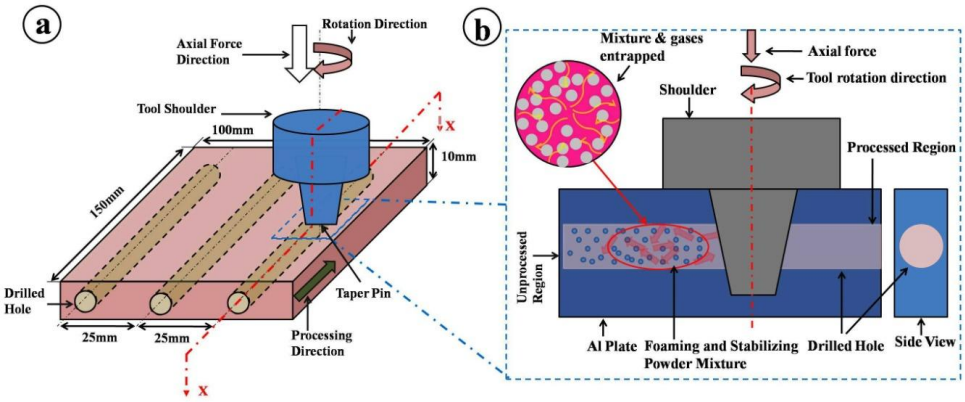

Fig. 3.6: (a) Buried hole technique and (b) process mechanism

3.2.2 Open groove technique

In this technique, the open V-shape grooves are made on the AA7075 plate and then filled with a mixture of blowing and stabilizing agents, as shown in Fig 3.7 (a). The groove size is maintained to contain an equal amount of mixture in volume like in the buried hole technique. For the same reason, the depth of the groove is approximately taken as 4mm and inclination angle is 65^0.

3.2.3 Sandwich technique

In the sandwich technique, a layer of the foamable mixture is placed between two plates of AA7075. Both plates are clamped together with the help of a clamping fixture. The grooves are made in the plates to put the mixture in between the substrates, just like the open V-groove technique for maintaining the equal volume of foaming mixture. Then FSP is carried out for mixing this mixture into the substrate, as shown in Fig. 3.7 (b).

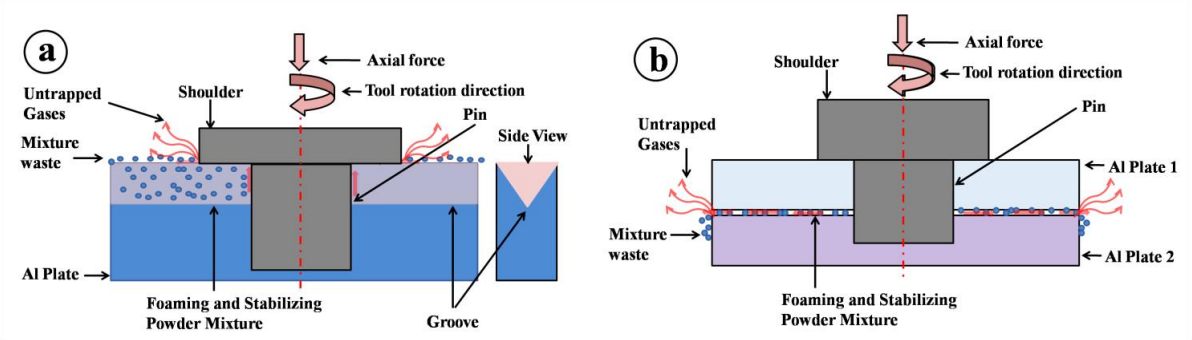

Fig. 3.7: Process Mechanism of (a) Open V-groove and (b) Sandwich techniques

Experiments are performed for each plate configuration, Fig. 3.8 (a, b and c) displays the original experimental plates on which the FSP is carried out to manufacture the precursor and at least three precursors are extracted from each plate.

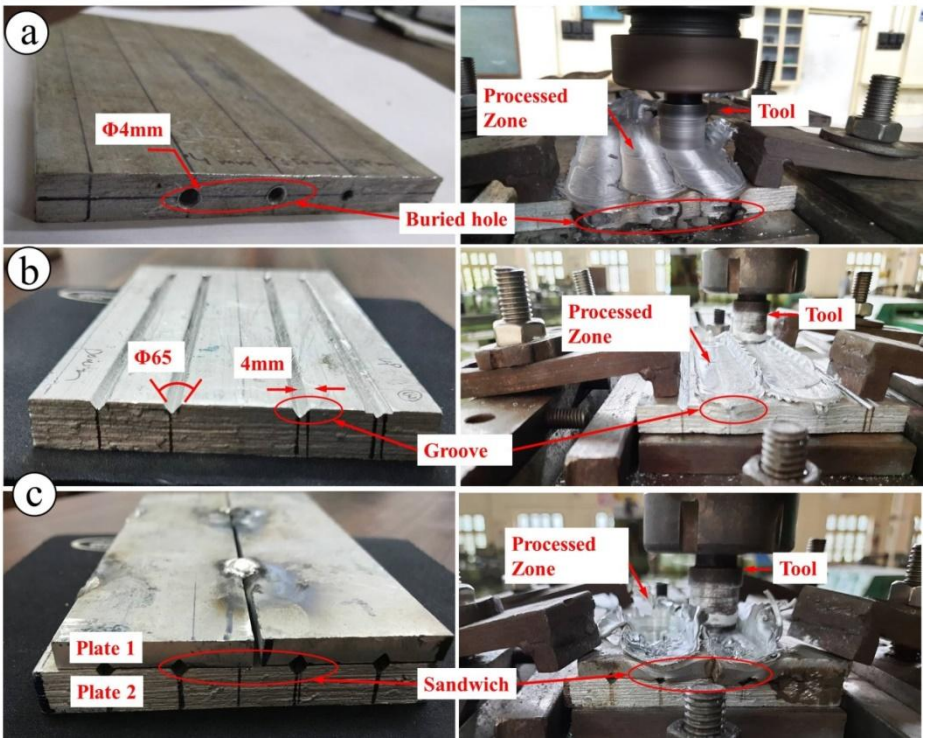

Fig. 3.8: Development of precursor by FSP route (a) Buried hole; (b) Groove and (c) Sandwich architecture

3.3 Effect of Tool Pin Profiles on Buried Hole Strategy (2nd Phase)

Now for further improvement on foam formation, the optimized technique of phase 1 is further examined for different tool pin profiles in the next phase of experiment. Three different tool geometries are used to mix the foaming mixture into the substrate. Tool geometry is one of the most important process parameters that affect the grain size of the processing zone. These tool geometries are straight threaded cylindrical (STC), triangular (TR), and square (SQ) pin profiles as shown in Fig. 3.9.

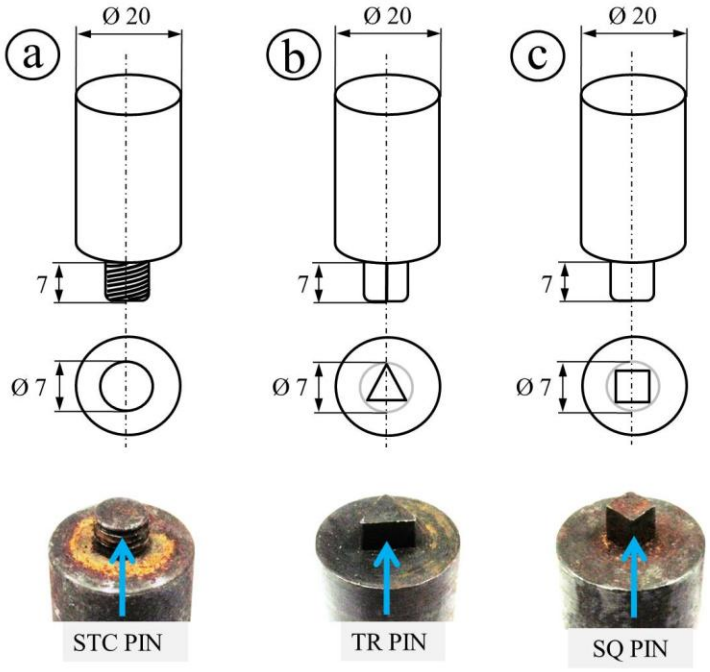

Fig. 3.9: Tool Geometries; (a) Straight threaded cylindrical (STC), (b) Triangular (TR) and (c) Square (SQ)

These three pin profiles have been selected to see the effect of their contact area/points during the stirring action [137]. The length of the pin is 7 mm for all the three pin profiles. The diameter of the pin is taken as inscribed circle of 7 mm to maintain the uniformity in the design

of the pin profile. It has been seen from the literature review that TR and SQ pin produce higher grain refinement due to pulsating action of the selected tool during the weld joint. Therefore, same mechanism needs to be explored during foam development. With this intension various pin profiles have been selected.

3.4 Parametric Selection

The manufacturing of aluminum metal foam by FSP is influenced by a number of process parameters as shown in ishikawa diagram (Fig. 1.8). The density and quality of the foam produced are influenced by the amount of blowing agent powder and stabilizing agent utilized. These mixtures include a combination of TiH_2, AA7075 and $CaCO_3$ powders. The foaming agent and the stabilizer are mixed by weight % of the constituents, as depicted in Table 3.5.

Table 3.5: Composition of the mixture

Sr. No.	Composition (wt. %)	Notation
1	TiH_2 (20%) + Al 7075(60%) + $CaCo_3$ (20%)	A
2	TiH_2 (30%) + Al 7075(60%) + $CaCo_3$ (10%)	B
3	TiH_2 (40%) + Al 7075(50%) + $CaCo_3$ (10%)	C

Since the primary objective of this research is to consistently distribute TiH_2 particles throughout the Aluminium matrix, this has also led to uniform pore distribution. Therefore, multi pass FSP are also employed here to achieve the proper mixing in the stir zone. The composition of mixture and number of passes of FSP is used as variable factors, as shown in Table 3.6. The levels for different factors have been decided based on the trial runs. After various trial runs, for optimum traverse speed and rpm, the experiments are performed at a range of rotational speeds of 1400

rpm and traverse speed of 100 mm/min. For uniform pressing of the foamable mixture the tool is tilted at angle of 2° on vertical axis of the machine. An L-27 orthogonal array [138] is being used as design of the experiments. The set of experimentation obtained from the Taguchi method is shown in Table 3.7. The other factors like tool parameters such as tool shoulder, tool pin profile are constant and presented in Table 3.8.

Table 3.6: Control factors and their levels

S. No.	**Factors**	**Levels**	**Level 1**	**Level 2**	**Level 3**
1	Technique	3	Buried	Sandwich	Groove
2	Composition (Wt. %)	3	A	B	C
3	No. of Passes	3	1	2	4

Table 3.7: Experimental Process Parameters

Sr. no.	Techniques	Composition	No. of Passes
1	Buried	A	1
2	Buried	A	2
3	Buried	A	4
4	Buried	B	1
5	Buried	B	2
6	Buried	B	4
7	Buried	C	1
8	Buried	C	2
9	Buried	C	4
10	Sandwich	A	1

11	Sandwich	A	2
12	Sandwich	A	4
13	Sandwich	B	1
14	Sandwich	B	2
15	Sandwich	B	4
16	Sandwich	C	1
17	Sandwich	C	2
18	Sandwich	C	4
19	Groove	A	1
20	Groove	A	2
21	Groove	A	4
22	Groove	B	1
23	Groove	B	2
24	Groove	B	4
25	Groove	C	1
26	Groove	C	2
27	Groove	C	4

Table 3.8: Constant factors used in the experimentation

Sr. No.	Parameters	Values
1	Rotational Speed (rpm)	1400
2	Feed Rate (mm/min)	100
3	Tool Shoulder (mm)	20

4	Tool Pin Length(mm)	9
5.	Tool Tilt Angle(Degree)	2

After employing the L-27, the foam quality is evaluated on the basis of following output parameters:

1. Pore size

2. Porosity

3. Compressive strength

These properties govern the quality of foam on the basis of mechanical behavior. A proper distributed optimum pore size with optimum density provide large plateau zone which represents better sock absorption.

In order to generate the precursor, the foaming agent (TiH_2) and stabilizing agent (Al powder and $CaCO_3$) are first combined in the appropriate quantities and filled into the Al plate using various filling techniques. Clamps are then used to hold these plates to the FSP fixture. After that, the FSP procedure is carried out on it by inserting the rotated tool into the plate as shown in Fig. 3.10 (a). The heat that deforms the material is produced by the friction between the plates and the shoulders. With this spinning tool, the filled mixture is mixed with the metal matrix. The Fig. 3.10 (b) shows processed zones on which the FSP is carried out for mixing.

The precursors (approximate 15 × 10 × 10 mm size) are extracted from each experiment's at beginning, middle, and last section/location, as shown in Fig. 3.11. The different location has been chosen to check the uniformity of the mixture.

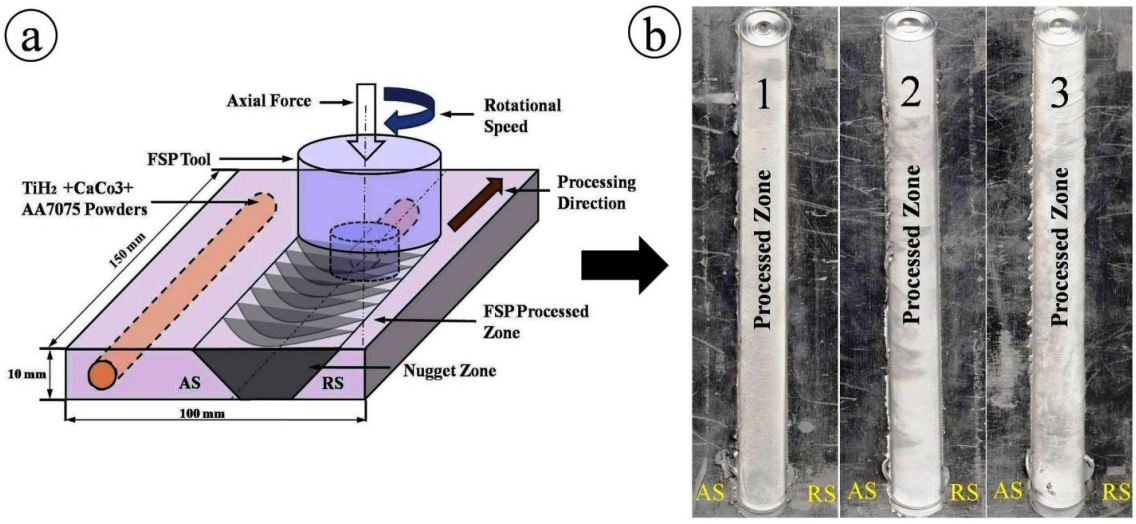

Fig. 3.10: Precursor fabrication; (a) schematic of FSP process, (b) FSP processed plates

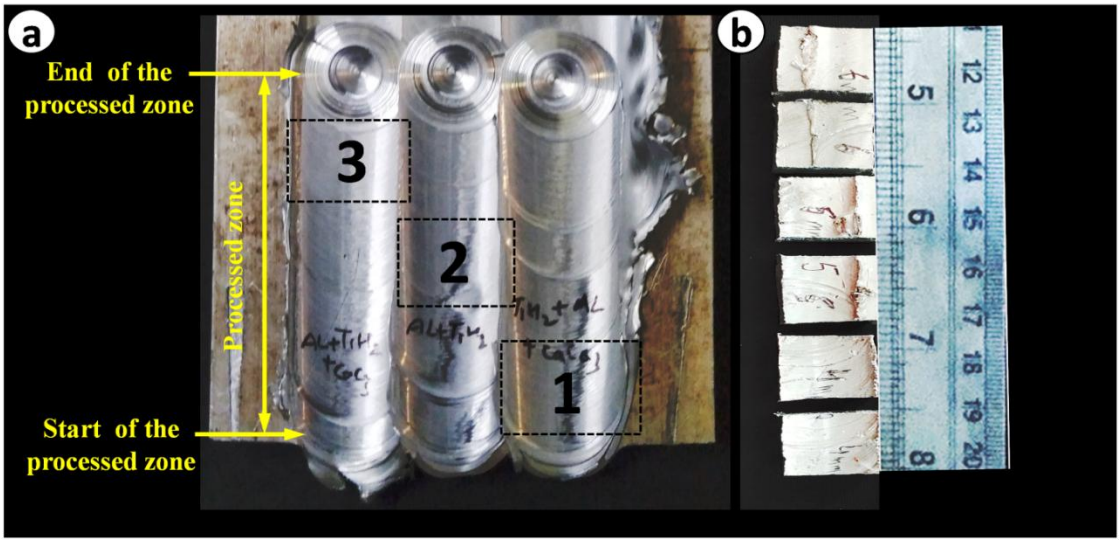

Fig. 3.11: Precursor Extraction from processed plate zone; (a) Different locations; (b) Extracted precursors

3.5 Precursor Heat Treatment Techniques for Foam Development

After extracting the precursor, the samples are heat treated to release gases by decomposition of the blowing agent, which creates pores and the precursor is foamed. The quality of the foam is

dependent on heat treatment techniques and, therefore, needs to be explored. Thus, in the present work, microwave heating is also applied for foam development and being compared with furnace heating. To check influence of time on the properties of the foam, the samples are heated at different intervals of the time. Thus, in this experiment, the required soaking time for both heating techniques is examined.

3.5.1 Furnace heating treatment

In furnace heating technique the extracted samples are heated for the decomposition of the foaming agent for the foam development. For this purpose the electric furnace is used for heating as shown in Fig. 3.12. The samples are heated for a long range of time intervals from 2 to 20 min to check the pore growth in the developed foam. The optimized time has been deduced from these intervals for the decomposition temperature. The temperature is noted down on the furnace display itself.

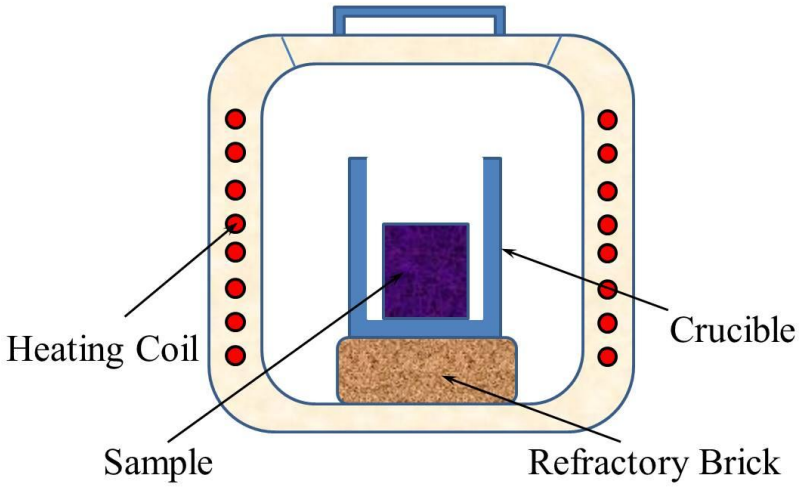

Fig. 3.12: Sample heating in furnace

3.5.2 Microwave heating treatment

For the development of foam, the microwave heating technique also applied. A domestic LG microwave unit with 900 W powers is used for heating purposes, as shown in Fig. 3.13. In this procedure, the entire precursor samples are placed on a refractory brick platform. The thin sheet of graphite separator is placed on the top of the precursor sample and further covered by a thick layer of charcoal powder. This charcoal powder acts as a susceptor of microwaves. The sample is heated above the decomposition temperature of TiH_2 for the development of foam. It is difficult to measure the temperature raised in the microwave; thus, time is selected as the controlling factor of heating. Again, the same technique is used in the microwave heating case. But, as the microwave energy is a spontaneous heating approach the time intervals are selected here were in seconds range. Hence, a range of 20 sec to 100 seconds were selected for the foam development.

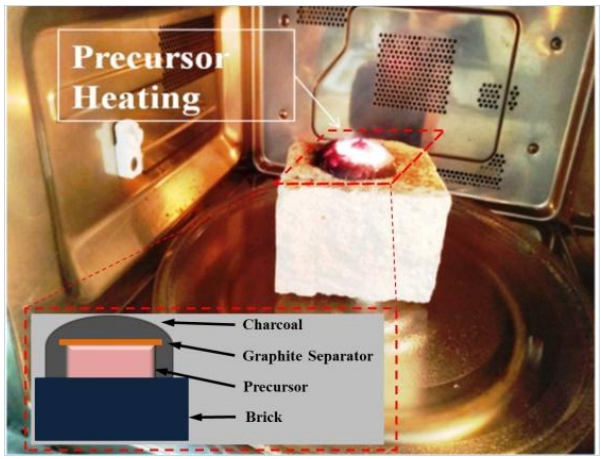

Fig. 3.13: Sample heating in microwave

3.6 Characterization of Precursor and Al foam

However, since foaming is a phenomenon that cannot be completely controlled due to the mechanisms involved at the micro and nanoscales, this study has been able to optimize the input

parameters involved in FSP in order to achieve a metal foam that has all the qualities of a high-quality porous material, including low density, high compressive strength, and energy absorption capacity, along with almost spherical pores and thick cell walls. In order to look at how input parameters are influence the quality of the foam, the metal foam is characterized for different optimized parameters. The density, shape and size of pores are determined using morphological characterization, while mechanical characterization helped determine the mechanical behaviour of the developed foam sample. The structure of the AA7075 precursor is studied using an optical microscope (Carl zeiss) to analyze foaming agent uniformity in the FSP zone. The dispersion of TiH_2 particles and the grain size of the etched samples are examined using scanning electron microscopy (Jeol, JSM-6510). The microhardness of nugget and base material is determined using a Vickers micro-hardness tester (made of Omni tech Mvh1, India) with a load of 0.98 N for 20 s. The compressive strength of the developed foam samples is conducted on a universal testing machine (Zwick/Roell with 10 kN loading capacity) and correlated with pore size distribution. The pore size distribution of the generated foam samples is calculated using the 'ImageJ' software.

3.7 Experiment Results

After the phase 1 experimentation the different pore size and porosity results are obtained according to L-27 experimental design. Table 3.9 shows the average pore and porosity results and Fig. 3.14 (a-c), shows developed foam samples which are produced by these three techniques.

Table 3.9: Results of pore size and porosity

Sr. no.	Techniques	Composition	No. of Passes	Average Pore Size (mm)	Porosity (%)
1	Buried	A	1	1.45	22.1
2	Buried	A	2	0.89	28.73

3	Buried	A	4	0.23	31.58
4	Buried	B	1	1.73	30.92
5	Buried	B	2	1.12	46.03
6	Buried	B	4	0.51	57.18
7	Buried	C	1	1.89	37.49
8	Buried	C	2	1.26	69.32
9	Buried	C	4	0.57	81.57
10	Sandwich	A	1	1.82	21.92
11	Sandwich	A	2	1.07	33.48
12	Sandwich	A	4	0.36	34.26
13	Sandwich	B	1	2.03	24.56
14	Sandwich	B	2	1.16	40.29
15	Sandwich	B	4	1.05	45.64
16	Sandwich	C	1	2.3	29.33
17	Sandwich	C	2	1.38	56.83
18	Sandwich	C	4	0.99	69.17
19	Groove	A	1	2.06	20.45
20	Groove	A	2	1.1	22.93
21	Groove	A	4	0.41	31.47
22	Groove	B	1	2.21	21.84
23	Groove	B	2	1.24	32.72
24	Groove	B	4	1.4	39.13
25	Groove	C	1	2.5	26.02
26	Groove	C	2	1.55	39.98
27	Groove	C	4	1.49	47.63

After optimizing the process techniques with given process parameters, the selected technique is further examined with varying the tool pin profiles. The rest of the process parameters are taken

similar as previously explained. The developed foam samples these pins are shown in Fig. 3.15 (a-c).

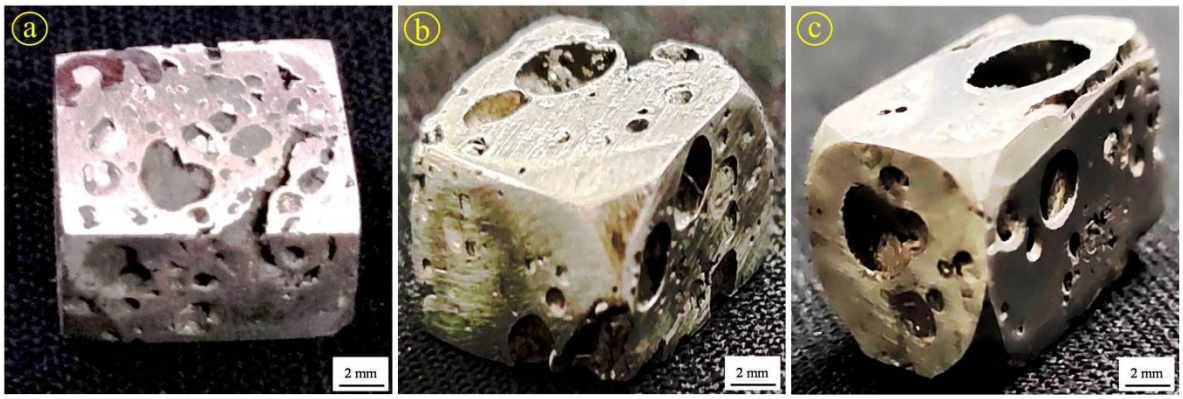

Fig. 3.14: Structure of the developed foam samples of (a) buried hole, (b) sandwich and (c) groove techniques

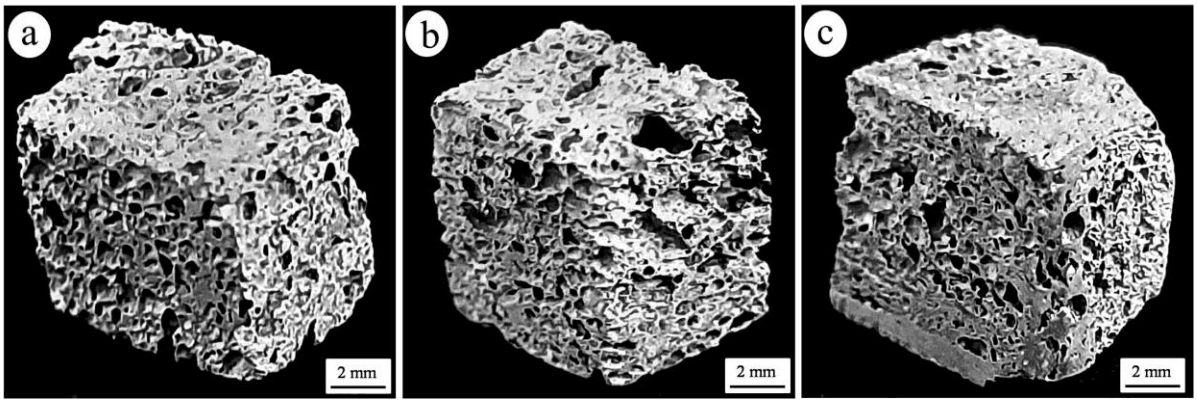

Fig. 3.15: Foam samples developed by different tool pin profiles: (a) STC, (b) TR, and (c) SQ pins

Chapter 4: Results and Discussions

The effect of various input parameters on the properties of developed metal foam is covered in this chapter. The experimentation starts with utilization of FSP technique to mix a foamable mixture containing foaming and stabilizing agent with the substrate by different filling strategies. The impact of these filling strategies on the development of the foam is then analyzed. The analysis has been done to investigate the distribution of trapped mixture of stabilizing and blowing agent in the processed zone. Along with that, the metallurgical characterization has also been done using optical microscopy, scanning electron microscopy (SEM), and Energy-dispersive X-ray spectroscopy (EDX) analysis. The mechanical properties of developed foam has been obtained by compression test on a fully automatic servo controlled UTM. The purpose of this study is to obtain best parameters like pin profile, number of passes, powder composition, filling strategies and heating technique for development of foam.

4.1 Characterization of Filling Strategies on Developed Foam

The filling of the foamable mixture in the substrate is done by three different strategies named: buried hole, sandwich and groove architecture. The developed precursor is then heated for the development of foam. A comparison is made between the different filling techniques, number of passes and composition of the foamable mixture on the distribution of pores, size, porosity and compressive behavior of the foam. After development of precursor, samples are extracted from processed sample. Then, abrasive papers of various grits are used to polish the extracted samples. Samples are then etched using a modified Keller's reagent, which contains 190 ml distilled water, 5 ml nitric acid, 3 ml hydrochloric acid, and 2 ml hydrofluoric acid to reveal the macro and microstructure of the processed zone.

4.1.1 Macro and microstructure analysis of precursor

The typical friction stir processed cross-section of substrate is depicted in Fig. 4.1 (a-c). The flow pattern indicates that the material flows from the advancing side (AS) to the retreating side (RS) in all macrographs. The material flow takes place in one direction only because of clock wise tool stirring. In the case of the buried hole technique, it seems that the foamable mixture distribution is uniform, and no macro-segregation or defect present in the processed zone (Fig. 4.1 (a)). But in case of sandwich and groove type strategy (Fig. 4.1 (b & c)), tunneling defect is observed. This may happen due to the decomposition of TiH_2 during stirring produces H_2 gas, which can easily, entrapped in the processed zone and creates tunneling defect and cavity. Also, due to easy flow of material away from processing zone in sandwich and groove technique, the chances of occurrence of defect are common.

The microstructural analysis of the processed zone has also been carried out. The microstructural analysis helps to identify the distribution of embedded particles in the stir zone. This investigation is also done to study the microstructural changes in the processed zone. The samples for this study are taken from the best result obtained from macroscopic examination at 4 passes with 40% TiH_2. The optical microscope revealed the flow pattern of material in form of onion rings which is clearly visible in all samples in the processed zone as shown in Fig. 4.1 (d, e and f). This onion ring occurred at a higher number of passes because of churning effect of rotating tool which eventually promotes more material processing. The uniform mixing of particles is seen in all microstructures. However, agglomeration of foamable particles can also be seen at specific locations in the matrix in some samples.

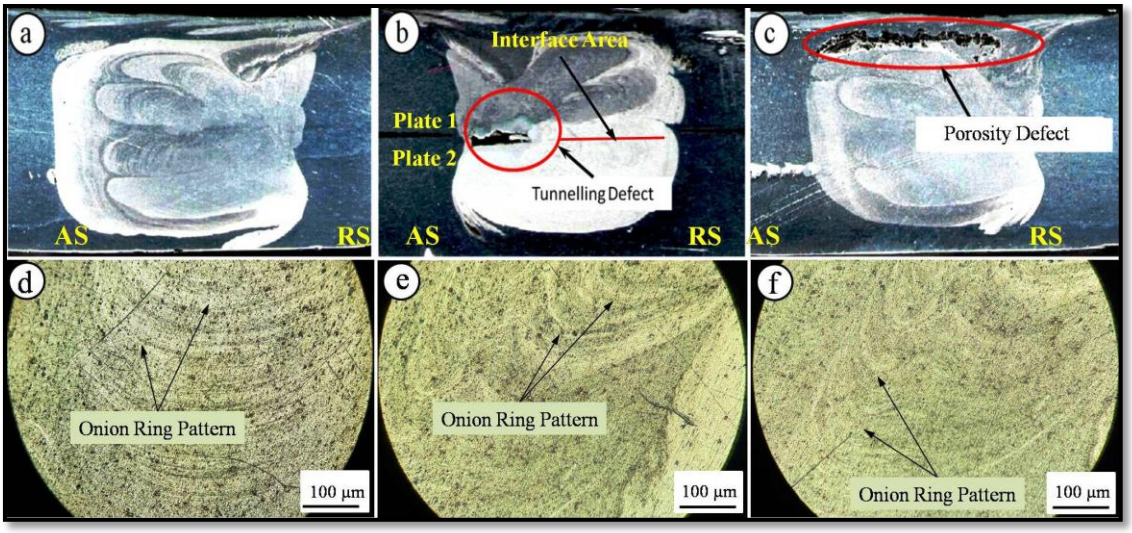

Fig. 4.1: Macrostructure of processed zone of (a) buried hole, (b) sandwich and (c) groove techniques and microstructure of samples developed with (d) buried hole, (e) sandwich and (f) groove techniques at 'C' composition with 4 passes

The Fig. 4.1 (d) shows the microstructure of the buried hole technique. The microstructure reveals a large number of small particles (pointed as black dots) entrapped in the matrix of Aluminium. The rotating tool churns the particles in the processed zone and distributes the particle throughout the processed zone. The large numbers of small particles ensure higher number of pores. However, due to closed boundaries, the foaming mixture tends to agglomerate at the boundaries of the processed zone, which may cause irregularity in the pores. Similarly, Fig. 4.1 (e) shows the microstructures of the sandwich technique in which comparatively less number of small particle are present and agglomeration are seen. This is because open space is present between two plates, and the material can easily flow out from the processing zone due to rotation of the tool during stirring. A similar trend is also observed in the groove technique, as shown in Fig. 4.1 (f).

4.1.2 Effect of heating techniques and time on development of foam

The developed precursors are then heated by two heating methods i.e., furnace and microwave heating to produce foam. The macrostructure of the precursor does not reveal the distribution of foaming material in the processing zone. To reveals the distribution of the foaming mixture, the precursor with similar hole size of 4 mm and "C" composition is heated for a small duration. Due to this heating, small pores are developed in the processed zone due to decomposition of TiH_2. Then based on these small pores, the flow pattern in the processed zone can be clearly analyzed. Also, it is required to optimize the heating time for development of good quality of foam. Thus, samples are extracted at different soaking times to evaluate the time required for development of proper foam in both microwave and furnace heating. It is observed that the time taken in case of microwave heating is much lower as compared to furnace heating. The developed foam samples show varying pores size dependent on the soaking time. The progressive development of pores with time during heating shows the foaming behaviour of the mixture in the processed zone.

The samples heated in the microwave with different soaking time are shown in Fig. 4.2 (a-c). The development of foam occurred in three stages [139]. The sample shows in Fig. 4.2 (a) reveals the microwave heating of the precursor for 30 s. In this sample, foam is not properly developed due to insufficient heating of the sample and porosity is achieved only 5-10%. The lower porosity is due the fact that sample is not heated up to the solidus temperature of matrix and the Aluminium matrix has sufficient strength to resist the pressure of foaming gases. Fig. 4.2 (b) shows the foam developed at 60 s duration in which small pores are visible and foaming starts. The pores are observed in all the processing zones in this stage and porosity reaches 23 to 36%. But when the sample is heated up to 90 seconds, as shown in Fig. 4.2 (c), the proper foam

has been developed with excessive sample expansion. This is known as the third stage, which is a stable stage in which the porosity increases between 50 to 70%. This is because, within this time frame, the formed pores gradually merge into large pores. During this heating, sample is expanded 1.5 to 1.8 times higher than the original sample. At this stage, excess pressure of H_2 gas enhances pore size and small pores collide to form big pores. Also, at this time period, the Aluminium matrix heated uniformly and soft enough to deform easily by the pressure of H_2 gas. After this stage, the decline phase starts in which pore size increases due to the collision of small pores in larger pores and the porosity steadily decreases.

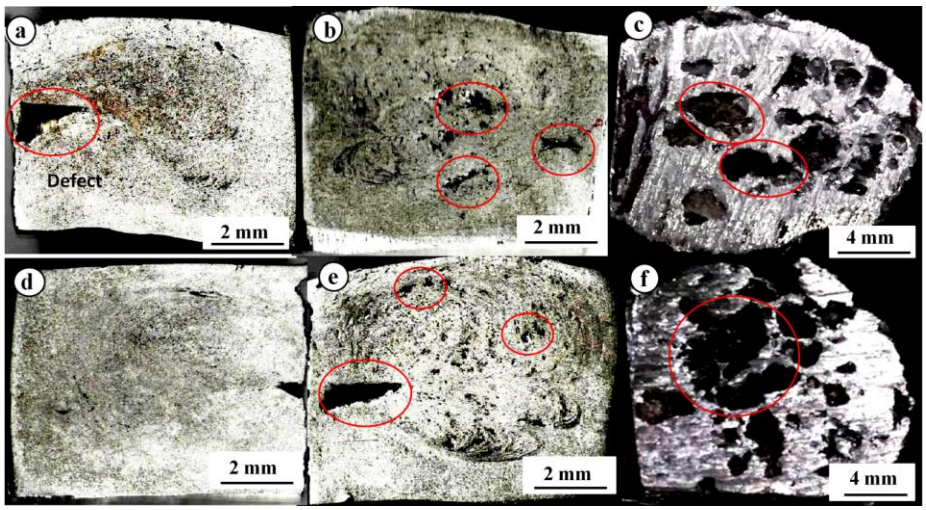

Fig. 4.2: Effect of time on the development of foam in microwave heating (a) 30 s, (b) 60 s, (c) 90 s and furnace heating (d) 5 min, (e) 10 min, (f) 15 min at "C" composition

The second heating is furnace heating, in which samples are placed in a pre-heated furnace at a temperature of 6650C. Fig 4.2 (d-f) shows the sample soaked for different duration in furnace. The first sample removed from the furnace after 5 min shows a small decomposition TiH_2. The area covered by the foamable mixture is visible, as shown in Fig. 4.2 (d). The small pores are formed when samples are heated for this duration. Further increasing the soaking time increases

the pore size, as shown in Fig. 4.2 (e), in which samples are extracted after 10 minutes. Reasonably decent foam has been obtained when the precursor is soaked for 15 min duration, as shown in Fig. 4.2 (f). At this stage, proper heating causes the decomposition of TiH_2 and the formation of pores with smaller wall thickness. During the first heating stage (for 5 minutes), the porosity of 4 - 9% is achieved. In the second stage, in which samples are soaked for 10 min, the porosity is obtained between 28 to 45%. The last stage is the growing stage, in which pores cover the maximum area of the matrix. After this stage, the decline in porosity starts due to increased deformation of big pores and the release of gases from the matrix, this increases the wall thickness and reduces the porosity. Increasing the holding time by more than 15 min, the porosity steadily decreases.

4.1.3 Effect of composition on the formation of pores

The variation of pore size concerning composition in different heating techniques is shown in Fig 4.3 (a-c) for the samples obtained in microwave heating. Fig. 4.3 (a) shows the processed zone sample which containing 100% TiH_2. Because there is a greater quantity of TiH_2 present in the processed zone, smaller pores combine to form larger pores, resulting in the pores formed in this sample are less and larger in size. Fig. 4.3 (b) shows the pores in the processed zone with 50% TiH_2 and 50% Aluminium powder. It is clear from this figure that pores are smaller, but they are also less in quantity, which is not favorable for the characteristics of developed foam. Fig. 4.3 (c) shows the processed zone with 40% TiH_2, 40% Aluminium powder and 20 % CaCO3. The processed zone has the smallest pores than other samples and uniformly distributed. Obviously, as the amount of TiH_2 decreases, the formation of H2 gases decreases. Similarly, the foam samples developed in the furnace are shown in Fig. 4.3 (d-f). The foam developed has circular pores and the pores are of different sizes and shapes as like in microwave heating. The pore size

and distribution in the developed foam depend on the composition of the powder. It is found that as the composition of the TiH_2 decreases, the size of pores decreases. It is observed that the microwave heating causes suitable heating of the particles and thus, gases are formed properly before heating of Aluminium matrix. As the temperature reaches an appropriate temperature, Aluminium becomes soft and due to the pressure of gases present in the matrix, pores are formed. This pressure uniformly deforms the Aluminium and forms circular pores. But in case of furnace heating, the Aluminium matrix is heated first because the heating takes place due to conduction mode (from outside to inside). Thus, the foam developed in the Aluminium matrix is irregular in shape.

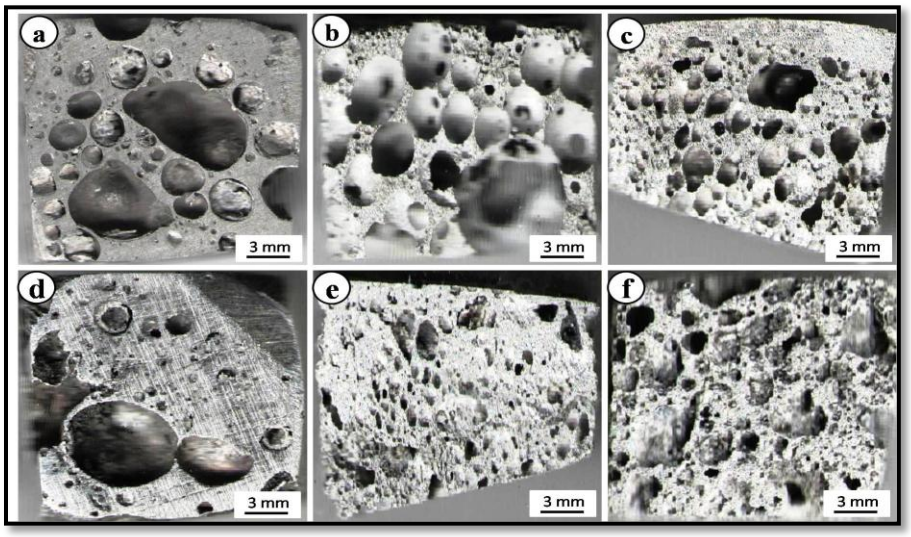

Fig. 4.3: Pores growth at different compositions (a) A, (b) B, (c) C in the microwave heating for 90 s and (d) A, (e) B, (f) C in furnace heating for 15 min at 4 passes

4.1.4 Effect of no. of passes on the formation of pores

The friction stir processing is used for mixing the foamable mixture in the processing zone. The effect of FSP can be observed on the foaming behavior and required to set a limit on the number

of FSP passes. Thus, foaming behavior has been observed based upon a number of passes. It is reported that increasing the number of FSP passes results consistent distribution of particles within the nugget [140]. But at the same time, excessive stirring causes tunneling defects, which may reduce the quality of foam. Thus, different numbers of passes have been selected to check the effect of number of pass on development of foam. Samples with a 4 mm hole size and a composition of "C" were taken and heated to examine the effect of different number of passes. As mentioned above, this composition produced better results than others. The precursors are heat treated by microwave and furnace heating for 90 seconds and 15 minutes, respectively. Thereafter the foam samples are polished to reveal the foam structure. Fig. 4.4 (a-f) shows the foam samples obtained with different number of FSP passes and different heat treatment techniques.

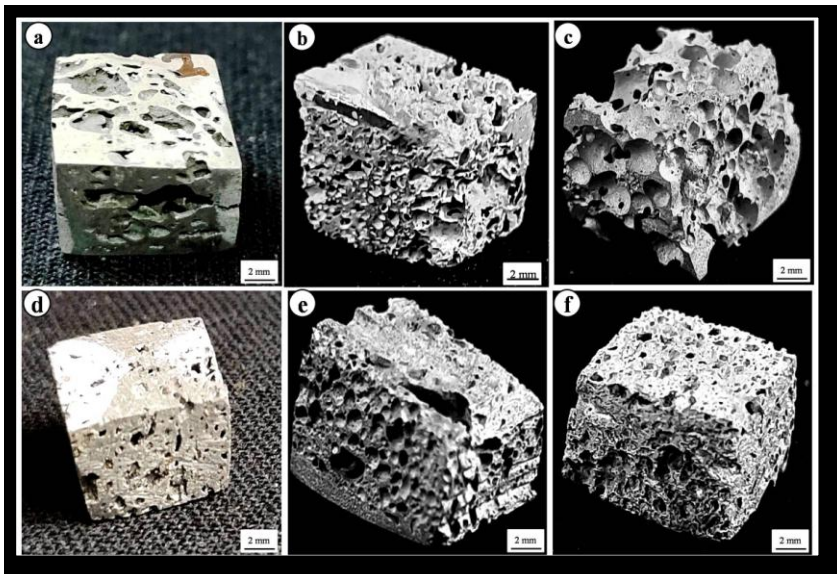

Fig. 4.4: Pores growth at ‘C’ composition with 4 mm hole diameter in (a) one pass, (b) two passes, (c) four passes in microwave heating for 90 s and (d) one pass, (e) two passes, (f) four passes in furnace heating for 15 min

The Fig. 4.4 (a), (b), and (c) shows the sample obtained in microwave heating with one, two and four number of passes, respectively. Similarly, Fig. 4.4 (d), (e), and (f) shows the sample obtained in furnace heating with one, two and four number of passes, respectively. The Fig. 4.4 (a) reviles that the pores occurred during single pass are bigger in size, but at the same time, they occupied less area. The pore size obtained in single pass is between the ranges of 0.8 mm to 1.4 mm in microwave heating, while the range in furnace heating is 1.1 to 2.4 mm. Also, the area covered by the pores is 40 to 61% in the case of the microwave, while it is 37 to 56% in the case of furnace heating. As the number of passes increases to two, the pore size decreases in both the heating cases. Microwave heating has uniform pores as compared to furnace heating. The pore sizes are between 0.65 to 1.1 and 0.78 to 1.47 for microwave and furnace heating. Also, the pores' area is slightly increasing in two passes. The area covered by pores in microwave heating is 47-69%, while it is 43-65% in furnace heating. As the number of passes further increases, the pores are reduced. The pores are very smaller at four passes in both the heating conditions. In microwave heating, it is in between 0.23 to 0.45, while in furnace heating, the pores are in the range of 0.31 to 0.47. The area covered by pores is also increased by increasing the number of passes and the area covered by pores in cases of microwave heating is 57 to 76%. Similarly, the area covered by pores in furnace heating is 56 to 77%. It is clear from these observations that pore size decreases with an increase in number of passes. This is because as the number of passes increases, uniform distribution of foamable mixture occurs. When the precursor with the uniformly distributed foamable mixture is heated, pores are developed at all precursor locations. These pores are small because of less clustering of the foamable mixture. The pore size directly depends on the gases produced during heating and heating time. The gas produced now depends on mixture distribution, but the pores depend on soaking time. If the soaking time is longer, the

pores collapse and form big pores.

4.1.5 Pore size and porosity measurement

The pore size has been measured after heat treatment of the samples. The pores are revealed after proper polishing of the foamed samples. After polishing, ultrasonic cleaning has also been done to remove adhered particles on the foamed samples. After appropriate cleaning, the captured images are used for pore size measurement by using 'Image J' software. The pore size is then utilized for obtaining the effect of processing parameters, composition and heating technique on the developed foam. The wall thickness of the foam has also been measured using the line intersection method. Fig. 4.5 (a) shows the foam sample taken for pore size measurement and Fig. 4.5 (b) shows the distribution of pores. The average pore size has been measured by measuring the volume of the sample and the area of the measured pores on the surface.

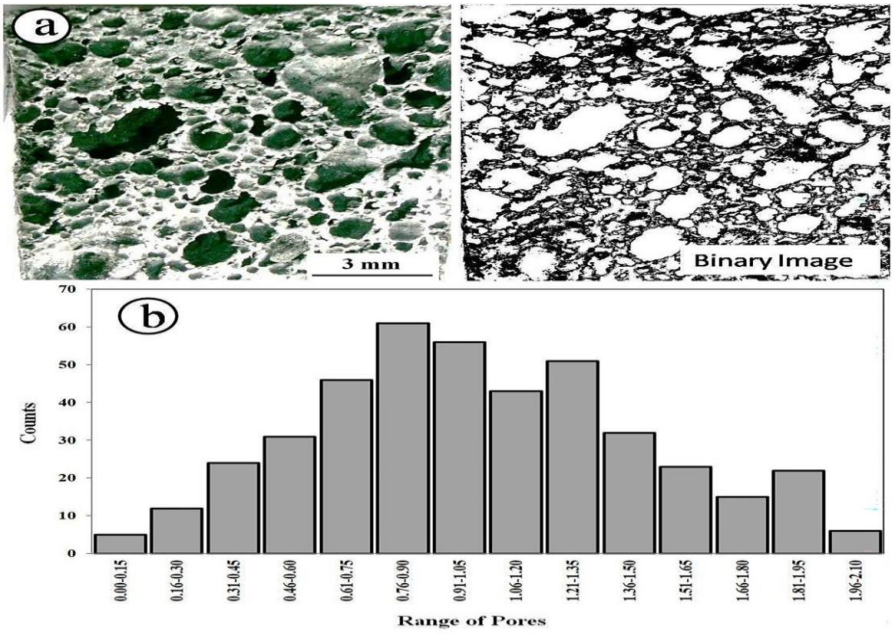

Fig. 4.5: (a) Foam sample for pore size measurement (with binary image) and (b) distribution of pores at "C" Composition

The porosity of the foam has been measured by measuring precursor density before heating and foamed sample after heating. The density of precursor and foam has been calculated by measuring the volume and weight of the samples. To ensure proper measurement of volume, the length, width and height have been measured after proper polishing of all faces of the samples.

The porosity of the samples is measured as follows:

$$Porosity = (\rho_{specimen} - \rho_{foam}) / \rho_{specimen} \times 100\% \quad \ldots \text{(i)}$$

The specimen density is represented as $\rho_{specimen}$ and the density of the foam is ρ_{foam}.

The effect of process parameters on foam formation has been analyzed based on properties such as pore size and porosity. The pore size is measured from the surface analysis of the foam after proper polishing. This pore size is then used to analyze the effect of various input parameters on the properties of the foam. Along with this, the porosity covered on the polished surface of the developed foam has also been analyzed by measuring the weight and volume of the sample. Table 4.1 displays the test results, representing the average pore size and porosity (%) of developed foam obtained by the above-said techniques. The effect of process parameters like the number of passes and powder composition on the test results is then analyzed.

Table 4.1: Result outcomes of L27 orthogonal array after the experiment

Weld no.	Composition	No. of Passes	Average Pore Size (mm)			Porosity (%)		
			Buried	**Sandwich**	**Groove**	**Buried**	**Sandwich**	**Groove**

1	A	1	1.45	1.82	2.06	22.1	21.92	20.45
2	A	2	0.89	1.07	1.1	28.73	33.48	22.93
3	A	4	0.23	0.36	0.41	31.58	34.26	31.47
4	B	1	1.73	2.03	2.21	30.92	24.56	21.84
5	B	2	1.12	1.16	1.24	46.03	40.29	32.72
6	B	4	0.51	1.05	1.4	57.18	45.64	39.13
7	C	1	1.89	2.3	2.5	37.49	29.33	26.02
8	C	2	1.26	1.38	1.55	69.32	56.83	39.98
9	C	4	0.57	0.99	1.49	81.57	69.17	47.63

4.1.6 Interaction plots for pore size and porosity

The pore size distribution has been measured concerning filling techniques, composition and number of passes of the FSP. Fig. 4.6 (a, b, and c) shows the variation of pore size (diameter) with respect to these three factors. The results presented here are the average of three samples. It was found that as increase the composition, the pore size improves. However, the buried hole technique gives less pore size diameter as compared to other approaches. Further, it is also depicted that the buried hole technique provides less pore size with increase in number of passes, as shown in Fig. 4.6 (a). The diameter of the pores increases as the weight % of TiH_2 increases. This is because the amount of release of H_2 gases increases with an increase in weight % of

TiH_2. The interaction graph shows the pore size with respect to the number of passes (Fig. 4.6 (b)). As the number of passes increases with respect to varying composition, the pore size decreases. This is because the mixing of TiH_2 particles is distributed more uniformly at a higher number of passes thus reduces pore size. The same trends have been found in Fig. 4.6 (c) where increasing the number of passes with different techniques (from buried to sandwich and further to groove). The buried hole technique gives the minimum pore size at 4 passes.

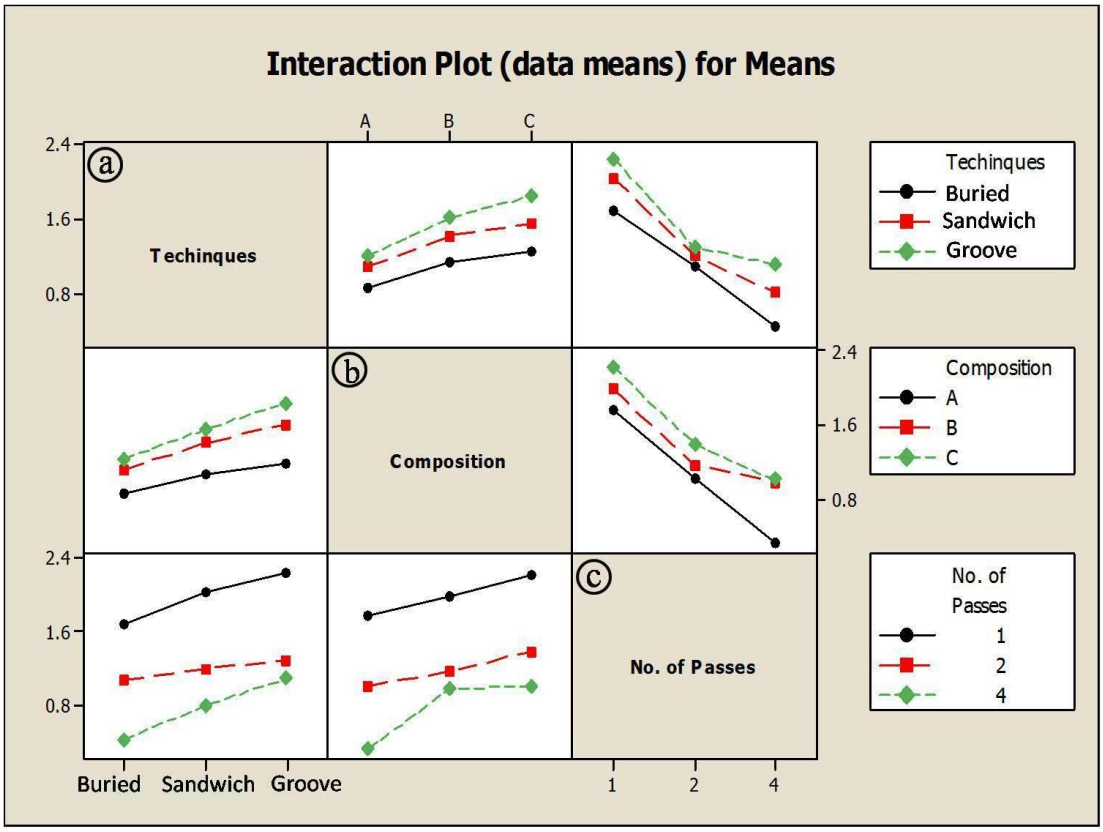

Fig. 4.6: Pore size interaction plot between techniques, composition and no. of passes

The porosity variation is represented concerning parameters like filling techniques, composition, and the number of passes revealed in Fig. 4.7 (a, b and c). The porosity of the foam is affected by composition (weight % of TiH_2) and the number of passes when it is linked with different filling techniques, as refer the in Fig. 4.7 (a). It was found that the porosity of the developed foam is

continuously increasing with increasing the % of TiH_2 and the number of passes of FSP. The porosity variation based on composition is also analyzed. The results show that all filling techniques present a better porosity percentage at higher TiH_2 composition. Still, the buried hole technique attained the highest porosity at a higher % of TiH_2 composition, as seen in Fig. 4.7 (b). A similar type of result is also observed in Fig. 4.7 (c), where the porosity % increased as the number of passes increases which is due to the fact that highr more stirring action by tool on the processed zone. Higher stirring of foamable mixture causes uniform distribution of foaming agents in the matrix. Thus, the foam with higher porosity has higher proportions of pores.

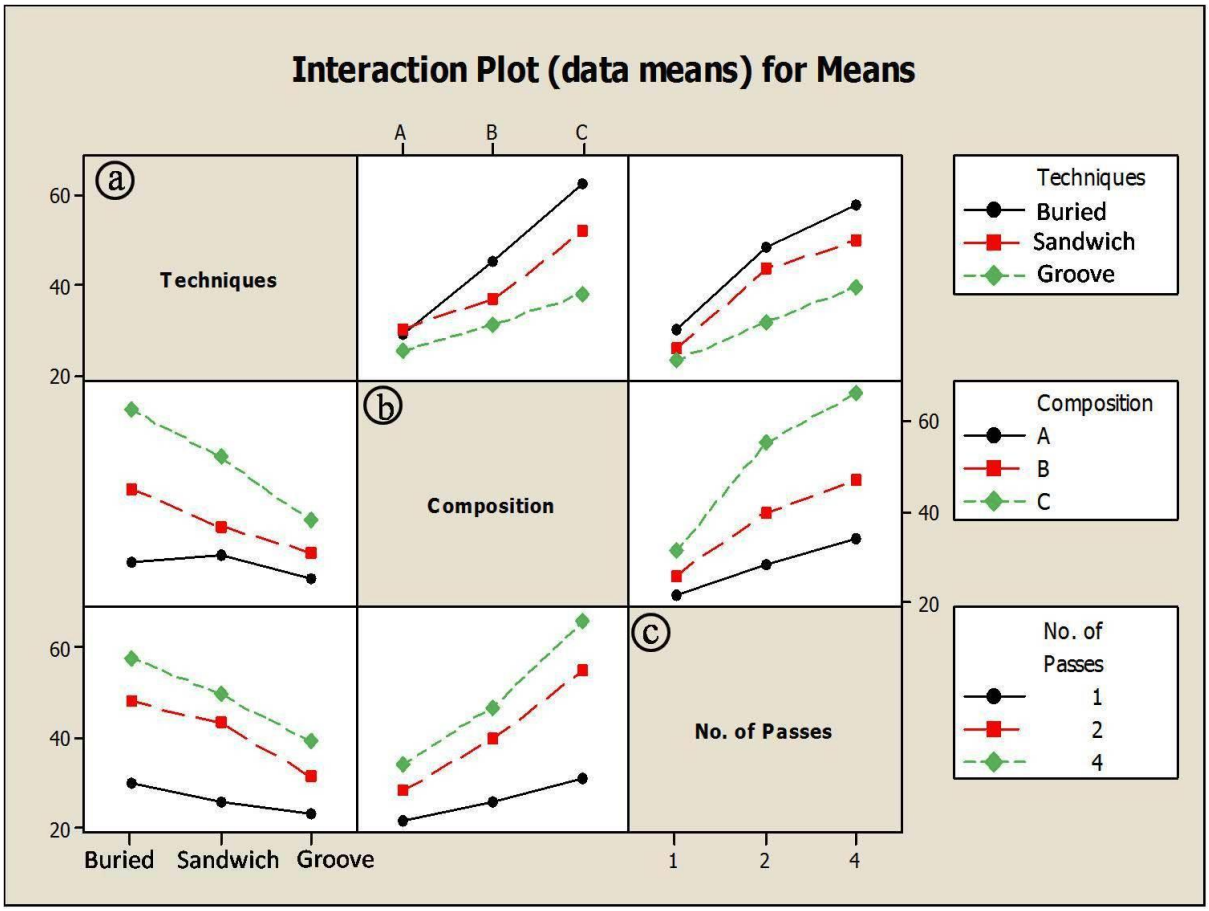

Fig. 4.7: Porosity % interaction plot between techniques, composition and no. of passes

4.1.7 Quasi-static compression behavior of foam

The mechanical behavior of developed foam has been analyzed by quasi-static compression test. The plateau stress measured in quasi-static compression across the sample's strain range [141]. Beat sample from each technique is selected during the test based on the composition and number of passes. It is found from the previous results that the composition 'C' (40% TiH_2) and four numbers of passes are giving better porosity as compared to other parameters. So, the compression testing has been done for these samples only. The work is focused on finding out the best technique of mixture filling, and thus the parameters which provide better porosity have been selected for compression testing. As illustrated in Fig. 4.8 (a-d), the developed foams show deformation bands during the compression test.

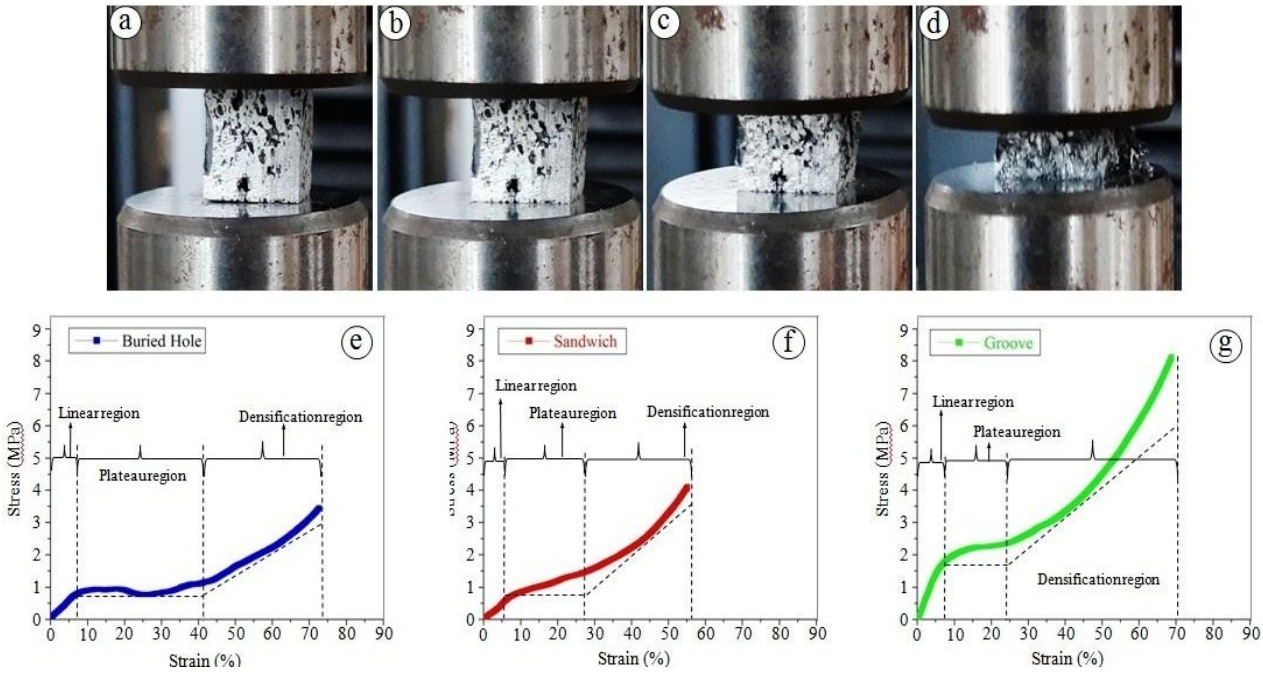

Fig. 4.8: Compression test showing deformation; (a) 0%, (b) 10%, (c) 40% and (d) 90% and Stress-strain curve after compression test; (e) Buried Hole, (f) Sandwich and (g) Groove techniques

Mapelli et al. (2013) [142] and Cambronero et al. (2009) [143] demonstrated that three distinguish zones have been observed during the compression test of foam, in which the first zone is an almost linear elastic zone, the second zone is a constant plateau zone, and the third zone is densification. These zones are observable in the experimental result shown in Fig. 4.8 (e-g). It is expected that the pores in the structure are uniformly distributed and that the developed foam has the maximum porosity. In that case, the second region becomes larger, observed in the buried hole technique as shown in Fig. 4.8 (e). The foam developed by this technique achieved 82% porosity, and pores are uniformly distributed. Similarly, the pores are uniformly distributed in the sandwich technique, but the porosity is 69%and more wall thickness between the pores [144], as compared to buried hole technique. Due to this, the plateau region of this technique is less, as seen in Fig. 4.8 (f). The first region of an unequally distributed porous structure is longer, while the second region is shorter, as illustrated by the groove technique in Fig. 4.8 (g). This is because of the less porosity, which is 48% and less number of pores. Thus the results obtained in the compression test are in line with previous research.

4.2 Effect of Tool Pin Profile on Development of Foam

It has been observed from the above results that the buried hole is more suitable for foam development owing to uniform distribution of foaming agent. The decomposed gases were fully utilized by trapping into the substrate. It is also observed that increasing the number of passes and weight % of TiH_2, improves the distribution of pores. The quality of the foam developed also depends on the FSP parameters that control the distribution of foamable particles. Thus in phase two experiment, the impact of tool pin profiles and numbers of passes on the distribution of foamable mixture of AA7075/ TiH_2 in the substrate has been investigated on the buried hole strategy technique at best suited of parameters. The three different tool pin profile i.e. straight

threaded cylindrical (STC), triangular (TR) and square (SQ) pin are used with 2, 4, and 6 number of FSP passes.

4.2.1 Macro and microstructure of the stir zone

A macroscopic image of the stirred zone (SZ) cross-section of processed samples after 4 passes by various pin profiles is shown in Fig. 4.9. The macrostructure of all three samples demonstrated that the tool pin stirs the material in SZ without any defect.

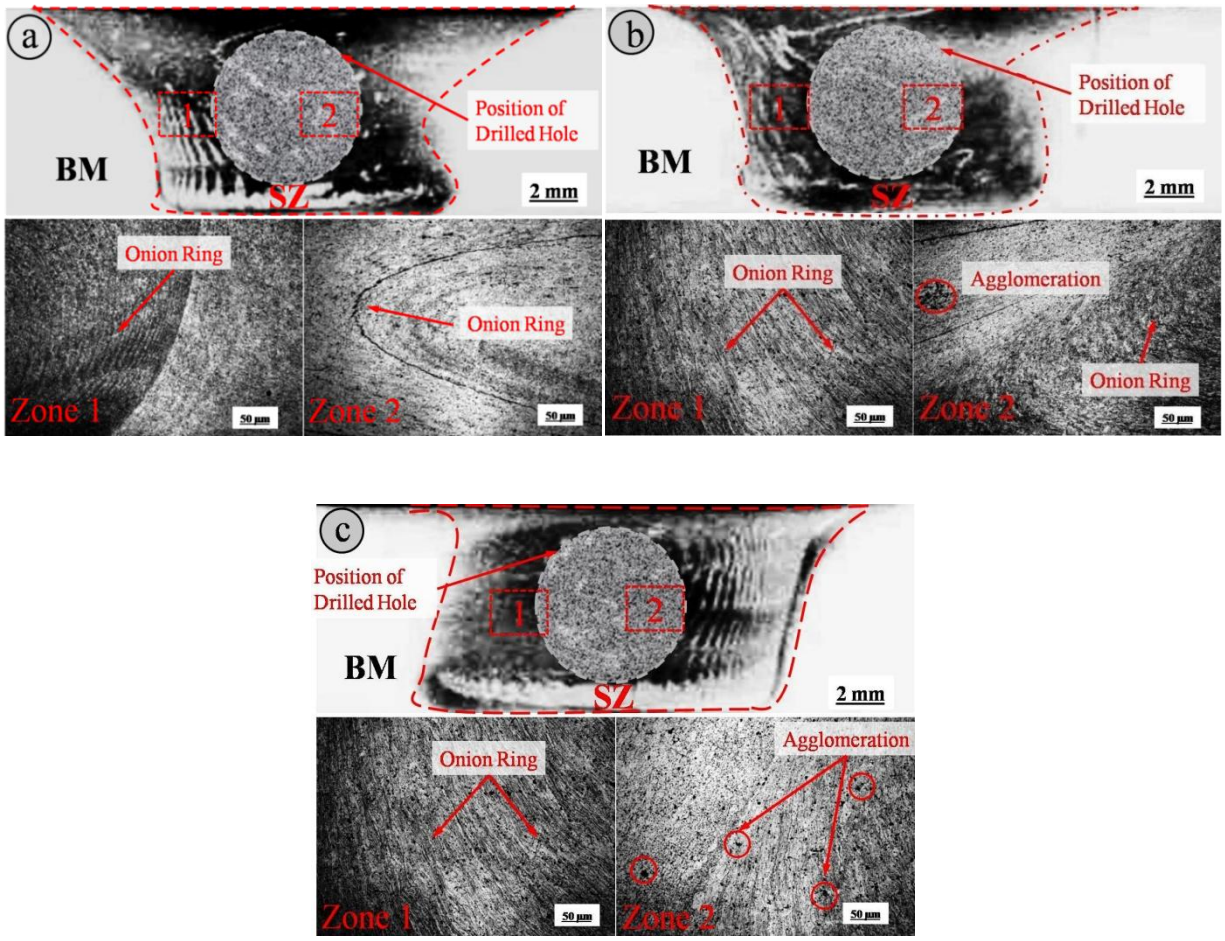

Fig. 4.9: Macroscopic view of cross-section of stirred zone SZ of (a) STC, (b) TR and (c) SQ pin

The cross-sections of the FSP-processed sample at 4 passes with STC pin is shown in Figure 4.9

(a). The cross-section of the samples indicates void free stir zone along with uniform distribution of foaming mixture particles. The downward movement of materials along the probe threads improves material flow in this sample. Along with that, circular onion ring patterns can be seen in the samples, indicat foaming mixture is relatively well mixed [145]. Lesser onion ring patterns has been detected in the micrographs of the TR pin profile at 4 passes, as seen in Fig. 4.9 (b) because of stirring action is restricted to the tool's edge faces. Due to inadequate material flow around the pin in the stirred zone, the particles segregation occured at some locations [28]. Similarly, in the SQ pin profile, the 4 edges participate in mixing of foamable mixture into the substrate. Therefore, better-stirring action occurred as compare to TR pin but an agglomeration of the particles is also seen in the SZ as shown in Fig. 4.9 (c). In both the pin profiles, the homogeneity of the samples is lower than the STC probe which may be due to pulsating action of tool. Similarly, Fig. 4.10 illustrates optical micrographs of the stir zone of materials processed with STC, TR, and SQ pin profiles at 4 passes. Dynamic recrystallization increases grain refinement in the SZ compared to the base material.

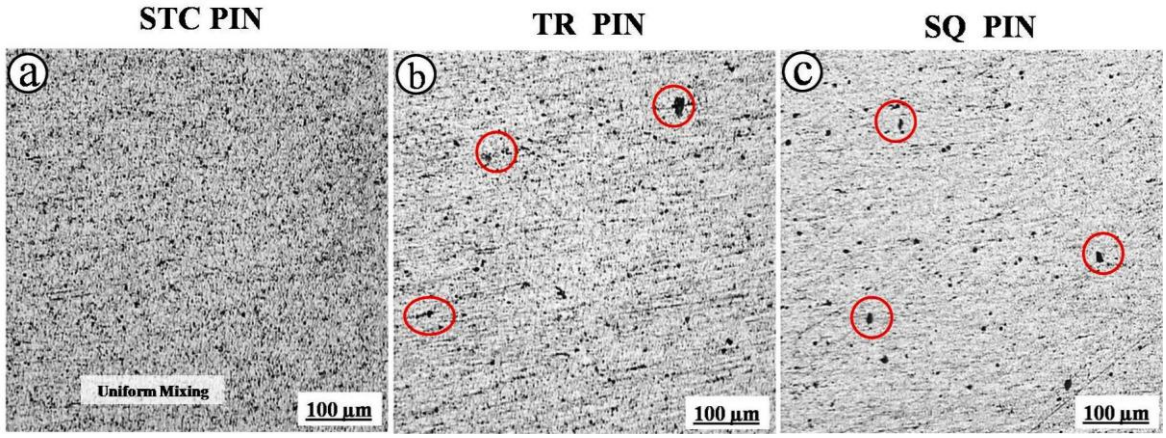

Fig. 4.10: Micrographs of the stir zone of materials processed with STC, TR, and SQ pin profiles at 4 passes.

As shown in Fig. 4.10 (a), the FSP with STC pin profile did not trigger particle clustering at 4 passes, resulting in a homogenous distribution of particles in the Aluminium matrix due to sufficient stirring action by tool. The clustering of foamable mixture is minimum, thus the distribution of particles is readily evident at any location of processed zone. But TR and SQ pin profiles, as illustrated in Fig. 4.10 (b) and (c), respectively, the clustering of particles observed at some location which is because only the edge faces are involved in the material flow process. This edges causes pulsating action during material stirring and enhance chances of clustering.

4.2.2 Scanning electron microscopy (SEM) of processed zone

The processed zone of the precursor is also studied by Scanning electron microscopy (SEM), as shown in Fig. 4.11 (a, b, and c). The SEM images demonstrate the dispersion of TiH_2 particles by different tool geometries of STC, TR, and SQ. For more clear view of particle distribution in SZ, the SEM images of particle dispersion in the processed zone is converted in binary images too. The STC profile pin illustrates the uniform distribution of TiH_2 particles on the matrix, as shown in Fig. 4.11 (a). This is due to the significant dynamic recrystallization by threaded tool. Furthermore, the defect-free structure can be seen in the microstructure, indicating that the material is churned more throughout the process. The clustered particles of foamable mixture, on the other hand, are present in clusters at a specific area of the TR and SQ profile pins processed zone, as indicated in the circled region in Fig. 4.11 (b and c). Along with that, several pores are formed due to decomposition of TiH_2 particle during processing. This is because higher number of passes, the amount of heat developed in the processed zone is appropriate for particular sites where decomposition of TiH_2 particle happens.

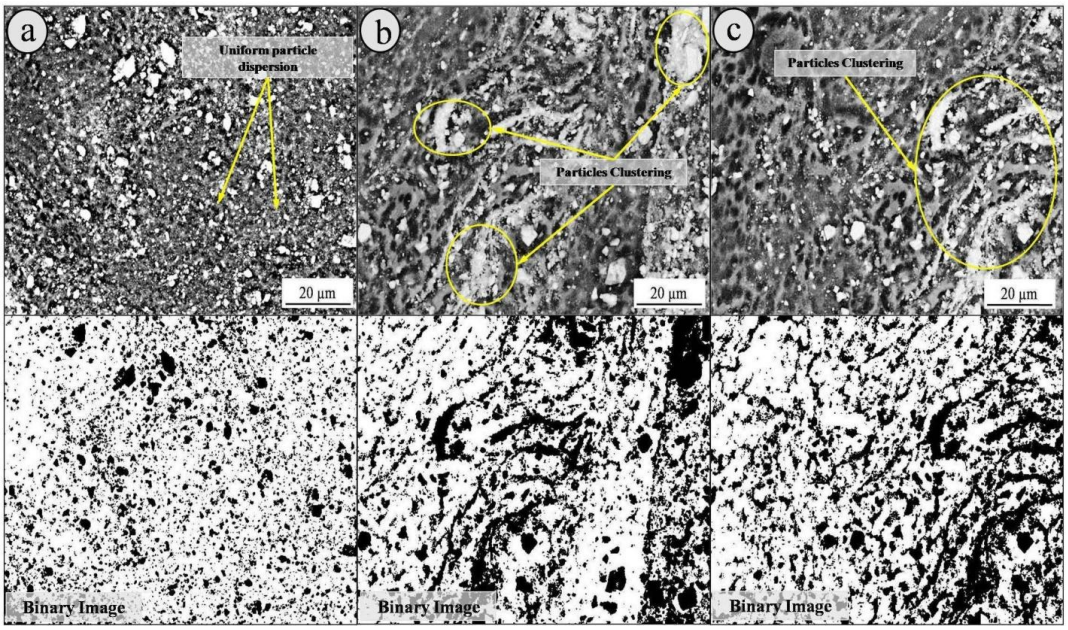

Fig. 4.11: SEM micrographs showing the particle dispersion of processed zone of: (a) STC-4P, (b) TR-4P, (c) SQ-4P

4.2.3 Evolution of temperature during FSP

To evident the heat generation in processing zone due to material flow and plastic deformation, temperature at the bottom of processed zone has been obtained. Fig. 4.12 depicts temperature distributions by different pins profiles. The upward slope in the graph shows the heating curve, while the downward slope is cooling curve. The temperature history of the samples is determined by using a K-type thermocouple which is schematic represented in Fig. 12 (a). The frictional heat is generated in two different ways. The first is the contact between the tool and the work-piece. The second heat is developed from the plastic deformation of material in the stir zone. To check the influence of tool pin profile, in this experiment, the shoulder area is kept constant so that the difference in heat input can observed in different pin profiles. During stirring, all pin profiles covered a comparable volume of material, but the plastic deformation of the material differs

owing to the mechanism of pin edges contact with the substrate [146]. The STC pin comes in continuous contact with the material, while SQ and TR pin are pulsating mechanisms of contact where the edges are involved in mixing. Thus, the STC pin has a broader temperature range during FSP. The temperature graphs can be used to compare the temperature profiles of different pin profile samples.

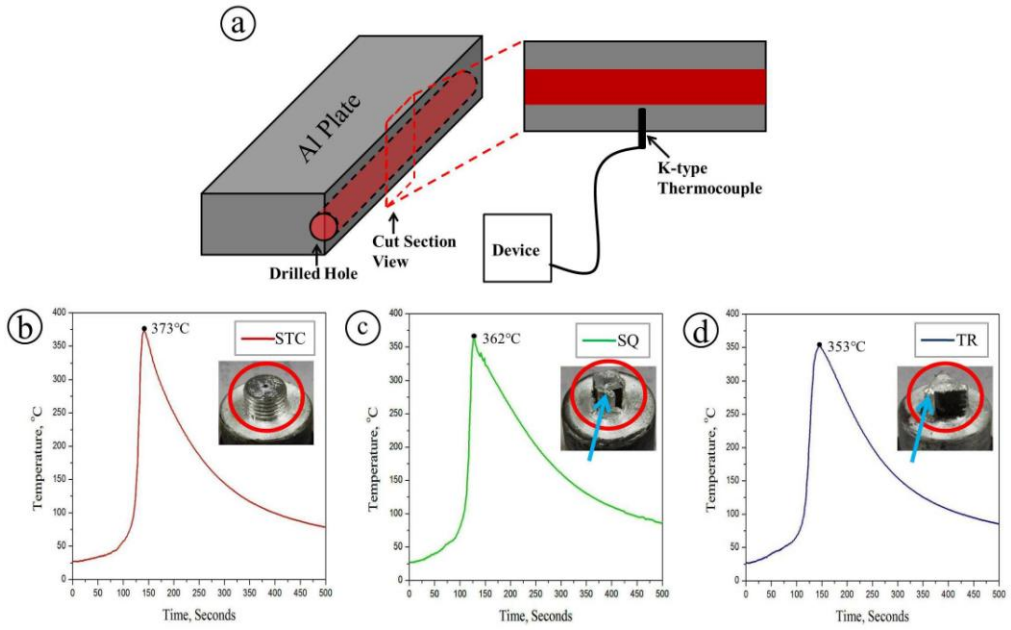

Fig. 4.12: Temperature profile at 4 passes by: (a) STC, (b) TR, (c) SQ pins

During the FSP process, the STC pin reached a maximum temperature of 373°C, as shown in Fig. 4.12 (b). The temperature generated during the STC pin is highest because the entire tool participates in mixing and pushes the material downside owing to the threads on the perimeter. The effective area around the STC pin is substantially higher than the other profiles. Similarly, the maximum temperature of TR and SQ pins is 362°C and 353°C, respectively, which is lower than the STC pin, as illustrated in Fig. 4.12 (c and d). This is due to a smaller area surrounding the TR and SQ profile pins during FSP and only the edge faces are involved in material mixing

which lowering the contact volume of the tool. The shoulder and pin in the STC profile create the majority of the heat in SZ because the tools energetic churning and shearing of the material, results in higher temperature generation during processing.

4.2.4 Microhardness characterization

The hardness distribution across the processed samples processed with 4 passes is shown in Fig. 4.13.

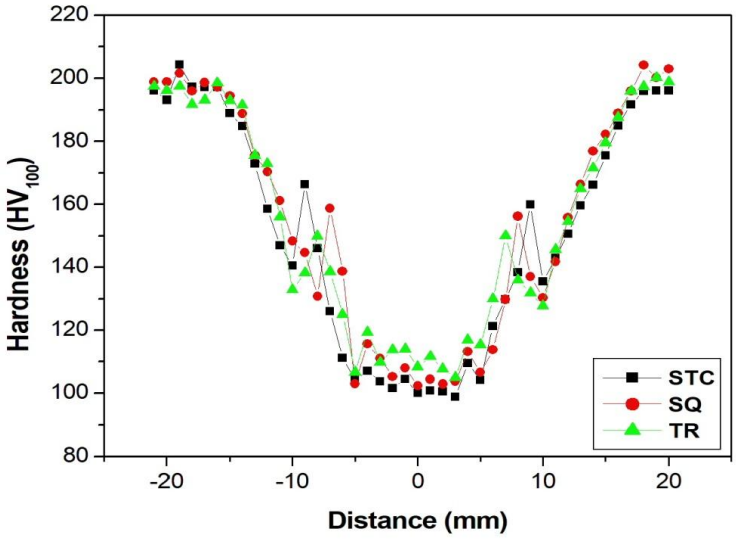

Fig. 4.13: Microhardness distributions after 4 passes by: STC, TR, and SQ pins

The central area of the graph depicts microhardness in the SZ of the samples. For STC, TR, and SQ pin samples, the highest microhardness in the SZ is observed 106, 114, and 119 HV, respectively. In TR and SQ pin samples, the hardness levels are practically comparable. This is because the plasticized materials are subjected to similar turbulence due to the pulsating actions induced by both pins throughout the process [146]. The pulsating action and intensity of plastic deformation are reduced when the number of faces in the pin is reduced [28]. This plastic

deformation in TR and SQ pin samples also increases the dislocation, resulting in increased hardness. The STC pin sample produces the highest peak temperature during the process, resulting in a low hardness value in the SZ. The hardness distribution in the SZ in the STC pin sample is more uniform than TR and SQ pin samples, as seen in Fig. 4.13. Compared to TR and SQ pins, the STC pin creates more heat due to the continuous tool motion, causing less turbulence in the plastic deformation. As a result, due to appropriate material flow around the pin, homogeneous hardness distribution occurred in SZ.

4.2.5 Pore size distribution and compressive strength

Fig. 4.14 (a, b and c) depicts distribution of pores in the developed foam. As mentioned in the previous section, the foam developed by STC pin creates circular pores that are uniformly dispersed throughout the developed foam which is because the foaming agent appropriately mixed into the substrate. It was found that the pore diameters of the STC foams are approximately under the range of 0.45 mm to 1.30 mm as seen in Fig. 4.14 (a). Similarly, other pin profiles (TR and SQ) are evaluated and found that the counting of larger pores is more, as shown in Fig. 4.14 (b and c). The pores are not uniformly distributed, because of improper mixing of the foaming agent into the substrate. The large pores into the foam samples decrease the compressive behaviour of the foam by decreasing the plateau zone.The stress strain curve obtained from the testing of developed foam made by different tool pin profile of STC, TR and SQ is shown Fig. 4.14 (d, e and f). The stress-strain curve shown in figure is showing different deformation behavior of foam developed with different pin profiles. The deformation behavior of foam depends on the average pore size and pore distribution. The fine and uniform pores obtained in STC pin shows lower plateau stress (Fig. 4.14 (d)) than the TR and SQ pin (Fig. 4.14 (e and f)). The foam developed by SQ pin has higher plateau stress as compare to STC pin and

little lower strain (Fig. 4.14 (f)). This is because of clustering of foamable mixture occurred in SQ pin profile, causes big pores at certain location and also uneven distribution of cell walls. This unequal distribution of pore size and cell walls restricted uniform deformation of foam. The foam developed by TR pin not shows a clear plateau zone and stress continuously increases with strain as seen in Fig. 4.14 (e). This happens due to continuous force is required to deform the material because of bigger wall thickness. The wall thickness is depends on the pore size and pore distribution and it is found that the larger wall thickness (in the range of 0.5 to 1.37 mm) has been obtained in the foam developed by TR pin. Also the wall thickness varies in all over the foam as the clustering of foaming mixture is highest in this pin profile. Thus the stress shows a linear response to the strain.

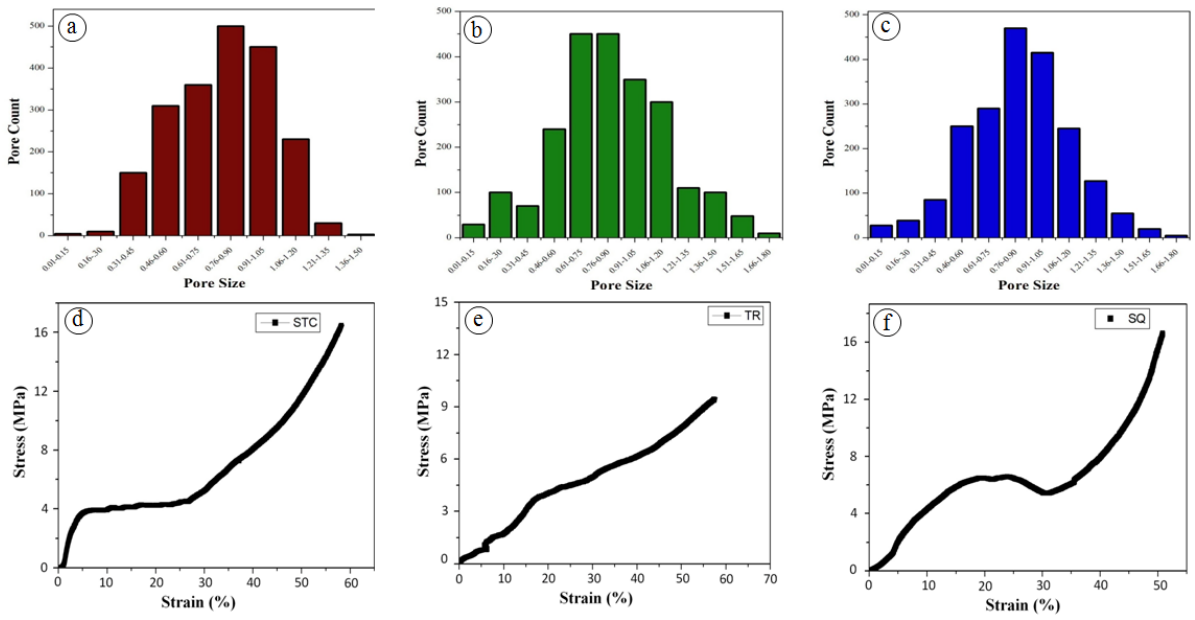

Fig. 4.14: Pore Size distribution of samples processed by (a) STC, (b) TR, and (c) SQ pins and compressive strength of samples produced by (d) STC, (e) TR, and (f) SQ pins

Chapter 5: Development of Foam by Friction Stir Deposition Technique

The friction stir processing is used for development of Aluminium foam. But this process has many constraints which limits the usefulness of this process. One common constraint is preparation of plates for FSP for development of precursor. Also, the utilization of foaming mixture is dependent on the FSP technique used for foam development. Thus, it is require to working on some other technique which can overcome the limitation of FSP for development of foam. So, in present work, friction stir deposition (FSD) technique is employed for the development of precursor. In this technique, the working tool acts as a consumable rod which is deposited on the substrate. This consumable rod contains a foaming mixture in the holes which then mixed with deposited material during deposition. The process is used the optimum parameters obtained from the foamable mixture filling technique and tool pin profile experiments, which were covered in the previous chapter for manufacturing of precursor.

5.1 Selection of Work Material and Machine

5.1.1 Work material

In this study AA6063 consumable rod with a diameter of 25 mm and length of 100 mm is used for deposition. The composition of the consumable rod is given in Table 5.1. This Al alloys shows good strength and high corrosion resistance which make it suitable for the variety of applications including aircraft, automobiles and shipbuilding and thus used for this experiment.

Table 5.1: Aluminum 6063 Composition [53]

Al	Si	Fe	Cu	Mn	Mg	Cr	Zn	Ti	Al

98.41%	0.2%	0.35%	0.10%	0.10%	0.55%	0.10%	0.09%	0.10%	Balance

5.1.2 Machine setup

Similar to the foamable mixture filling technique and tool pin profile experiments, the FSD experimentation work is also conducted on a traditional milling machine (HMT: Model-FN2V). The optimized process parameters of previous experiments are used for the development of precursor which is presented in Table 5.2.

Table 5.2: Optimized factors used in the experimentation

Sr. No.	Parameters	Values
1	Rotational Speed (rpm)	1400
2	Feed Rate (X direction) (mm/min)	100
3	Feed Rate (Z direction) (mm/min)	20
4	Tool Shoulder (mm)	25
5.	Tool Tilt Angle(Degree)	0

5.2 Mixture Filling Strategy

These deposited rods are filled with foamable mixture which is deposited on the substrate along with Aluminium rod. For filling the foamable mixture, these rods are bored with a twist drill along its length up to 70 mm. The stabilizing agent is selected with almost same composition of base plate of AA6061 powder and the titanium hydrate (TiH_2) has been selected as a blowing

agent powder. The 50-50 (%) weight composition of the TiH_2 and AA6061 powders is used as a foamable mixture because this composition gave better results on pore size and porosity as discussed in previous chapters. The rods have varying number of holes along the length from one to six. The diameter of the hole is selected in such a way that the total area covered by holes is almost uniform and volume of foamable powder is constant per unit length. The holes are made in such a way that during deposition of rod, the holes cover maximum area. The schematic diagram of a consumable rod with drilled holes is shown in Fig. 5.1 (a), and the original pictures of the consumable rods after preparation of holes are shown in Fig. 5.1 (b-g).

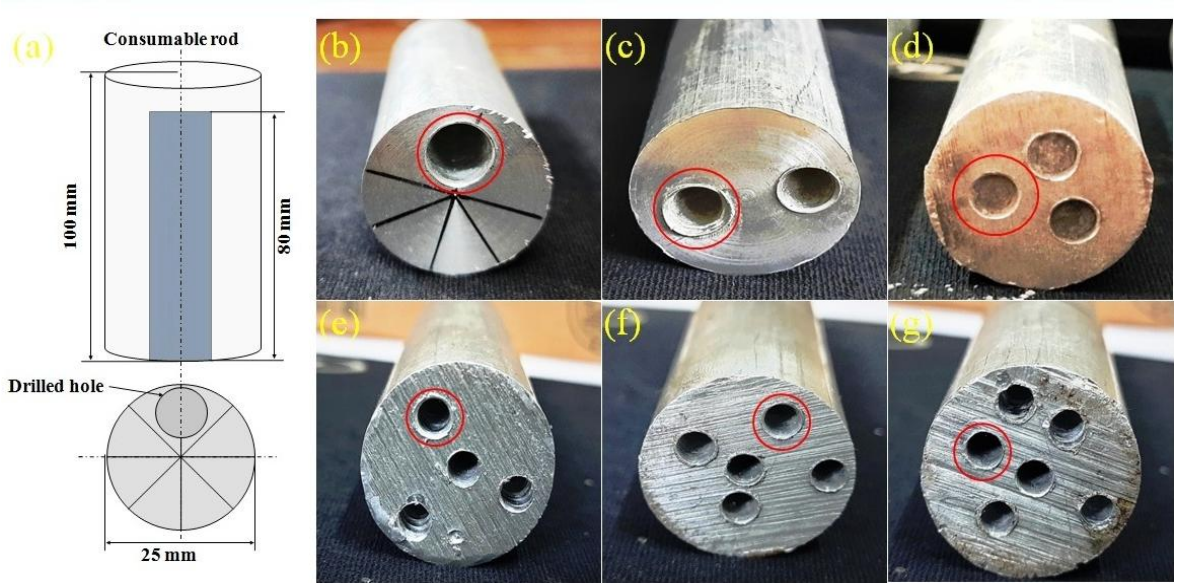

Fig. 5.1: (a) Schematic diagram of the consumable rod, (b-g) Original images of the rod after drill

The foamable mixture filling technique is done in stages to ensure that the mixture tightly filled throughout length without any air gap. Then, after filling the mixture, the ends of the holes are closed with a commercially available Aluminium foil paper to prevent escape of the mixture during start of deposition.

5.3 Fabrication of Precursor by FSD

Then these foamable mixture-filled consumable rods are deposited layer by layer onto the substrate, as shown in Fig. 5.2 (a-d). The rubbing interface is transmitted to the substrate surface. It is securely bonded by an inter-diffusion process induced by pressure and heat. FSD allows the creation of a continuous deposit from the gradual decay of the consumable rod, as seen in Fig. 5.2 (d). The process is also characterized by the constant creation of a rotating flash of visco-plastic material at the rod tip, as shown in Fig. 5.2 (c), responsible for the smooth mushroom-shaped upset on the consumable rod [147].

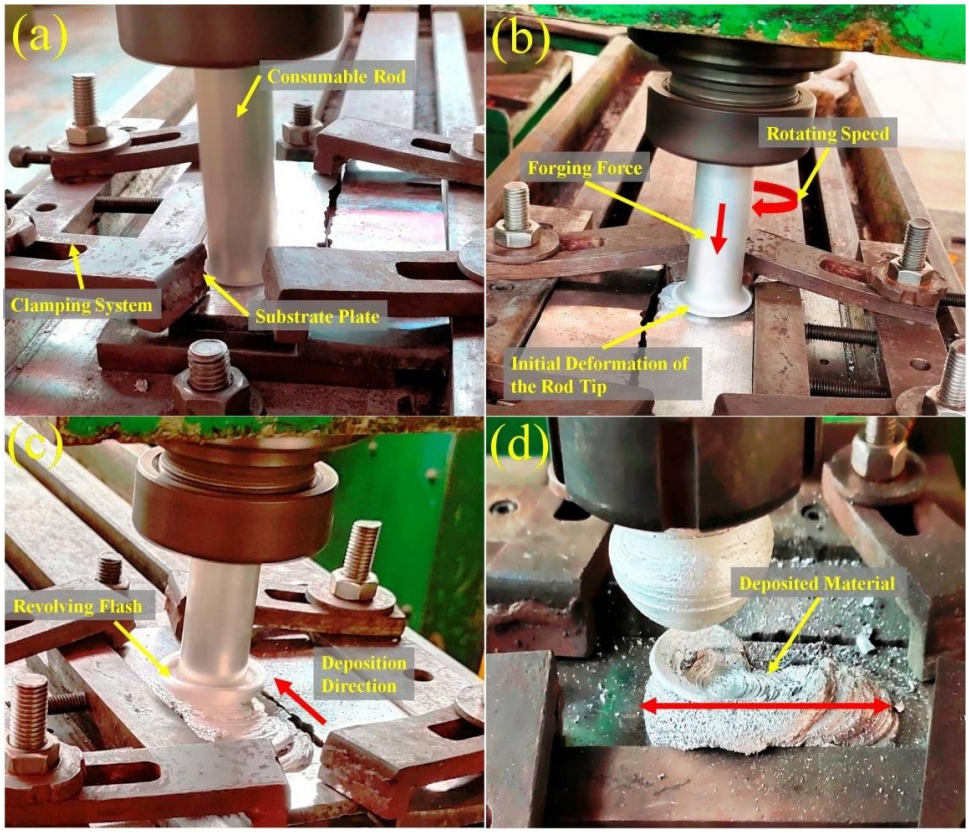

Fig. 5.2: (a) Deposition of AA6063 by friction; (a) Experimental setup; (b) Initial plunging phase; (c) Deposition; (d) Deposited material.

The deposits formed by FSD at optimized process parameters are shown in Fig. 5.3 (a-f). The curve wave markings indicate the consumable rod's deposition direction and clockwise movement of material during deposition. Wave markings may be seen on the surface of all deposits, which is an intrinsic feature of the FSD process. The type of material transport is related to surface roughness and the creation of wave markings. The plasticized metal is applied in separate layers in an elliptical pattern, one after other. This shows that the substrate's union process proceeds from advancing to the retreating side. In all mixture filling hole profile procedures shown by a red line, adequate height and length of the deposits are attained. This demonstrates that the substance is adequately bonded to the substrate.

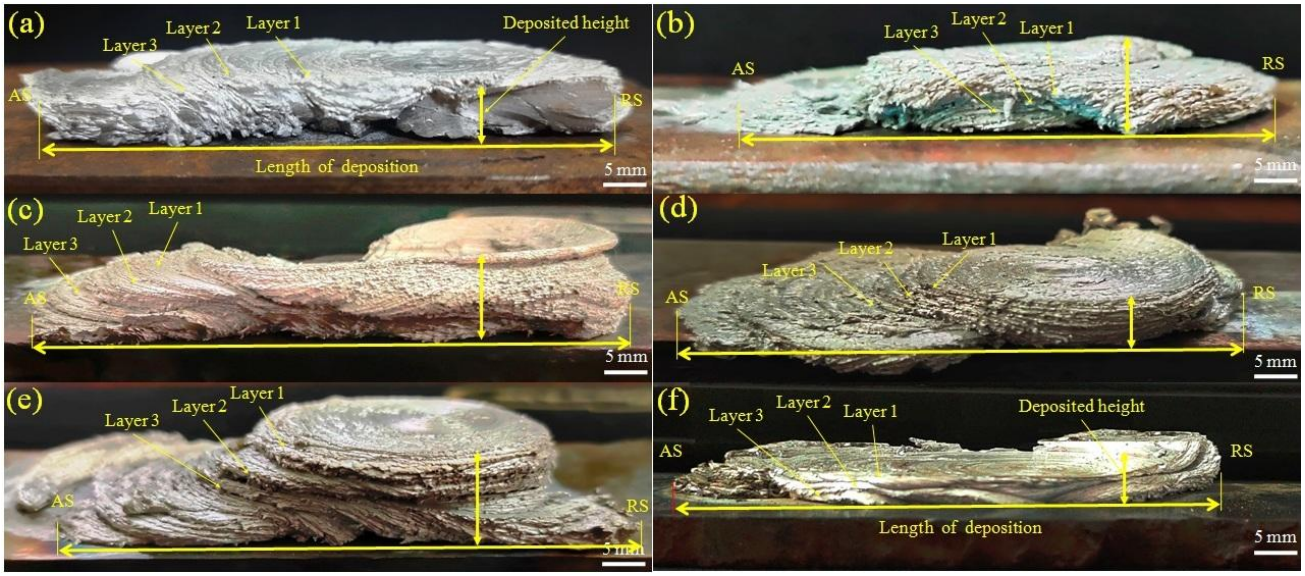

Fig. 5.3: Successive deposition by FSD using; (a) 1 hole, (b) 2 hole, (c) 3 hole, (d) 4 hole, (e) 5 hole and (f) 6 hole consumable rods

Once the deposits are produced, at least three precursors are retrieved from each FSD zone. As illustrated in Fig. 5.4, the precursors (about 10 x 10 x 10 mm size) are retrieved from each

experiment from beginning, middle, and end. These locations are chosen to check the mixture distribution uniformity over the FSD zone.

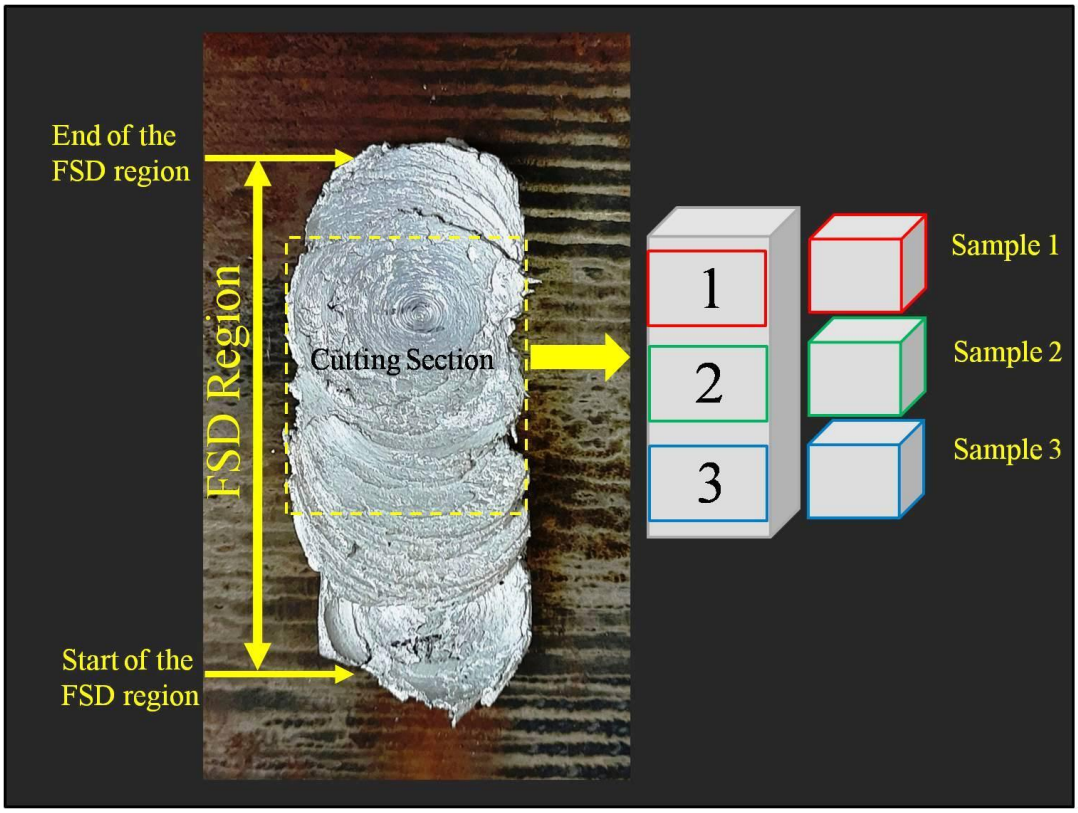

Fig. 5.4: Sample extraction from the FSD region

5.4 Characterization of Samples

To observe the distribution of foaming agent in the processed zone, optical microscopy and scanning electron microscopy (SEM, JSM-6510) are employed to study the macrostructure and microstructure of AA6063 precursors. To polish the retrieved samples, abrasive sheets of various grits are utilized. The samples are then etched with a modified Keller's reagent to show the deposited material's macrostructure. A K type thermocouple with an Extech (SDL200) data collection device with a temperature range up to 800^0C is used to monitor the temperature and

assess the heat generation effect during the FSD. Using a Vickers micro-hardness tester (manufactured by Omni tech Mvh1, India) with a load of 0.98 N for 20 seconds, the microhardness of deposited and base material is determined. Finally, the compressive strength of the produced foam samples is optimized based on pore size and porosity. The produced foam samples' pore size distribution is calculated using the software 'ImageJ,'.

5.5 Material Flow Analysis

In the deposited zone (DZ), the microstructure assisted in characterizing the distribution of foamable mixture particles/material flow. The flow pattern of material in the shape of onion rings in the DZ is apparent in all rod profiles, as demonstrated in Fig. 5.5 (a-f). In all microstructures, the material flow is observable with the foamable mixture. The microstructure of the DZ of the one hole profile rod deposition is shown in Fig. 5.5 (a). In the middle of the deposits, the microstructure displays a lot of mixture clustering (marked as black colour). This occurs because the whole mixture is present in the rod profile's centre. During deposition, the rod profile covers the less stirring area for mixture distribution, resulting in a significant quantity of mixture particles in a localized location. The clustering of the mixture is decreased following the deposition of two and three-hole profiles in the rod, as seen in Fig. 5.5 (b and c). Adjusting the hole position in the rod profile enhanced the outcomes of mixture dispersion because it covers the greater area for distribution during deposition. As shown in Fig. 5.5 (d), a four-hole profile in the rod produces homogeneous mixture mixing compared to a lower hole profile in the rod. Defects in the processing zone have been discovered when the number of holes is increased to more than four (5 and 6 holes) due to inadequate material processing in the stir zone, as illustrated in Fig. 5.5 (e and f). A more homogeneous distribution ensures more spherical pores.

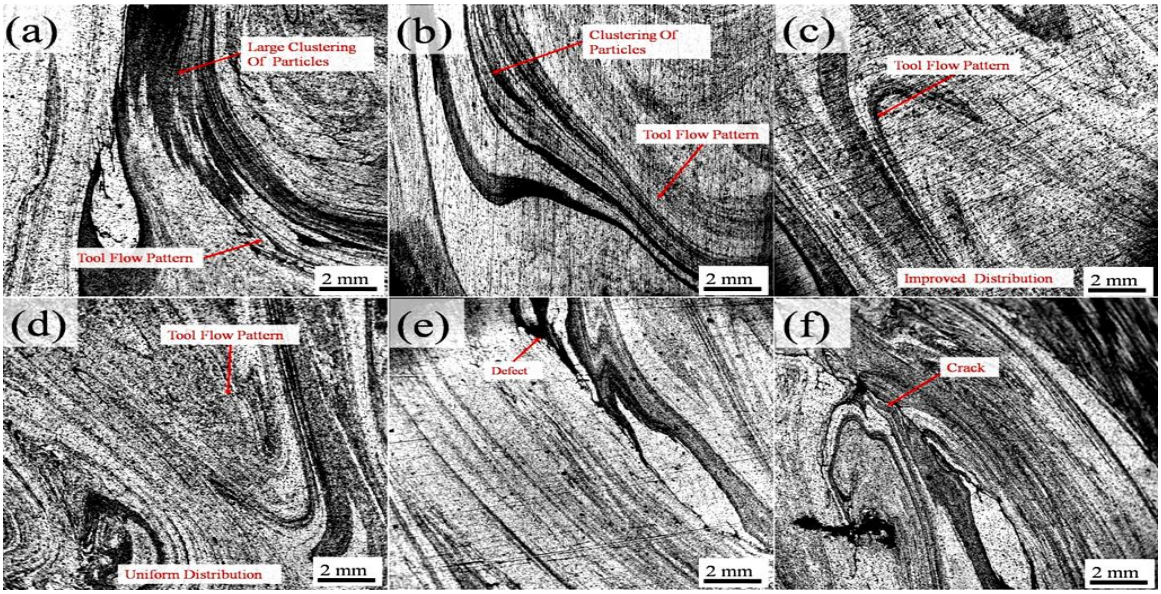

Fig. 5.5: Material flow pattern of ; (a) 1, (b) 2, (c) 3, (d) 4, (e) 5 and (f) 6 hole profile rods during FSD process

5.5.1 Scanning electron microscope (SEM):

To examine the microstructural changes in DZ, different mixture-filled hole profile rods are also subjected to SEM analysis. Based on the findings of the optical microscope examination, three different hole profile (4, 5 and 6 holes) rods are selected to obtain the material flow patterns and microstructure of the deposited material. The results of the SEM study are comparable to those of the optical microscope. The more uniform material flow pattern is visible in the 4 hole rod samples at low magnification as shown in Fig 5.6 (a). The SEM analysis shows that as the number of hole increases more than four (5 holes) then crack like defects observed in the DZ (Fig. 5.7 (b)). As the number of holes increases more than five, large defects like cavities are observed in the DZ as shown in Fig. 5.6 (c). From these result it is observed that the four-hole rod profile offers more consistent results due to the homogeneous mixing of the foaming agent.

5.6 Microstructure Analysis

Fig. 5.7 (a) depicts a deposited section of a four-hole rod profile after FSD. Three separate areas are chosen to examine the microstructural evolution of the rod during processing: the advancing side, centre, and retreating side. Fig. 5.7 (b) depicts the microstructure of the consumable material (AA6063) before processing in its as-received state. The consumable rod undergoes thermomechanical changes during deposition, resulting in a reduction in the grain size of the deposited material. Fine-grain morphology on the advancing (AS), central region, and retreating sides (RS) of Fig. 5.7 (c-e) demonstrates minor differences in grain size between deposited layers. The typical microstructure of refined grains is a property of the deposits, which occurs due to heat and deformation, allowing dynamic recrystallization of the material to appear, where the original set of deformed grains gives rise to a group of new equiaxial grains.

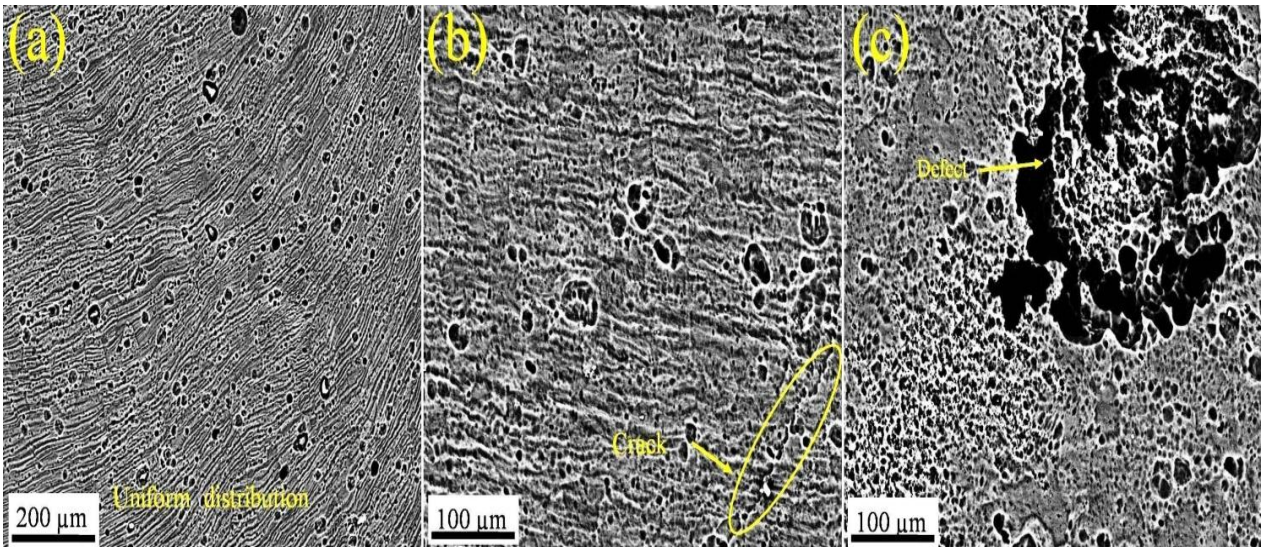

Fig. 5.6: SEM images of material flow pattern of; (a) showing flow pattern, (b) crack in the processed zone with five holesand (c) cavity like defect in processed zone with 6 hole profile rods

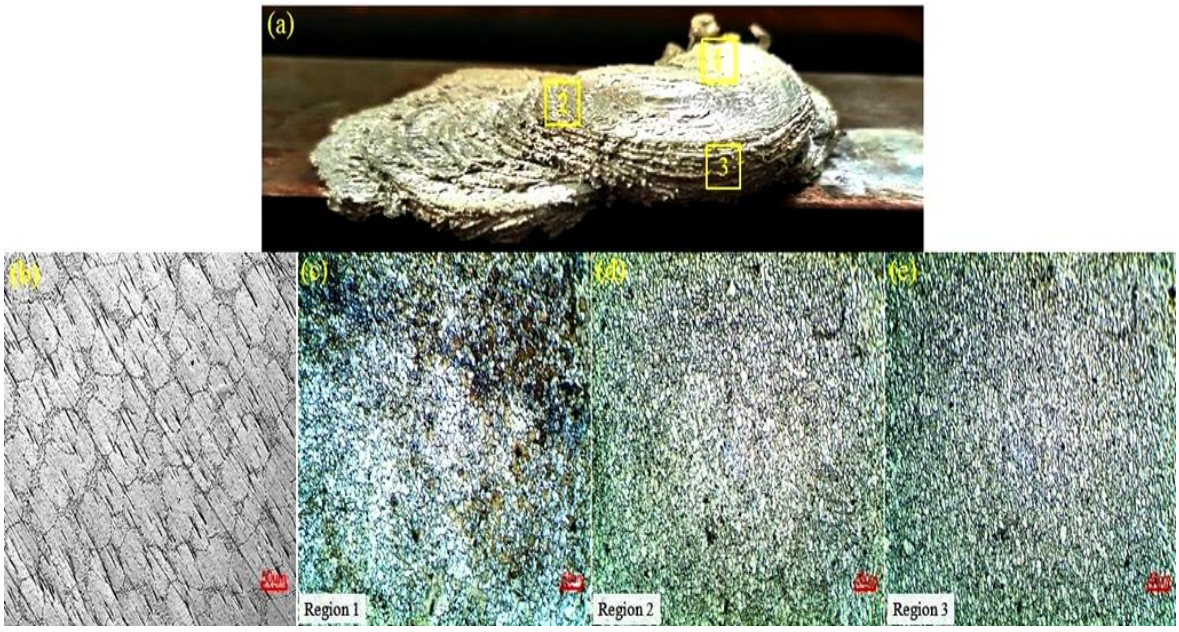

Fig. 5.7: (a) The deposits four-hole profile sample showing the (b) microstructure of the AA6063 consumable rod in its as-received condition, (c) the microstructure of the advancing side, (d) centre portion and (e) retreating side

5.6.1 Scanning electron microscope (SEM):

SEM analysis of the DZ section is also done to check the verify for microstructure alterations that result from deposition. The microstructure of four-hole rod profile deposited section from two locations (location 1 and location 3 from Fig. 5.7 (a)) is taken. Fig. 5.8 (a) shows the microstructure taken from advancing side of deposited material and Fig. 5.8 (b) shows the microstructure from retreating side. The microstructure of deposited material reviles that the during friction stir deposition, thermo-mechanical processing reduces the grains size of the deposited material. Fine-grain morphology is observed because the original set of large grains in the extruded rod gives way to a new group of small equiaxial grains during the processing.

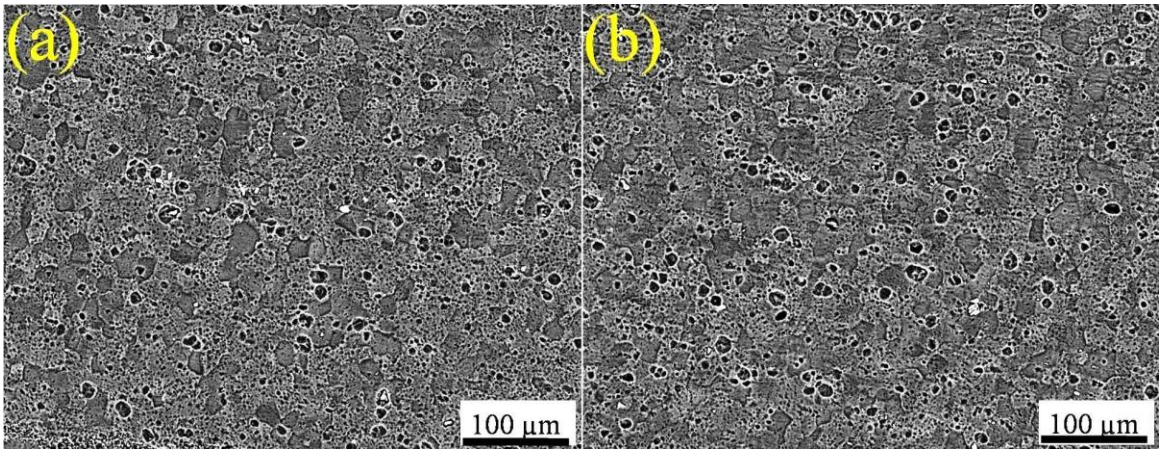

Fig. 5.8: SEM microstructure of the deposits of four-hole profile sample taken from (a) location 1 and (b) location 3 as shown in the Fig. 5.7

5.7 Energy Dispersive Spectroscopy (EDS) Analysis

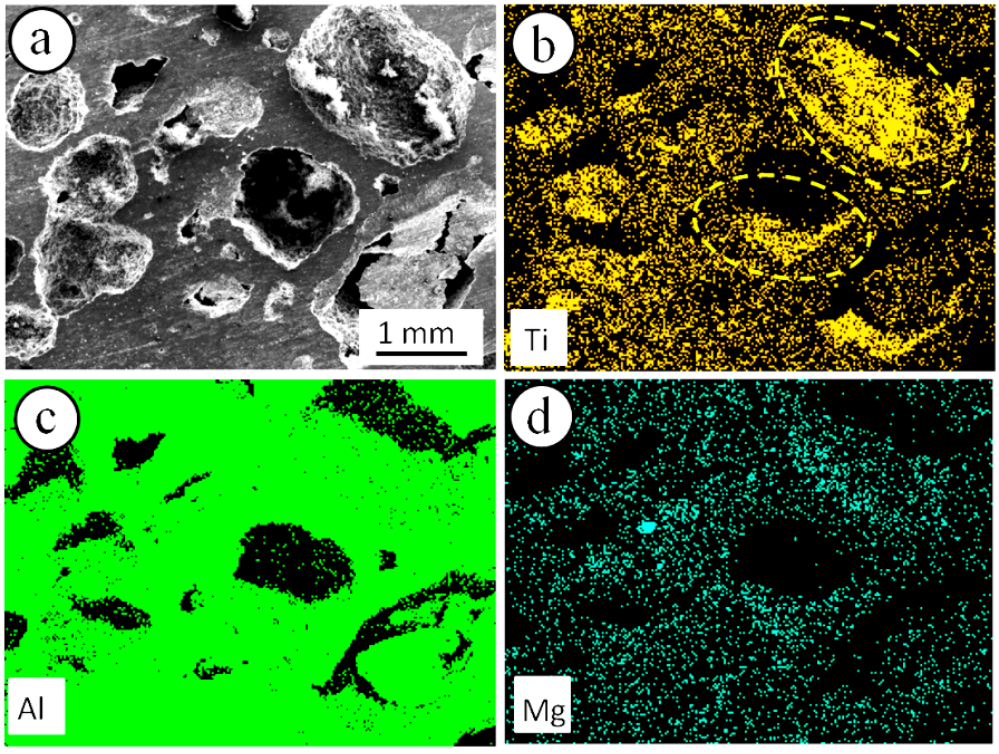

Fig. 5.9: Mapping of different alloying elements using EDS

The elemental mapping is done to see the distribution of different elements in the developed foam 5.9 (a-d). The SEM images of the sample used for EDS analysis is shown in Fig. 5.9 (a). It is observed that Ti element segregated nearby the big pores as observed and circled in Fig. 5.9 (b). It represents segregation of TiH_2 at that location during deposition which further decomposes during heating and produces high amount of gases to form big pores. The other alloying elements of the Aluminium matrix are uniformally distributed thorougout the foam as observed in Fig. 5.9 (c and d).

5.8 Hardness Behavior of Precursors

The hardness values of the deposits carried out with one to six holes in the rod are approximately 40-51 HV, as shown in Fig. 5.10, but the hardness of as-received state consumable rod is 76.04 HV. The hardness values were tested along the length of the deposits, from left to right, at various points with a 0.5 mm spacing interval. The hardness values of the deposits are lower than the consumable rod's hardness values because of the heat generated during the process, the drop in hardness values in the deposits is more prominent in the central area, which provides the circumstances for recovery and recrystallization events of the deformed grains in the rolling direction. This may impact the microstructural properties in this area, directly impacting the hardness values [148]. The results reveal that the hardness values of all six processing conditions are almost same. Still, the difference is due to other factors such as microstructure and the existence of defects, which can influence the hardness values in each deposit.

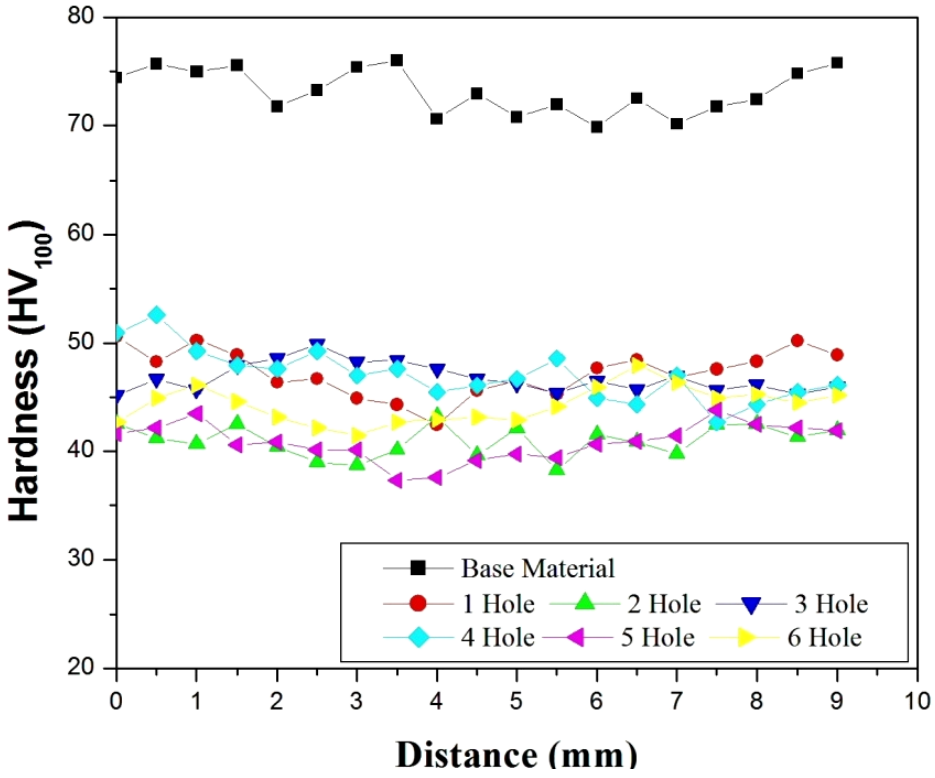

Fig. 5.10: Microhardness profile of base material and the deposits

5.9 Temperature Evaluation during FSD

The temperature distribution in DZ resulting from material flow and plastic deformation should be evident. This heat plastifies the substance and causes it to bind with other. There is no melting involved in the process. The temperature of the friction region is predicted using the measurement of heat during deposition. As shown schematically in the Fig. 5.11 (a). The temperature evolution surrounding the rod throughout the deposition process is depicted in Fig. 5.11 (b-g). The upward slope represents a heating curve in the graph, while the downward slope represents a cooling curve. Although all rod profiles covered the same area for deposition during stirring, the plastic deformation of the material differed due to the holes in the rod. The

temperature graphs may be used to compare the temperature changes caused by different hole profiles in the rod during FSD.

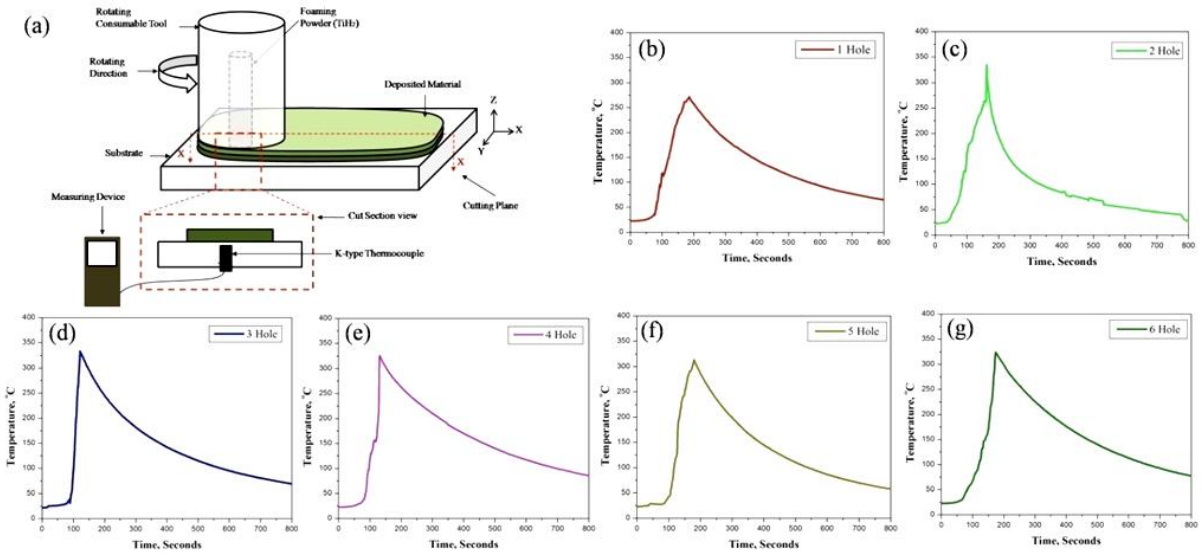

Fig. 5.11: (a) Sectional View of thermocouple and temperature generation during FSD process of: (b) 1 hole, (c) 2 hole, (d) 3 hole, (e) 4 hole, (f) 5 hole and (g) 6 hole

5.10 Foam Structure

Using the furnace heating technique, the precursor developed by the FSD process is heat-treated for foam development, the foam developed samples are shown in Fig. 5.12 (a-f) with binary images. The binary images show the distribution of the pores on the surface of the foam sample. Fig. 5.12 (a) shows a developed foam sample deposited by one hole rod. In the image, a bigger size hole (highlighted in yellow circled) is visible in the foam, which shows the clustering of the foaming particles at a particular location. This happens because a single hole is present at the centre of the rod, and the foaming material is not distributed from inside to the outer side of the processed area. The mixture's clustering decreases following the deposition of two and three holes in the rod, as seen in Fig 5.12 (b and c), because it covers the greater area for distribution

of material during deposition. By increasing the number of holes in the rod, some improved results in material distribution are obtained. As shown in Fig. 5.12 (d and e), four and five holes in the rod produce homogeneous mixture mixing compared to a lower hole profile. This results in uniform distribution of foaming material and reduced particle clustering. The binary images of the foam samples also show that the pores are uniformly distributed throughout the sample and cover the maximum area.

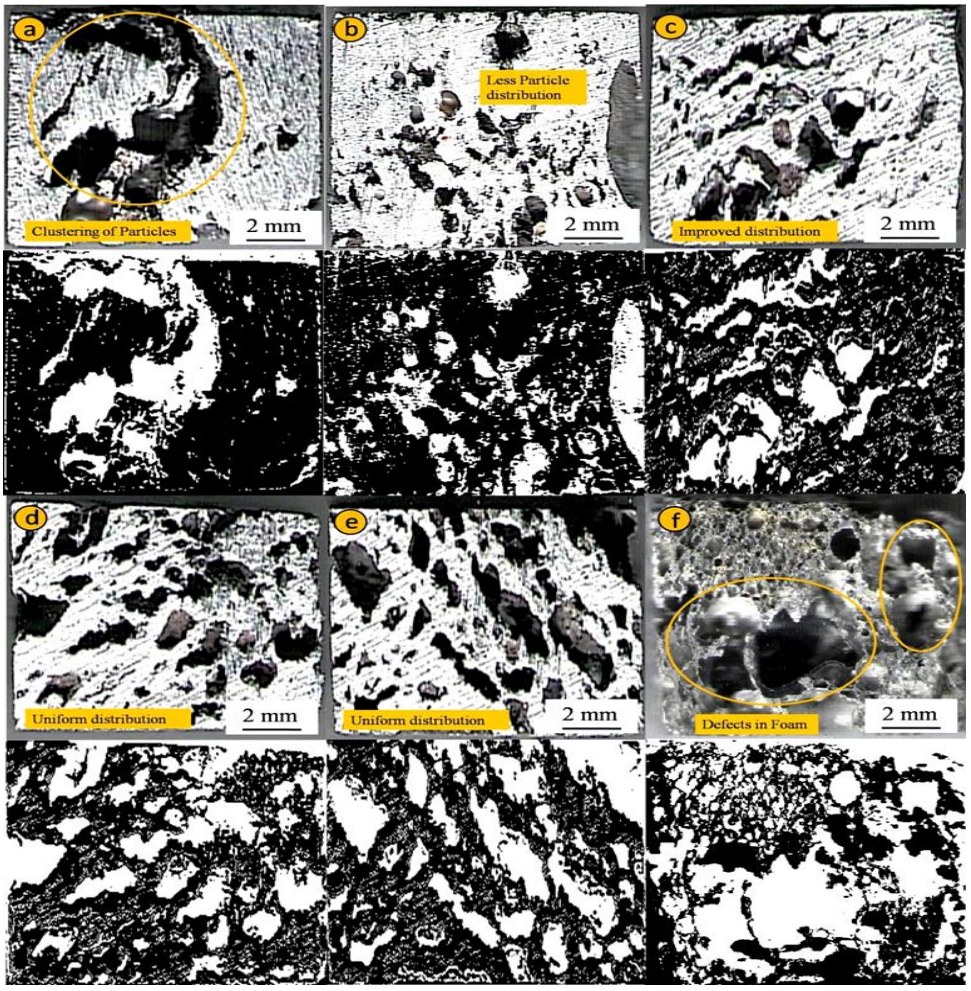

Fig. 5.12: Foam samples with their binary images developed by the FSD process using: (a) 1 hole, (b) 2 hole, (c) 3 hole, (d) 4 hole, (e) 5 hole and (f) 6 hole in the rod

When the number of holes increased to more than five, the defects in the developed foam were seen (highlighted in yellow circled), as shown in Fig. 5.12 (f). By drilling the six holes in the rod, the quantity of the foamable mixture is more in the rod than the Aluminium matrix. Due to this, a small pores are merged and creates large holes, decreasing the foam's absorbing capacity. A more homogeneous distribution ensures more spherical pores. Due to the homogeneous mixing of the foaming agent, the four and five holes rod is predicted to offer more consistent results after viewing the developed foam samples of the deposits.

5.11 Stress-Strain Curve of Developed Foam Samples of FSD Technique

Compression tests are the most common mechanical testing methods for evaluating foams' compressive behaviour and energy absorption capacity. Gibson and Ashby present a comprehensive overview of the mechanical behaviour of cellular solids [149]. The compression behaviour of these Al foams is influenced by several factors like pore size, alloy composition, and defects present in the foam structure. The three samples of less pores, average pores and maximum pores are selected for the compression test, obtained at 3, 4 and 5 holes in the rod.

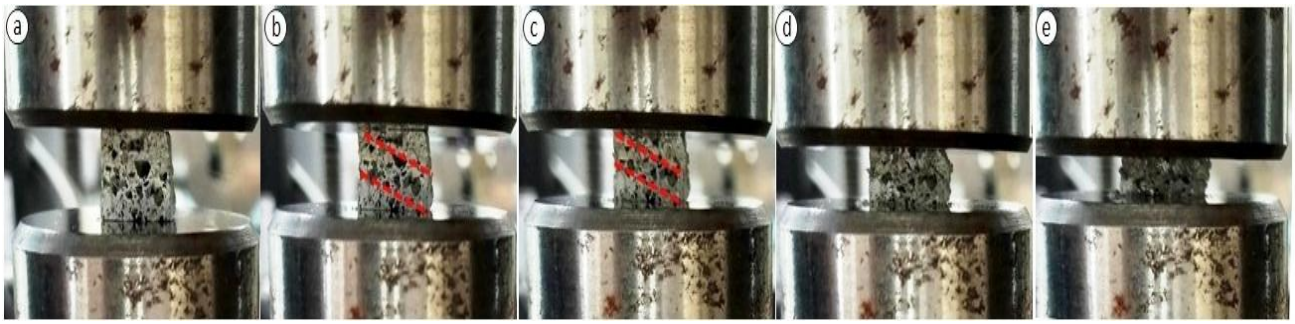

Fig. 5.13: Deformation of the foam during compression; (a) 0 %, (b) 10 %, (c) 20 %, (d) 40 % and (e) 60 %

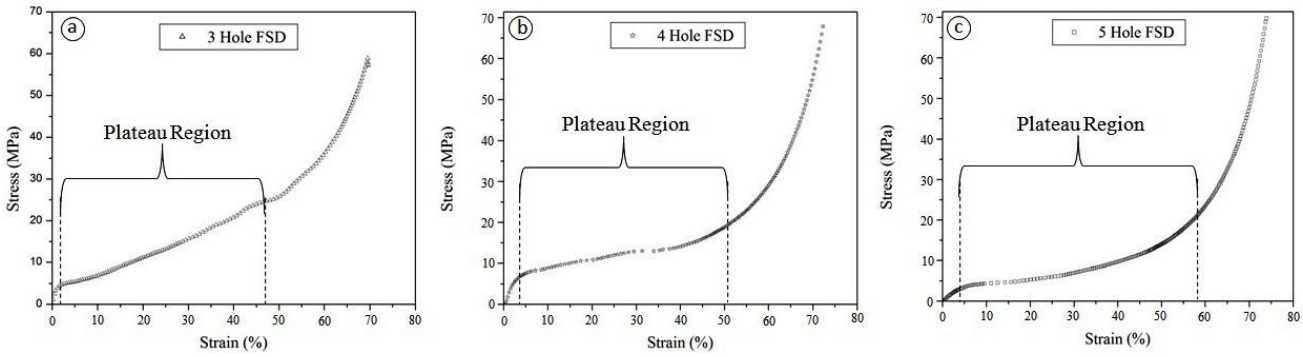

Fig. 5.14: Stress-strain diagram of foam developed in different conditions: (a) 3 holes, (b) 4 hole and (c) 5 holes

A compression test has been done on a constant strain rate of 1 mm/sec and the stress-strain behaviour has been obtained. The deformation pattern of sample in compression test is presented in Fig 5.13. This figure shows the deformation at different stages of the samples from 0 to 60 % in the image 5.13 (a-e). The compression test shows three stages of deformation [150]. In the first stage deformation start faster due to initial required stress for deformation of structure. The second stage is constant deformation zone where strain increases without increasing stress due to the deformation of foam cell walls. This deformation is observed during the second stage of compression test in form of a band as shown in Fig 5.13 (b and c). The second region shows the stable deformation range and called as plateau zone as observed in the stress-strain graph in Fig. 5.13. This plateau stress is an important property for the compression performance of foam and is used to define its energy absorption behaviour. The third stage is densification stage which causes increase in stress with strain. The average stress of plateau zone can be used to indicate the deformation behaviour of foam. Also, the length of this zone is taken as deformation range of foam [151]. It is observed that the foam developed with 3 number of hole has very less first stage whereas the slope gets increases in second stage which shows densification of foam with

increasing strain. The foam developed with 4 and 5 holes deposited rod has large plateau zone shows constant deformation of foam. But the range of this zone is larger in 4 holes as compare to 5 holes deposits. The reason of this is that the plateau deformation depends on the pores distribution, pores size and the wall thickness in between pores. As the number of pores increase, the plateau stress increases up to certain limit then decreases. This is because an optimum wall thickness is required for larger deformation. This phenomenon is also observed in this research that as the pores are less and wall thickness are more as in 3 holes deposited foam, the deformation causes increase in stress with strain. As increasing the number of pores in 4 and 5 holes deposit, the plateau zone is uniform because of lower wall thickness and proper distribution of pores. But little bit variation has been observed in the first stage of deformation and the length of plateau stress which is due to variation in pores in these samples.

Chapter 6: Conclusions and Scope for Future Work

6.1 Conclusions

1. The three different filling techniques have been successfully used for the development of foam. Based on the characteristic of the developed foam, it has been observed that the distribution of foamable mixture improved in the buried hole technique by restrict the mixture to flow away and produce a porous Aluminium with a porosity of approximately 81% at 4-passes with 40% TiH_2 composition.
2. As the number of FSP passes increases, pore size decreases and this decreasing % of pore size from one pass to four passes is observed at 17.78 % in the microwave heating and 14.76 % in furnace heating.
3. The results observed that the porosity in sandwich and groove techniques is 69% and 48%, respectively. The buried hole technique has 17.92% and 71.25% higher porosity as compared to sandwich and groove techniques, respectively. More the porosity, more is the foam quality.
4. It takes only 90 sec to develop the foam in a domestic microwave as compare to 15 min of a furnace heating. Hence, 83.33 %age of time saving may be observed during new heating method i.e. microwave heating.
5. The distribution of the foaming mixture improves with continuous material deformation by straight threaded cylindrical (STC) tool pin compared to the pulsating effect produced by square (SQ) and triangular (TR) pin.
6. Hardness is lowest in the weld nugget with straight threaded cylindrical (STC) pin due to higher deformation and thus, higher heat generation.
7. The developed foam with straight threaded cylindrical (STC) shows uniform distribution of pores of similar size which shows uniform foaming properties throughout structure. Whereas, square (SQ) and triangular (TR) pin shows big pores at the certain location due to segregation of foamable mixture during pulsating action of tool pin in the stir zone.
8. The foam developed at straight threaded cylindrical (STC) pin shows uniform deformation behavior during compression test than the foam developed by other tool profiles. Also,

almost constant plateau stress has been obtained in straight threaded cylindrical (STC) pin profile causes better foaming properties.

9. The friction stir deposition (FSD) technique shows uniform distribution of foaming powder in more numbers of holes in the consumable rod. The hardness of the deposited precursor is lower than the base metal which lies in range of 38-53 HV.
10. The microstructure of the deposited material during FSD shows equiaxed fine grains which occurred due to dynamic recrystallization during deposition. The foam developed with more number of holes has longer plateau stress due to optimum pore size which absorb energy at longer duration.

6.2 Scope for Future Work

As friction stir process requires less energy, hence it can be regarded as the sustainable technique for the foam fabrication in the future era of green technology. This study presented the analysis and investigations of the effects of various input parameters on the density and mechanical behavior of the Aluminium metal foam. The Alloy used in this study was Aluminum 6063 and 7075 but other variant of Aluminium alloys can also be used to produce foam. Also, the materials other than Aluminium is also required to explore for development of foam such as composite and functionally graded materials [152, 153].

From the research point of view, the particle size of stabilizing agent and blowing agent can be varied and its effect may be analyzed for development of better foam performance.

The cell wall composition after foaming is different than the parent metal because of the reaction at high temperatures. An intricate micro structural analysis can be performed in order to ascertain the phases and intermetallic formed in the cell wall, leading to the analysis of micro deformation mechanisms during compressive loading. This can be used as a research objective in a separate study.

Future studies can utilize this technique for bulk foam formation and fabrication of foam filled parts used in heavy duty machines for shock and vibration absorption.

REFERENCES

[1] N. Kumar, P. K. Jain, P. Tandon, and P. M. J. M. T. P. Pandey, "Experimental investigations on suitability of polypropylene (PP) and ethylene vinyl acetate (EVA) in additive manufacturing," vol. 5, no. 2, pp. 4118-4127, 2018.

[2] D. Singh *et al.*, "Experimental assessment of biomechanical properties in human male elbow bone subjected to bending and compression loads," vol. 17, no. 2, p. 2280800018793816, 2019.

[3] V. Srivastava and K. J. I. M. N. Sahoo, "Metallic foams: current status and future prospects," vol. 9, no. 4, pp. 9-13, 2006.

[4] Y. Cheng, Y. Li, X. Chen, X. Zhou, N. J. J. o. M. E. Wang, and Performance, "Compressive properties and energy absorption of aluminum foams with a wide range of relative densities," vol. 27, pp. 4016-4024, 2018.

[5] B. Zhao, A. K. Gain, W. Ding, L. Zhang, X. Li, and Y. J. T. I. J. o. A. M. T. Fu, "A review on metallic porous materials: pore formation, mechanical properties, and their applications," vol. 95, pp. 2641-2659, 2018.

[6] A. Kennedy, "Porous metals and metal foams made from powders," *Powder Metallurgy,* vol. 2, pp. 31-46, 2012.

[7] L. P. Lefebvre, J. Banhart, and D. C. J. A. e. m. Dunand, "Porous metals and metallic foams: current status and recent developments," vol. 10, no. 9, pp. 775-787, 2008.

[8] J. David Raja Selvam, I. Dinaharan, P. J. T.-M. Mashinini, Surfaces, and Interfaces, "High temperature sliding wear behavior of AA6061/fly ash aluminum matrix composites prepared using compocasting process," vol. 11, no. 1, pp. 39-46, 2017.

[9] M. Durante, A. Formisano, A. Viscusi, and L. J. T. I. J. o. A. M. T. Carrino, "An innovative manufacturing method of aluminum foam sandwiches using a mesh-grid reinforcement as mold," vol. 107, pp. 3039-3048, 2020.

[10] E. Koza, M. Leonowicz, S. Wojciechowski, and F. J. M. l. Simancik, "Compressive strength of aluminium foams," vol. 58, no. 1-2, pp. 132-135, 2004.

[11] F. García-Moreno, "Commercial applications of metal foams: Their properties and production," *Materials,* vol. 9, no. 2, p. 85, 2016.

[12] S. Chen, J. Marx, and A. Rabiei, "Experimental and computational studies on the thermal behavior and fire retardant properties of composite metal foams," *International Journal of Thermal Sciences,* vol. 106, pp. 70-79, 2016.

[13] N. Dukhan, *Metal foams: fundamentals and applications*. DEStech Publications, Inc, 2013.

[14] F. J. M. García-Moreno, "Commercial applications of metal foams: Their properties and production," vol. 9, no. 2, p. 85, 2016.

[15] J. Banhart, "Manufacture, characterisation and application of cellular metals and metal foams," *Progress in materials science,* vol. 46, no. 6, pp. 559-632, 2001.

[16] I. Duarte and J. Banhart, "A study of aluminium foam formation—kinetics and microstructure," *Acta materialia,* vol. 48, no. 9, pp. 2349-2362, 2000.

[17] K. Kitazono, E. Sato, and K. Kuribayashi, "Novel manufacturing process of closed-cell aluminum foam by accumulative roll-bonding," *Scripta Materialia,* vol. 50, no. 4, pp. 495-498, 2004.

[18] M. Banea and L. F. da Silva, "The effect of temperature on the mechanical properties of adhesives for the automotive industry," *Proceedings of the Institution of Mechanical Engineers, Part L: Journal of Materials: Design and Applications,* vol. 224, no. 2, pp. 51-62, 2010.

[19] T. Miyoshi, M. Itoh, S. Akiyama, and A. Kitahara, "ALPORAS aluminum foam: production process, properties, and applications," *Advanced Engineering Materials,* vol. 2, no. 4, pp. 179-183, 2000.

[20] R. S. Mishra, M. Mahoney, S. McFadden, N. Mara, and A. Mukherjee, "High strain rate superplasticity in a friction stir processed 7075 Al alloy," *Scripta materialia,* vol. 42, no. 2, pp. 163-168, 1999.
[21] S. Rathee, M. Srivastava, S. Maheshwari, T. Kundra, and A. N. Siddiquee, *Friction based additive manufacturing technologies: principles for building in solid state, benefits, limitations, and applications*. CRC Press, 2018.
[22] R. Kumar, R. Singh, I. Ahuja, M. J. A. i. M. Hashmi, and P. Technologies, "Friction-stir-spot welding of 3D printed ABS and PA6 composites: flexural, thermal and morphological investigations," vol. 8, no. 1, pp. 909-916, 2022.
[23] S. Haro-Rodríguez *et al.*, "On influence of Ti and Sr on microstructure, mechanical properties and quality index of cast eutectic Al–Si–Mg alloy," vol. 32, no. 4, pp. 1865-1871, 2011.
[24] J. D. R. Selvam, I. Dinaharan, S. V. Philip, P. J. J. o. A. Mashinini, and Compounds, "Microstructure and mechanical characterization of in situ synthesized AA6061/(TiB2+ Al2O3) hybrid aluminum matrix composites," vol. 740, pp. 529-535, 2018.
[25] M. Arulraj, J. Davim, M. J. A. i. M. Hashmi, and P. Technologies, "Prediction of tensile strength in squeeze casted hybrid aluminium matrix composites using conventional statistical approach," vol. 8, no. 2, pp. 2216-2228, 2022.
[26] Y. Hangai and T. Utsunomiya, "Fabrication of porous aluminum by friction stir processing," *Metallurgical and Materials Transactions A,* vol. 40, no. 2, pp. 275-277, 2009.
[27] N. Sharma, A. N. Siddiquee, Z. A. Khan, M. T. J. M. Mohammed, and M. Processes, "Material stirring during FSW of Al–Cu: Effect of pin profile," vol. 33, no. 7, pp. 786-794, 2018.
[28] M. Azizieh, A. Kokabi, and P. Abachi, "Effect of rotational speed and probe profile on microstructure and hardness of AZ31/Al2O3 nanocomposites fabricated by friction stir processing," *Materials & Design,* vol. 32, no. 4, pp. 2034-2041, 2011.
[29] S. Rathee, S. Maheshwari, A. N. Siddiquee, and M. Srivastava, "Analysis of microstructural changes in enhancement of surface properties in sheet forming of Al alloys via friction stir processing," *Materials Today: Proceedings,* vol. 4, no. 2, pp. 452-458, 2017.
[30] C. Langlade, A. Roman, D. Schlegel, E. Gete, and M. Folea, "Formation of a tribologically transformed surface (TTS) on AISI 1045 steel by friction stir processing," *Materials and manufacturing processes,* vol. 31, no. 12, pp. 1565-1572, 2016.
[31] S. Rathee, S. Maheshwari, A. N. Siddiquee, M. Srivastava, and S. K. Sharma, "Process parameters optimization for enhanced microhardness of AA 6061/SiC surface composites fabricated via Friction Stir Processing (FSP)," *Materials Today: Proceedings,* vol. 3, no. 10, pp. 4151-4156, 2016.
[32] S. Rathee, S. Maheshwari, A. N. Siddiquee, and M. Srivastava, "Effect of tool plunge depth on reinforcement particles distribution in surface composite fabrication via friction stir processing," *Defence technology,* vol. 13, no. 2, pp. 86-91, 2017.
[33] F. Baumgärtner, I. Duarte, and J. Banhart, "Industrialization of powder compact foaming process," *Advanced Engineering Materials,* vol. 2, no. 4, pp. 168-174, 2000.
[34] I. Papantoniou, D. Pantelis, and D. J. P. S. I. Manolakos, "Powder metallurgy route aluminium foams: A study of the effect of powder morphology, compaction pressure and foaming temperature on the porous structure," vol. 10, pp. 243-248, 2018.
[35] S. Haro, J. Ramírez, D. K. Dwivedi, E. J. M. S. Martínez, and Technology, "Influence of solutionising and aging temperatures on microstructure and mechanical properties of cast Al–Si–Cu alloy," vol. 25, no. 7, pp. 886-891, 2009.
[36] G. Marinzuli, L. A. C. De Filippis, R. Surace, and A. D. J. P. M. S. Ludovico, "Effect of processing parameters on morphology and plateau stress of AlSi and AlSiMg foams," vol. 4, pp. 121-126, 2014.

[37] J. Banhart, "Light-metal foams—history of innovation and technological challenges," *Advanced Engineering Materials,* vol. 15, no. 3, pp. 82-111, 2013.
[38] S. Singh and N. Bhatnagar, "A survey of fabrication and application of metallic foams (1925–2017)," *Journal of Porous Materials,* vol. 25, no. 2, pp. 537-554, 2018.
[39] S. Benjamin, "Process for making foamlike mass of metal," ed: Google Patents, 1948.
[40] J. C. Elliott, "Method of producing metal foam," ed: Google Patents, 1956.
[41] S. O. Fiedler, J. A. Bjorksten, and W. S. Fiedler, "Method of foaming granulated metal," ed: Google Patents, 1961.
[42] G. H. Erb, "Method for shaping products made of foam metal by progressive localized crushing of foam structure," ed: Google Patents, 1971.
[43] C. B. B. Jr, "Foamed metal " Patent U.S. Patent, 3,671,221, 1972.
[44] C. J. L Niebylsk, "Lead-zinc foams ", ed: Google Patent, 1974.
[45] L. M. Niebylski, C. P. Jarema, and T. E. Lee, "Reinforced foamed metal," ed: Google Patents, 1976.
[46] B. Kendall, "Vacuum applications of metal foams," *Journal of Vacuum Science and Technology,* vol. 17, no. 6, pp. 1385-1385, 1980.
[47] G. Davies and S. Zhen, "Metallic foams: their production, properties and applications," *Journal of Materials science,* vol. 18, no. 7, pp. 1899-1911, 1983.
[48] F. H. Cocks, "Ultralight reactive metal foams in space-A novel concept," *Journal of Spacecraft and Rockets,* vol. 21, no. 5, pp. 510-512, 1984.
[49] I. Jin, L. D. Kenny, and H. Sang, "Method of producing lightweight foamed metal," ed: Google Patents, 1990.
[50] C. Chen and R. Lakes, "Holographic study of conventional and negative Poisson's ratio metallic foams: elasticity, yield and micro-deformation," *Journal of Materials science,* vol. 26, no. 20, pp. 5397-5402, 1991.
[51] R. Clancy, J. Cochran, and T. Sanders, "Fabrication and properties of hollow sphere nickel foams," *MRS Online Proceedings Library (OPL),* vol. 372, 1994.
[52] W. Knott, B. Niedermann, M. Recksik, and A. Weier, "Process for producing metal foam and metal body produced using this process," ed: Google Patents, 2005.
[53] F. Dobesberger, H. Flankl, and D. Leitlmeier, "Process and device for manufacturing free-flowing metal foam," ed: Google Patents, 2006.
[54] D. C. Dunand and A. Bansiddhi, "Method of making metallic foams and foams produced," ed: Google Patents, 2010.
[55] T. U. Y Hangai, "Using friction stir processing to form foamed metal precursors," ed: Google, Patent, 2010.
[56] A. Jung, H. Natter, R. Hempelmann, and E. Lach, "Metal foams," *EP,* vol. 2261398, p. A1, 2009.
[57] J. Banhart and F. Garcia-Moreno, "Method for the powder-metallurgical production of metal foamed material and of parts made of metal foamed material," ed: Google Patents, 2013.
[58] N. Babcsán, S. Beke, and P. Makk, "Method of producing a metal foam by oscillations and thus obtained metal foam product," ed: Google Patents, 2015.
[59] B. H. Reesink, "Open-celled, porous shaped body for heat exchangers," ed: Google Patents, 2016.
[60] T. H. Wood, T. G. Wetzel, J. G. Luedke, and T. M. Tucker, "Combined surface cooler and acoustic absorber for turbomachines," ed: Google Patents, 2018.
[61] R. R. Aronsson, B. S. Iseard, and P. Kalal, "Method of manufacturing hybrid metal foams," ed: Google Patents, 2020.
[62] J. J. A. e. m. Banhart, "Metal foams: production and stability," vol. 8, no. 9, pp. 781-794, 2006.

[63] J. Banhart, F. García-Moreno, K. Heim, H.-W. J. L. W. f. D. Seeliger, Aerospace,, and Transportation, "Light-weighting in transportation and defence using aluminium foam sandwich structures," pp. 61-72, 2019.
[64] M. F. Ashby *et al.*, "Metal foams: a design guide," vol. 54, no. 6, pp. B105-B106, 2001.
[65] L. J. J. M. B. Gibson, "Cellular solids," vol. 28, no. 4, pp. 270-274, 2003.
[66] J. J. J. Banhart, "Manufacturing Routes for Very Low Specific," vol. 52, pp. 22-27, 2000.
[67] A. J. P. M. Kennedy, "Porous metals and metal foams made from powders," vol. 2, pp. 31-46, 2012.
[68] J. Banhart, J. Baumeister, and M. Weber, "Powder metallurgical technology for the production of metallic foams," in *Proceedings of the European Conference on Advanced PM Materials*, 1995, vol. 201, p. 208.
[69] F. García-Moreno *et al.*, "The influence of alloy composition and liquid phase on foaming of Al–Si–Mg alloys," vol. 10, no. 2, p. 189, 2020.
[70] V. Pamidi, B. Muduli, and M. J. T. o. t. I. I. o. M. Mukherjee, "Al and Al-TiB 2 Foams Produced by Melt Injection Technique," vol. 73, pp. 191-198, 2020.
[71] K. Heim, G. Vinod-Kumar, F. García-Moreno, and J. J. J. o. M. S. Banhart, "Stability of various particle-stabilised aluminium alloys foams made by gas injection," vol. 52, pp. 6401-6414, 2017.
[72] F. Deng, Y. Liu, X. Lu, J. J. M. Fan, and M. International, "Improved stability of aluminum foam through heat treatment of foamable precursor," vol. 26, pp. 1596-1601, 2020.
[73] K. Kadoi, N. Babcsán, and H. J. M. t. Nakae, "Heat treatment of TiH2 powder to control decomposition phenomenon for aluminum foam fabrication by melt route," vol. 50, no. 4, pp. 727-733, 2009.
[74] S. Mahjoob, K. J. I. J. o. H. Vafai, and M. Transfer, "A synthesis of fluid and thermal transport models for metal foam heat exchangers," vol. 51, no. 15-16, pp. 3701-3711, 2008.
[75] K. Khan, P. Mahajan, and R. J. T. o. t. I. I. o. M. Prasad, "Synthesis and characterization of Al foam, Al alloy foam and Al-SiC composite foam," vol. 61, pp. 111-113, 2008.
[76] N. Mahmutyazicioglu, O. Albayrak, M. Ipekoglu, and S. J. J. o. M. R. Altintas, "Effects of alumina (Al2O3) addition on the cell structure and mechanical properties of 6061 foams," vol. 28, no. 17, pp. 2509-2519, 2013.
[77] Y. Hangai and T. Utsunomiya, "Using friction stir processing to form foamed metal precursors," ed: Google Patents, 2014.
[78] R. S. Mishra and Z. Ma, "Friction stir welding and processing," *Materials science and engineering: R: reports,* vol. 50, no. 1-2, pp. 1-78, 2005.
[79] B. Darras, M. Khraisheh, F. Abu-Farha, and M. J. J. o. m. p. t. Omar, "Friction stir processing of commercial AZ31 magnesium alloy," vol. 191, no. 1-3, pp. 77-81, 2007.
[80] Z. Ma, S. Sharma, R. J. M. S. Mishra, and E. A, "Effect of friction stir processing on the microstructure of cast A356 aluminum," vol. 433, no. 1-2, pp. 269-278, 2006.
[81] S. R. Sharma, Z. Ma, and R. S. J. S. M. Mishra, "Effect of friction stir processing on fatigue behavior of A356 alloy," vol. 51, no. 3, pp. 237-241, 2004.
[82] S. Rathee, S. Maheshwari, A. N. Siddiquee, M. J. C. R. i. S. S. Srivastava, and M. Sciences, "A review of recent progress in solid state fabrication of composites and functionally graded systems via friction stir processing," vol. 43, no. 4, pp. 334-366, 2018.
[83] V. Sharma, Y. Gupta, B. M. Kumar, U. J. M. Prakash, and M. Processes, "Friction stir processing strategies for uniform distribution of reinforcement in a surface composite," vol. 31, no. 10, pp. 1384-1392, 2016.
[84] A. Feng and Z. J. S. m. Ma, "Enhanced mechanical properties of Mg–Al–Zn cast alloy via friction stir processing," vol. 56, no. 5, pp. 397-400, 2007.

[85] M. Daneshifar, A. Papi, and M. J. M. L. Alishahi, "Fabrication of Al-Si/Mg2Si in-situ composite by friction stir processing," vol. 282, p. 128832, 2021.
[86] R. Shandley, S. Maheshwari, A. N. Siddiquee, S. Mohammed, and D. J. M. R. E. Chen, "Foaming of friction stir processed Al/MgCO3 precursor via flame heating," vol. 7, no. 2, p. 026515, 2020.
[87] R. Bauri, D. Yadav, C. S. Kumar, and G. J. J. D. i. b. Ram, "Optimized process parameters for fabricating metal particles reinforced 5083 Al composite by friction stir processing," vol. 5, pp. 309-313, 2015.
[88] Y. Kwon, I. Shigematsu, and N. J. S. m. Saito, "Mechanical properties of fine-grained aluminum alloy produced by friction stir process," vol. 49, no. 8, pp. 785-789, 2003.
[89] Z. Liu, B. Xiao, W. Wang, and Z. J. C. Ma, "Singly dispersed carbon nanotube/aluminum composites fabricated by powder metallurgy combined with friction stir processing," vol. 50, no. 5, pp. 1843-1852, 2012.
[90] P. Vijayavel, V. Balasubramanian, S. J. M. Sundaram, and Design, "Effect of shoulder diameter to pin diameter (D/d) ratio on tensile strength and ductility of friction stir processed LM25AA-5% SiCp metal matrix composites," vol. 57, pp. 1-9, 2014.
[91] M.-N. Avettand-Fènoël, A. Simar, R. Shabadi, R. Taillard, B. J. M. De Meester, and Design, "Characterization of oxide dispersion strengthened copper based materials developed by friction stir processing," vol. 60, pp. 343-357, 2014.
[92] N. Gangil, A. N. Siddiquee, S. J. J. o. A. Maheshwari, and Compounds, "Aluminium based in-situ composite fabrication through friction stir processing: A review," vol. 715, pp. 91-104, 2017.
[93] K. Li, X. Liu, and Y. J. C. Zhao, "Research status and prospect of friction stir processing technology," vol. 9, no. 2, p. 129, 2019.
[94] S. U. Nisa, S. Pandey, and P. Pandey, "Significance of Al2O3 addition in the aluminum 6063 metal foam formation through friction stir processing route–A comprehensive study," *Proceedings of the Institution of Mechanical Engineers, Part L: Journal of Materials: Design and Applications,* vol. 235, no. 12, pp. 2737-2745, 2021.
[95] Y. Hangai, T. J. M. Utsunomiya, and M. T. A, "Fabrication of porous aluminum by friction stir processing," vol. 40, pp. 275-277, 2009.
[96] T. Utsunomiya, Y. Hangai, Y. J. J. o. e. Ozeki, and engineering, "Effects of amount of added alumina and holding time on manufacture of porous aluminum by utilizing friction stir processing," vol. 5, no. 3, pp. 517-525, 2010.
[97] Y. Hangai, H. Kamada, T. Utsunomiya, S. Kitahara, O. Kuwazuru, and N. J. M. Yoshikawa, "Tensile properties and fracture behavior of aluminum alloy foam fabricated from die castings without using blowing agent by friction stir processing route," vol. 7, no. 3, pp. 2382-2394, 2014.
[98] Q. Pang, Z. Hu, and J. J. T. I. J. o. A. M. T. Song, "Preparation and mechanical properties of closed-cell CNTs-reinforced Al composite foams by friction stir welding," vol. 103, pp. 3125-3136, 2019.
[99] Y. Hangai, T. Utsunomiya, and M. J. J. o. M. P. T. Hasegawa, "Effect of tool rotating rate on foaming properties of porous aluminum fabricated by using friction stir processing," vol. 210, no. 2, pp. 288-292, 2010.
[100] Y. Hangai, T. Utsunomiya, O. Kuwazuru, S. Kitahara, and N. J. M. Yoshikawa, "Deformation and plateau region of functionally graded aluminum foam by amount combinations of added blowing agent," vol. 8, no. 10, pp. 7161-7168, 2015.
[101] Y. Hangai, Y. Oba, S. Koyama, T. J. M. Utsunomiya, and M. T. A, "Fabrication of A1050-A6061 functionally graded aluminum foam by friction stir processing route," vol. 42, pp. 3585-3589, 2011.
[102] I. Papantoniou, H. Kyriakopoulou, D. Pantelis, A. Athanasiou-Ioannou, and D. Manolakos, "Manufacturing process of AA5083/nano-γAl 2 O 3 localized composite metal foam fabricated

by friction stir processing route (FSP) and microstructural characterization," *Journal of materials science,* vol. 53, no. 5, pp. 3817-3835, 2018.
[103] Y. Hangai, Y. Nakano, S. Koyama, O. Kuwazuru, S. Kitahara, and N. J. M. Yoshikawa, "Fabrication of aluminum tubes filled with aluminum alloy foam by friction welding," vol. 8, no. 10, pp. 7180-7190, 2015.
[104] Y. Hangai *et al.*, "Fabrication of functionally graded aluminum foam using aluminum alloy die castings by friction stir processing," vol. 534, pp. 716-719, 2012.
[105] S. U. Nisa, S. Pandey, and P. M. J. M. T. P. Pandey, "Formation and characterization of 6063 aluminum metal foam using friction stir processing route," vol. 26, pp. 3223-3227, 2020.
[106] T. Utsunomiya, K.-i. Tamura, Y. Hangai, O. Kuwazuru, and N. J. M. t. Yoshikawa, "Effects of tool rotating rate and pass number on pore structure of A6061 porous aluminum fabricated by using friction stir processing," vol. 51, no. 3, pp. 542-547, 2010.
[107] I. Papantoniou, H. Kyriakopoulou, D. Pantelis, A. Athanasiou-Ioannou, and D. J. J. o. m. s. Manolakos, "Manufacturing process of AA5083/nano-γAl 2 O 3 localized composite metal foam fabricated by friction stir processing route (FSP) and microstructural characterization," vol. 53, pp. 3817-3835, 2018.
[108] M. Azizieh *et al.*, "The application of friction stir processing to the fabrication of magnesium-based foams," vol. 62, no. 4, pp. 1957-1962, 2017.
[109] M. H. Abidi, K. Moiduddin, A. N. Siddiquee, S. H. Mian, and M. K. J. C. Mohammed, "Development of Aluminium Metal Foams via Friction Stir Processing by Utilizing MgCO3 Precursor," vol. 13, no. 1, p. 162, 2023.
[110] M. Azizieh, K. Goudarzi, R. Pourmansouri, H. Kafashan, Z. Balak, and H. S. J. T. o. t. I. I. o. M. Kim, "Influence of friction stir processing parameters on the microstructure of aluminum foams," vol. 71, pp. 483-491, 2018.
[111] S. Rathore, R. K. R. Singh, and K. Khan, "Development of aluminium-yttrium oxide metal matrix composite foam through FSP," in *Recent Advances in Mechanical Engineering: Select Proceedings of NCAME 2019*, 2020, pp. 367-373: Springer.
[112] K. Yamamura and T. Nishihara, "Development of Local Reinforcement and Local Metallic Foam Using FSP," in *Materials Science Forum*, 2010, vol. 638, pp. 1267-1272: Trans Tech Publ.
[113] D. Lim, T. Shibayanagi, A. J. M. S. Gerlich, and E. A, "Synthesis of multi-walled CNT reinforced aluminium alloy composite via friction stir processing," vol. 507, no. 1-2, pp. 194-199, 2009.
[114] C. Don-Hyun, K. Yong-Hwan, A. Byung-Wook, K. Yong-Il, and J. J. T. o. N. M. S. o. C. Seung-Boo, "Microstructure and mechanical property of A356 based composite by friction stir processing," vol. 23, no. 2, pp. 335-340, 2013.
[115] K. Y. McCullough, N. A. Fleck, and M. F. J. A. M. Ashby, "Uniaxial stress–strain behaviour of aluminium alloy foams," vol. 47, no. 8, pp. 2323-2330, 1999.
[116] X.-q. Cao, Z.-h. Wang, L.-m. ZHAO, and G.-t. J. T. o. N. M. S. o. C. YANG, "Effects of cell size on compressive properties of aluminum foam," vol. 16, no. 2, pp. 351-356, 2006.
[117] D. Papadopoulos, H. Omar, F. Stergioudi, S. Tsipas, H. Lefakis, and N. J. J. o. P. M. Michailidis, "A novel method for producing Al-foams and evaluation of their compression behavior," vol. 17, pp. 773-777, 2010.
[118] D. T. Queheillalt, Y. Katsumura, and H. N. J. S. M. Wadley, "Synthesis of stochastic open cell Ni-based foams," vol. 50, no. 3, pp. 313-317, 2004.
[119] N. Tuncer and G. J. J. o. m. s. Arslan, "Designing compressive properties of titanium foams," vol. 44, pp. 1477-1484, 2009.
[120] I. K. A. P. Z. PRIPRAVA, Z. POROZNOSTJO, Z. D. P. IZDELANIH, and K. S. Z. J. M. i. t. PENJENJE, "Synthesis and characterisation of closed cells aluminium foams containing dolomite powder as foaming agent," vol. 44, no. 6, pp. 363-371, 2010.

[121] Y. Luo, S. Yu, J. Liu, X. Zhu, and Y. Luo, "Compressive property and energy absorption characteristic of open-cell SiCp/AlSi9Mg composite foams," *Journal of Alloys and Compounds,* vol. 499, no. 2, pp. 227-230, 2010.
[122] D. K. Rajak, L. Kumaraswamidhas, and S. Das, "An energy absorption behaviour of foam filled structures," *Procedia Materials Science,* vol. 5, pp. 164-172, 2014.
[123] D. Kumar Rajak, L. Kumaraswamidhas, and S. Das, "Energy absorption capabilities of aluminium foam-filled square," *Advanced Materials Letters,* vol. 6, no. 1, pp. 80-85, 2015.
[124] Z. Fan, B. Zhang, Y. Gao, X. Guan, and P. J. S. M. Xu, "Deformation mechanisms of spherical cell porous aluminum under quasi-static compression," vol. 142, pp. 32-35, 2018.
[125] D. Yang *et al.*, "Coupling effect of porosity and cell size on the deformation behavior of Al alloy foam under quasi-static compression," vol. 12, no. 6, p. 951, 2019.
[126] T. Ohgaki *et al.*, "In situ observations of compressive behaviour of aluminium foams by local tomography using high-resolution X-rays," vol. 86, no. 28, pp. 4417-4438, 2006.
[127] A. Byakova, S. Gnyloskurenko, and T. J. M. Nakamura, "The role of foaming agent and processing route in the mechanical performance of fabricated aluminum foams," vol. 2, no. 2, pp. 95-112, 2012.
[128] J.-y. Yuan and Y.-x. J. T. o. N. M. S. o. C. Li, "Effects of cell wall property on compressive performance of aluminum foams," vol. 25, no. 5, pp. 1619-1625, 2015.
[129] N. Mahmutyazıcıoğlu, Ö. Albayrak, M. İpekoğlu, and S. Altıntaş, "Effects of alumina (Al2O3) addition on the cell structure and mechanical properties of 6061 foams," 2013.
[130] N. Movahedi, E. Linul, L. J. J. o. M. E. Marsavina, and Performance, "The temperature effect on the compressive behavior of closed-cell aluminum-alloy foams," vol. 27, pp. 99-108, 2018.
[131] U. Ramamurty and A. J. A. m. Paul, "Variability in mechanical properties of a metal foam," vol. 52, no. 4, pp. 869-876, 2004.
[132] J. Banhart and J. J. J. o. m. s. Baumeister, "Deformation characteristics of metal foams," vol. 33, pp. 1431-1440, 1998.
[133] M. F. Ashby, T. Evans, N. A. Fleck, J. Hutchinson, H. Wadley, and L. Gibson, *Metal foams: a design guide*. Elsevier, 2000.
[134] Y. Hangai, H. Kamada, T. Utsunomiya, S. Kitahara, O. Kuwazuru, and N. Yoshikawa, "Tensile properties and fracture behavior of aluminum alloy foam fabricated from die castings without using blowing agent by friction stir processing route," *Materials,* vol. 7, no. 3, pp. 2382-2394, 2014.
[135] S. Sakthivelu, T. Anandaraj, and M. Selwin, "Multi-objective optimization of machining conditions on surface roughness and MRR during CNC end milling of aluminium alloy 7075 using Taguchi design of experiments," *Mechanics and Mechanical Engineering,* vol. 21, no. 1, pp. 95-103, 2017.
[136] Z. Shen, T. Akbay, J. Bourne, and R. Reed, "Modelling of reaustenitization during welding of Fe-C steels," ASM International, Materials Park, OH (United States)1996.
[137] C. Atkinson and T. J. A. m. Akbay, "The effect of the concentration-dependent diffusivity of carbon in austenite on a model of reaustenitisation from ferrite/cementite mixtures in FeC steels," vol. 44, no. 7, pp. 2861-2868, 1996.
[138] P. Antil, S. Singh, and P. J. J. P. M. Singh, "Taguchi's methodology based electrochemical discharge machining of polymer matrix composites," vol. 26, pp. 469-473, 2018.
[139] Y. Hangai, H. Yoshida, O. Kuwazuru, and N. Yoshikawa, "Effect of die material on compressive properties of open-cell porous aluminum fabricated by friction powder compaction process," *Materials transactions,* p. M2013081, 2013.

[140] D. Storjohann, O. Barabash, S. David, P. Sklad, E. Bloom, and S. Babu, "Fusion and friction stir welding of aluminum-metal-matrix composites," *Metallurgical and Materials Transactions A,* vol. 36, no. 11, pp. 3237-3247, 2005.
[141] S. U. Nisa, S. Pandey, and P. Pandey, "A review of the compressive properties of closed-cell aluminum metal foams," *Proceedings of the Institution of Mechanical Engineers, Part E: Journal of Process Mechanical Engineering,* p. 09544089221112291, 2022.
[142] C. Mapelli, D. Mombelli, A. Gruttadauria, S. Barella, and E. Castrodeza, "Performance of stainless steel foams produced by infiltration casting techniques," *Journal of Materials Processing Technology,* vol. 213, no. 11, pp. 1846-1854, 2013.
[143] L. Cambronero, J. Ruiz-Roman, F. Corpas, and J. R. Prieto, "Manufacturing of Al–Mg–Si alloy foam using calcium carbonate as foaming agent," *Journal of Materials Processing Technology,* vol. 209, no. 4, pp. 1803-1809, 2009.
[144] Y. Hangai, H. Kato, T. Utsunomiya, S. Kitahara, O. Kuwazuru, and N. Yoshikawa, "Effects of porosity and pore structure on compression properties of blowing-agent-free aluminum foams fabricated from aluminum alloy die castings," *Materials Transactions,* vol. 53, no. 8, pp. 1515-1520, 2012.
[145] S. Rathore, R. K. R. Singh, and K. L. A. Khan, "Effect of Process Parameters on Mechanical Properties of Aluminum Composite Foam Developed by Friction Stir Processing," *Proceedings of the Institution of Mechanical Engineers, Part B: Journal of Engineering Manufacture,* p. 09544054211021341, 2021.
[146] V. V. Patel, V. Badheka, and A. Kumar, "Effect of polygonal pin profiles on friction stir processed superplasticity of AA7075 alloy," *Journal of materials processing technology,* vol. 240, pp. 68-76, 2017.
[147] G. Bedford, V. Vitanov, and I. Voutchkov, "On the thermo-mechanical events during friction surfacing of high speed steels," *Surface and Coatings Technology,* vol. 141, no. 1, pp. 34-39, 2001.
[148] U. Suhuddin, S. Mironov, H. Krohn, M. Beyer, and J. Dos Santos, "Microstructural evolution during friction surfacing of dissimilar aluminum alloys," *Metallurgical and Materials Transactions A,* vol. 43, no. 13, pp. 5224-5231, 2012.
[149] L. J. Gibson and M. F. Ashby, "Cellular Solids: Structure and Properties—Second Edition," *Published by the Press Syndicate of the University of Cambridge,* 1997.
[150] M. Kumar, R. K. Raj Singh, and V. Jain, "Effect of processing parameters and heat treatment techniques on foaming properties of aluminium foam developed by friction stir processing route," *Proceedings of the Institution of Mechanical Engineers, Part L: Journal of Materials: Design and Applications,* p. 14644207221117517, 2022.
[151] M. Kumar, R. K. R. Singh, and V. Jain, "Effect of tool pin profiles on the properties of foamable precursor developed by friction stir processing," *Proceedings of the Institution of Mechanical Engineers, Part E: Journal of Process Mechanical Engineering,* p. 09544089221113562, 2022.
[152] S. Singh, I. Singh, and A. J. I. J. o. C. M. R. Dvivedi, "Design and development of novel cost effective casting route for production of metal matrix composites (MMCs)," vol. 30, no. 6, pp. 356-364, 2017.
[153] R. Kumar, A. Singh, I. J. M. Singh, and M. Processes, "Electric discharge hole grinding in hybrid metal matrix composite," vol. 32, no. 2, pp. 127-134, 2017.